

UNIVERSITA' DEGLI STUDI DI PARMA

Dottorato di ricerca in Scienze Chimiche

Ciclo XXVIII (2013-2015)

Heterogeneous catalysts for environmentally
sustainable reactions

Coordinatore:

Chiar.mo Prof. Roberto Cammi

Tutor:

Chiar.mo Prof. Raimondo Maggi

Dottoranda: Veronica Santacroce

2016

Table of contents

1. Introduction	
1.1 Green chemistry	7
1.2 Heterogeneous catalysis	7
2. Metal oxides	
2.1 General introduction	9
2.2 Selective monoesterification of dicarboxylic acids	11
2.2.1 Introduction	11
2.2.2 Results and discussion	11
2.2.3 Conclusions	25
2.2.4 Experimental section	25
2.3 Oxidative dehydrogenation of butane to 1,3-butadiene	29
2.3.1 Introduction	29
2.3.2 Results and discussion	31
2.3.3 Conclusions	43
2.3.4 Experimental section	44
2.4 Non-oxidative dehydrogenation of butane to 1,3-butadiene	47
2.4.1 Introduction	47
2.4.2 Results and discussion	47
2.4.3 Conclusions	55
2.4.4 Experimental section	56
3. Supported sulfonic acids	
3.1 General introduction	59
3.2 Levulinic acid esterification	61
3.2.1 Introduction	61

3.2.2	Results and discussion	63
3.2.3	Conclusions	68
3.2.4	Experimental section	68
3.3	Friedel-Crafts acylation reaction	69
3.3.1	Introduction	69
3.3.2	Results and discussion	69
3.3.3	Conclusions	74
3.3.4	Experimental section	75
3.4	Reaction of α,β-Unsaturated Carbonyls with Epoxides	77
3.4.1	Introduction	77
3.4.2	Results and discussion	78
3.4.3	Conclusions	83
3.4.4	Experimental section	83
4.	Hydrotalcites	
4.1	General introduction	87
4.2	Phosphite Addition on Carbonyl Groups	89
4.2.1	Introduction	89
4.2.2	Results and discussion	90
4.2.3	Conclusions	99
4.2.4	Experimental section	99
4.3	Allylation reaction of β-dicarboxylic compounds	103
4.3.1	Introduction	103
4.3.2	Results and discussion	103
4.3.3	Conclusions	111
4.3.4	Experimental section	112
	References	115

1. Introduction

1.1 Green chemistry

Over the course of the past decade, green chemistry has demonstrated how fundamental scientific methodologies can protect human health and the environment in an economically beneficial manner.

Nowadays it is more and more increasing the attention towards a sustainable development, which should “*meet the needs of the present without compromising the ability of future generations to meet their own needs*”.¹ In this, green chemistry, that efficiently utilises renewable raw materials, eliminates waste and avoids the use of toxic and/or hazardous solvents and reagents in both products and processes,² represents a great potential.

By definition, Green chemistry is “*the design of chemical products and processes that reduce or eliminate the use and generation of hazardous substances*”.³

The design of environmentally benign products and processes may be guided by the 12 Principles of Green Chemistry.⁴ These principles are a categorization of the fundamental approaches taken to achieve the green chemistry goals of benign products and processes, and have been used as guidelines and design criteria by molecular scientists. Attempts are being made not only to quantify the greenness of a chemical process but also to factor in other variables such as chemical yield, the price of reaction components, safety in handling chemicals, hardware demands, energy profile and ease of product workup and purification. Thanks to these, significant progress is being made in several key research areas, such as catalysis, the design of safer chemicals and environmentally benign solvents, and the development of renewable feedstocks. Current and future chemists are being trained to design products and processes with an increased awareness for environmental impact.⁵

1.2 Heterogeneous catalysis

The area of catalysis is sometimes referred to as a “foundational pillar” of green chemistry.⁶ Catalytic reactions⁷ often reduce energy requirements and decrease separations due to increased selectivity; they may permit the use of renewable

feedstocks or minimize the quantities of reagents needed. Catalysis often permits the use of less toxic reagents, as in the case of oxidations using hydrogen peroxide in place of traditional heavy metal catalysts.⁸ Catalysis catalyzes the *greening* of chemistry,⁹ by reducing the environmental impact and the costs of processes.

Moreover, heterogeneous catalysis allows few more improvements over the homogeneous one. Homogeneous catalysts have better defined active sites, usually have all of the metal atoms available as the catalyst, and the steric and electronic environment of the metal atom can be, at least in principle, varied very widely. Nevertheless, homogeneous catalysts are difficult to separate off the reaction products and recover. This can be both complex and expensive. Other disadvantages are that these catalysts are relatively easily decomposed so temperatures must be well controlled, and that they can be deactivated if poisonous by-products are formed. In addition, corrosion of reactors by metal complexes is possible.

In contrast to homogeneous catalysts, heterogeneous catalysts bear specific advantages concerning especially the workup procedures. The separation of the catalyst from reactants and products can be facilitated by using simple mechanical techniques as filtration or centrifugation; in addition, they are generally not corrosive and could avoid the production of undesired side products.¹⁰ Moreover, the use of efficient solid acid catalysts has permitted to develop catalytic processes¹¹ with both environmental and economic benefits.

So, to minimize waste production and lower the economical impact of a given synthetic process, the replacement of homogeneous catalysts with potentially recyclable heterogeneous solid catalysts is an attractive proposition.¹² However, it is often difficult to predict the mode of action of a solid material, and then the design of the most suitable heterogeneous catalyst is with no doubt more complicated than in the case of homogeneous catalysis. Nevertheless, there are various materials that can be used for this purpose and the activity of these can also be improved by appropriate modification and functionalization.

This work mainly deals with the possibility of conducting organic reactions using as catalysts both commercial and prepared solid materials to minimize waste production and lower the economical impact of the studied synthetic processes.

2. Metal oxides

2.1 General introduction

Oxides are generally used as active catalytic components either in oxidation reactions under oxidizing conditions or in reactions in which the reduction of the oxide is prevented by kinetic or thermodynamic limitations.¹³ In selective oxidation reactions, the catalytically active oxide frequently acts according to the so-called MarsVan Krevelen mechanism, based on the idea that the adsorption of a molecule occurs on the top of another molecule which had previously been adsorbed.¹⁴ According to this mechanism, an oxidation reduction sequence occurs on the oxide surface. This requires that the metal ions of the oxide which constitutes the active phase have a variety of possible oxidation states.

Non-reducible oxides can function as solid acids or bases. For example, alumina has some acidic properties while MgO, CaO and BaO have basic properties. Non-reducible oxides can also be used as inert supports that help to stabilize the metal particles, examples being alumina (Al_2O_3), silica (SiO_2), magnesia (MgO) and zirconia (ZrO_2). However, even with these relatively stable oxides, it is not possible to completely exclude that the interface between the metal and the support provides a special type of site and that the catalytic reactions occurring on the supported catalysts depend on sites on both the metal and the oxide surface near the interface.

2.2 Selective monoesterification of dicarboxylic acids

2.2.1 Introduction

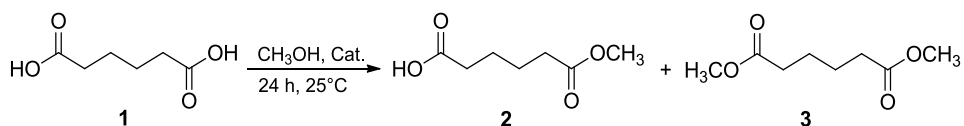
The selective protection of one of two identical functional groups is an important transformation in organic synthesis, especially when these groups are located in a symmetrical position in the molecule. While it is easy enough to protect a primary alcohol in the presence of a tertiary one, more problematic is for example the protection of only one of the two alcohol groups of 1,6-hexanediol.

In literature various strategies are shown for the selective protection of diols and symmetrical diketones under heterogeneous catalysis.¹⁵ For the selective protection of dicarboxylic acids, homogeneous acid catalysts have been used, for example sulfuric¹⁶ and boric acid,¹⁷ and various enzymes,¹⁸ for example the PPL (Porcine Pancreatic Lipase),¹⁹ by using methanol as reagent-solvent. The mono esterification of dicarboxylic acids has also been conducted using alkyl halides under transfer phase conditions.²⁰ Dicarboxylic can be selectively monoprotected also in the presence of heterogeneous catalysts by reaction with diazomethane or dimethyl sulfate in the presence of alumina or silica gel;²¹ the transesterification approach, utilizing butyl formate in octane was also reported.²²

The monoesterification of dicarboxylic acids with alcohols in the presence of heterogeneous acid catalysts has been studied and results are here reported.

2.2.2 Results and discussion

The model reaction studied was the one between adipic acid (hexanedioic acid) and methanol, used as a reagent-solvent (**Scheme 1**).



Scheme 1 Reaction between adipic acid and methanol.

At first the catalytic activity of different materials was considered. Acid and basic heterogeneous catalysts were tested, both commercially available or prepared by the

tethering methodology. The reaction was carried out at room temperature, for 24 hours, in excess of alcohol (2 ml of methanol per mmol of acid, ratio = 50/1 mmol). The amount of catalyst used was 50 mg per mmol of acid for clay, zeolites and oxides (**entries 3-7**) or 10% H⁺ per mmol of acid for sulfonic catalysts (**entries 1-2**). The results obtained are shown in **Table 1**.

Table 1 Catalytic activity of various heterogeneous acid catalysts.

Entry	Catalyst	1 Conversion (%)	2 Yield (%)	3 Yield (%)	2 Selectivity (%)
1	SiO ₂ -(CH ₂) ₂ -SO ₃ H	95	50	45	53
2	Amberlyst 15	68	40	28	59
3	Zeolite BEA 300	57	39	18	68
4	Zeolite HSZ 360	21	18	3	86
5	Acid Al ₂ O ₃	60	57	3	95
6	Basic Al ₂ O ₃	-	-	-	-
7	Hydrotalcite MG70	-	-	-	-

Basic catalysts, such as alumina and hydrotalcites of the MG series (synthetic clays) showed no catalytic activity (**entries 6-7**). Among the acid catalysts, those of zeolitic type (**entries 3-4**) have led to a moderate conversion of adipic acid (21-57%) together with a good selectivity (68-86%); sulfonic acids supported on silica or on polystyrene matrix (**entries 1-2**) showed the best results in terms of conversion (68-95%), but with very low selectivity (53-59%), as considerable amount of diester **3** were isolated. The best results were obtained by conducting the reaction using acid alumina, which leads to the formation of the desired monoester **2** with a yield of 57% coupled with a selectivity of 95% (**entry 5**). It should be emphasized that the reaction carried out in the same conditions but in the absence of catalyst, led to the total recovery of the starting acid material.

Since Al₂O₃ showed the best performances, the reaction was further tested with other commercial Al₂O₃ powders and ordered mesoporous aluminas prepared by a surfactant assisted synthesis.

Table 2 Catalytic activity of different aluminas.

Entry	Al ₂ O ₃ type	2 Yield (%)	2 Selectivity (%)
1	Janssen	3	100
2	Sigma Aldrich WA-1	29	98
3	Carlo Erba	57	95
4	AA	2	100
5	Al ₂ Zr ₉	3	100
6	Carlo Erba (basic)	0	-

The reaction was initially carried out for 24 hours at room temperature in order to evaluate the activity of these catalysts (50 mg each for 1 mmol of adipic acid). The best catalyst resulted the Carlo Erba acid alumina, superior to all the other commercial and prepared aluminas in term of yield, with an excellent selectivity value.

To understand the different catalytic behavior of all the tested aluminas, their physico-chemical proprieties were analyzed and compared.

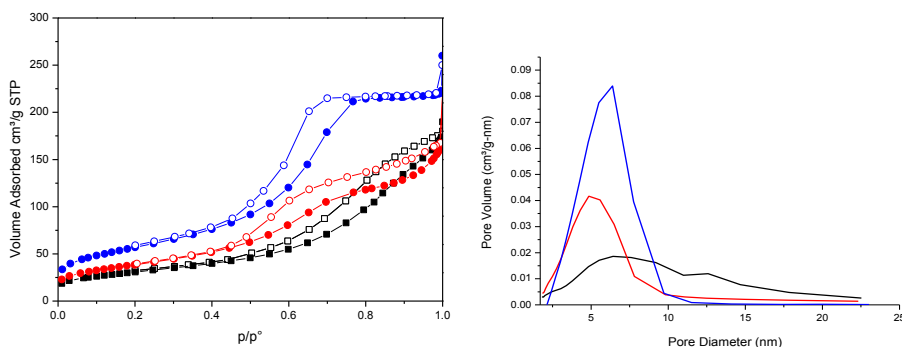
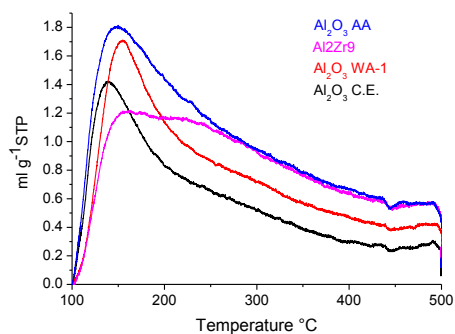
**Figure 1** Adsorption-desorption isotherms (left) and pore distribution (right) curves; from the top to the bottom: AA, WA1, C.E.**Figure 2** Temperature-programmed desorption of ammonia (NH₃-TPD).

Table 3 BET surface area of the tested aluminas.

	S.A._{BET} (m²g⁻¹)	V_p (cm³g⁻¹)	D_p (nm)	Acid sites (μmolg⁻¹)
WA-1	139	0.24	5.0	690
C.E.	110	0.25	7.0	560
AA	206	0.34	6.0	930
Al₂Zr₉	232	0.25	6.0	790

All the commercial and synthesized aluminas and the alumina zirconia have a type IV isotherms (IUPAC). In particular AA and Al₂Zr₉ alumina (an alumina doped zirconia) show type IV profile a with a H1 hysteresis loop (according to the IUPAC classification), typical of ordered and mesoporous material with one-dimensional cylindrical channels.

The BET surface areas (S.A._{BET}) are not so high for the commercial aluminas C.E. and WA-1 being the half of that of the synthesized AA and Al₂Zr₉ catalysts. The total pore volume of the commercial aluminas is very similar but C.E. alumina has a very broad distribution of the pore size centered at about 7 nm. WA-1 pore distribution is sharper and centered at about 5 nm. A.A. and Al₂Zr₉ synthetic ordered mesoporous aluminas have a pore distribution centered at about 6 nm, the former having the same total pore volume (V_p) of the commercial ones.

NH₃-TPD was successfully utilised to determine the total number of acid sites of the samples (**Figure 2**). The ammonia is a good probe basic molecule to quantify the amount of the total acid sites of a solid material. The strength of the acid sites can be determined by the desorption temperature. The samples show a characteristic tailed peaks, which means there are both weak and strong acid sites on the surface. A general slight decrease of the amount of desorbed ammonia (total peak area) indicates a global decrease of the concentration of the acid sites. Both C.E. and WA-1 samples have relatively weak acid sites and contain a low number of acidic sites (C.E contains the lowest quantity). On the contrary, AA and Al₂Zr₉ catalysts show a higher amount of strong acid sites.

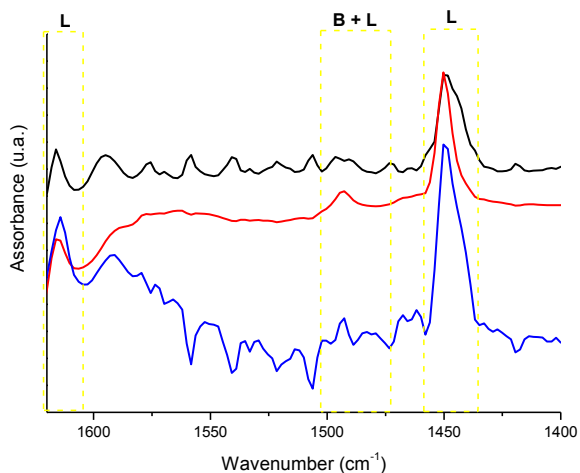


Figure 3 Infrared spectra of adsorbed pyridine.

The FT-IR analysis of the spectra of adsorbed pyridine in the 1400-1600 cm^{-1} range (**Figure 3**), allows a clear distinction between Brønsted and Lewis acid sites. The absorption bands at 1545 and 1455 cm^{-1} are unanimously assigned to adsorbed pyridinium ions and pyridine coordinated to Lewis acid sites, respectively. The peak at 1490 cm^{-1} is due to the C-C of the pyridine adsorbed on both Brønsted and Lewis acid sites. When pyridine was adsorbed, only bands indicative of weak Lewis acid sites were observed in the IR spectra of the studied aluminas.

The catalysts were also subjected to CO_2 adsorption in order to identify the presence of basic sites, as it is well known that these materials can act as bifunctional catalysts. Assuming that one CO_2 molecule interacts with one basic site, the total amount of basic sites on the catalysts have been calculated: 265 and 205 μmolg^{-1} for C.E. and AA alumina respectively. Moreover, for both materials two desorption peaks were obtained: at 447 and 470 $^{\circ}\text{C}$ for C.E. and at 461 and 489 $^{\circ}\text{C}$ for AA. This results confirm that both aluminas present a basic character and so they are able to form a carboxylate and permit the interaction with adipic acid. This interaction is favored with C.E. alumina which presents a slight bigger amount of basic sites.

In addition, the strength of the basic site is crucial: it is important to have the optimal base strength in order to permit the formation of the carboxylate group and to

avoid a too strong interaction between catalyst and reagent so that this can be released without poisoning the catalyst itself.

The interaction of the Al_2O_3 inorganic catalysts and the reactant/products was then studied mixing, in solid-phase and in a ball miller, each acid catalyst with a calculated amount of reagent or product, close to their estimated acid site quantity by NH_3 -TPD. When water was added 3% weight ratio $\text{H}_2\text{O}/\text{catalyst}$ was used ($1800 \mu\text{mol H}_2\text{O g}^{-1}\text{catalyst}$). The results are reported in **Figure 4**.

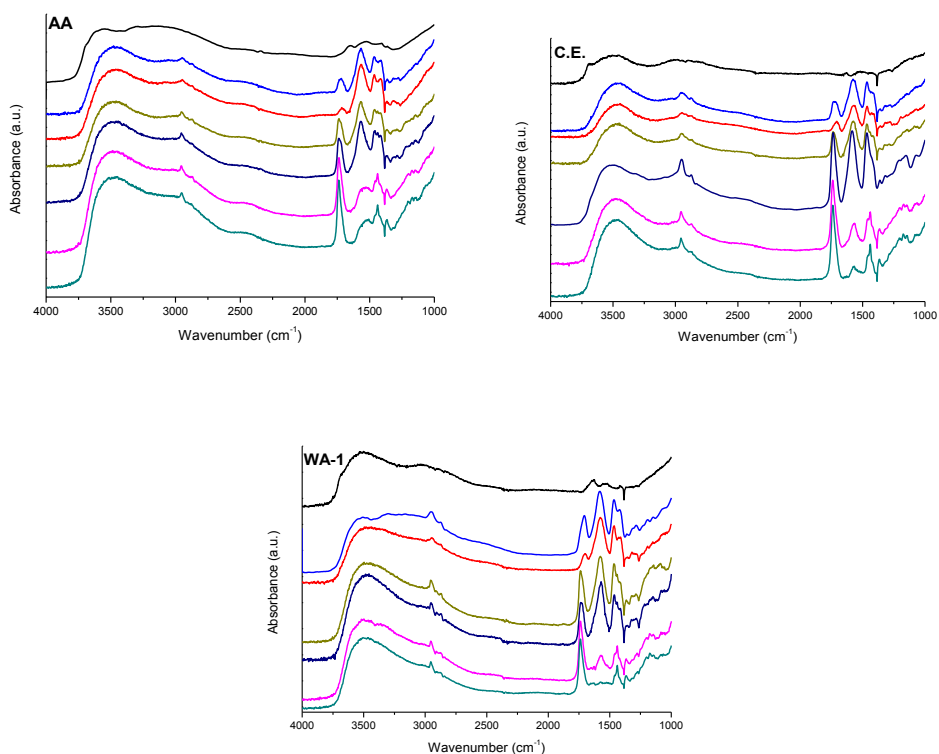


Figure 4 Infrared Spectra in Diffuse Reflectance (DRIFT-IR) of alumina samples: AA, C.E. and WA-1. From the top to the bottom: alumina sample; + adipic acid; + adipic acid, water; + monomethyl ester; + monomethyl ester, water; + dimethyl ester; + dimethyl ester, water.

Table 4 Stretching bands of the significant functional groups of reagent and products mixed with the three aluminas CE, WA-1 and AA with and without the presence of water.

	$\nu\text{C=O}$ (cm^{-1})	$\nu\text{carboxylate}$ (cm^{-1})	$\nu\text{C=O}$ (cm^{-1})	$\nu\text{carboxylate}$ (cm^{-1})	$\nu\text{C=O}$ (cm^{-1})
	Adipic acid		Monomethyl adipate		Dimethyl adipate
neat	(1760, dimer 1697)		(1735, 1714)		(1736)
CE	1726	1575	1735	1586	1738
WA-1	1700	1585	1736	1577	1737
AA	1719	1567	1735	1568	1736
in the presence of 1800 mmol H ₂ O g ⁻¹ of catalyst					
CE	1707	1575	1737	1573	1738
WA-1	1707	1574	1730	1570	1737
AA	1714	1567	1735	1568	1736

From the results reported, it is possible to state that the solid acid catalysts interact mainly with adipic acid and monomethyl adipate. Both of them interact with the basic sites of the catalysts forming a carboxylate specie (that consequently can not esterified) as already shown by using basic alumina.^{21a} Concerning the adipic acid, the other COOH group coordinates to the acid sites of the catalyst with the consequent activation of the C=O double bond that can undergo the attack by a methanol molecule giving the selectively monomethyl adipate.

When a very small amount of H₂O is present the C=O stretching of C.E. catalysts is shifted down to 1707 cm⁻¹, and this implies some interaction with the catalysts. It is possible to hypothesize that water can transform the Lewis acid sites into Broensted acid sites that can release H⁺ that active the adipic acid towards the nucleophilic attack of methanol by protonation of the C=O double bond.

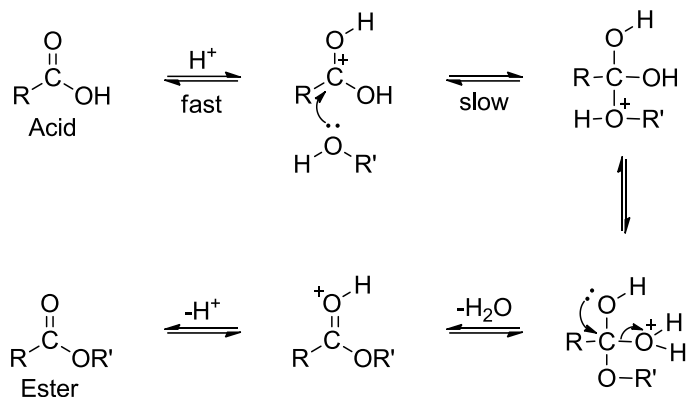


Figure 5 Proposed mechanism of activation of adipic acid promoted by a water molecule coordinated to the alumina catalyst.²³

The coordination through the carboxylate moiety avoids the attack of a second molecule of methanol to the so formed monomethyl adipate, but this coordination must be not so strong in order to allow the release of the monomethyl adipate thus avoiding the poisoning of the active sites. The good catalyst for this reaction must therefore be a bifunctional catalyst with basic and acid sites showing a good compromise concerning their number (not so high) and strength (not so high).

In order to increase the yield value, the model reaction was further carried out to find the best reaction conditions (catalyst amount, reaction temperature and reaction time). The first parameter evaluated was the temperature. Tests were conducted at 25, 50 and 65 °C (boiling point of methanol); the results are reported in **Table 5**.

Table 5 Catalytic activity of the acid alumina at various temperatures.

Entry	Temperature (°C)	1 Conversion (%)	2 Yield (%)	3 Yield (%)	2 Selectivity (%)
1	25	60	57	3	95
2	50	73	40	33	55
3	65	80	30	50	37

Even if an adipic acid conversion increasing was registered (up to 80%), the yield and the selectivity resulted very low due to the formation of big amounts of the unwanted diester **3** (33-50%). Since the selectivity of the present process is of fundamental

importance, it was decided to carry out the subsequent reactions for the optimization of the process at room temperature.

A further parameter studied was that of the amount of catalyst. It is well known that reactions which lead to the formation of products which can undergo subsequent transformations require precise amounts of catalyst and that an excess of this may result in further reaction of the desired product. It is therefore necessary to find an amount of catalyst that allows good conversion of the reactants but which at the same time maintains a good selectivity of the process. To this scope, the model reaction was conducted at room temperature using various amounts of acid alumina: 5, 25, 50 and 75 mg per mmol of adipic acid. The results obtained are reported in **Table 6**.

Table 6 Influence of the quantity of acid alumina on the yield and selectivity of the process.

Entry	Catalyst amount (g)	1 Conversion (%)	2 Yield (%)	3 Yield (%)	2 Selectivity (%)
1	5	30	29	1	97
2	25	40	38	2	96
3	50	60	57	3	95
4	75	61	58	3	95

The optimum amount of catalyst was found to be that of 50 mg per mmol of adipic acid, which leads to the desired monoester **2** with a yield of 57% and a selectivity of 95%. In fact, by halving its amount a significant decrease of the yield was observed (38%), while maintaining a good level of selectivity (96%). On the contrary, no variations were observed by increasing the amount of the acid alumina (58% yield, 95% selectivity).

On the contrary, the reaction time revealed to have a great influence on the process, as shown in **Figure 6**.

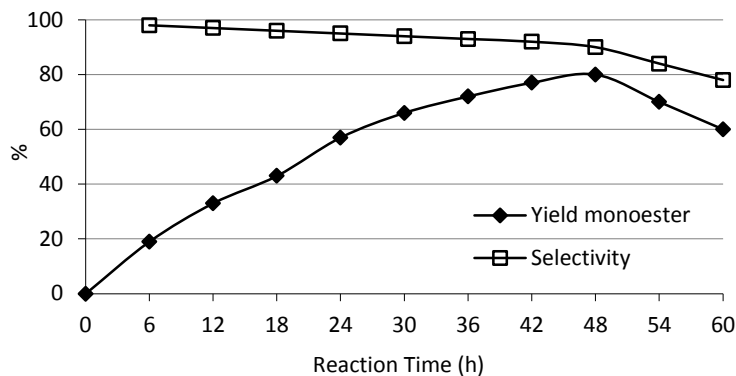


Figure 6 Yield and selectivity in function of the reaction time.

The conversion of adipic acid increases fairly linearly up to 89% after 48 hours, the threshold beyond which further increases are not observed; the yield of the product of mono-esterification reaches after this period the value of 80% resulting in a selectivity of 90%. It should be emphasized that during all the 48 hours of reaction, the selectivity remains always around very high values (90-98%). After 48 hours a decrease of the yield and the selectivity of the monoester **2** are noticed as the yield of the diester **3** increases significantly.

Finally, it was considered the amount of water present in the reaction, a very important parameter that can have a marked influence in reactions of this type. The amount of water is related to how much anhydrous are both the methanol and the acid catalyst. It should be underlined that the presence of water can also catalyze the reverse process of hydrolysis of the monoester obtained, leading in turn to a decrease of the conversion. It was therefore decided to carry out the reaction with different types of methanol, namely methanol HPLC (0.03 ~ % water), methanol HPLC left on molecular sieves overnight (with a water content close to zero), and methanol whit different amounts of water added (0.1 and 1.0%). The yields and selectivities obtained with the various types of methanol in the reaction model are given in **Figure 7**.

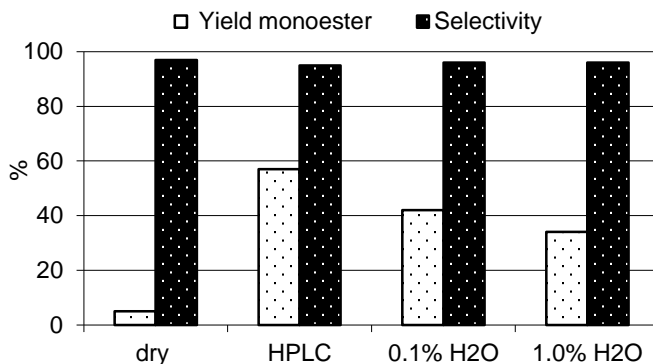


Figure 7 Yield and selectivity using methanol with different amount of water.

As can be deduced from the figure reported, the use of HPLC methanol over molecular sieves resulted in a nearly complete inhibition of the catalyst activity. The HPLC methanol itself (0.03% H₂O) revealed to be the best reaction medium, whereas by using technical methanol (0.1% H₂O) or methanol with 1% H₂O, a gradual yield decrease was observed. As above reported, a small amount of water is needed as it takes part in the catalytic process coordinating the active sites of alumina; of course, an excess of water is responsible of yield decrease due to the partial monoester hydrolysis.

It was finally evaluated the applicability of the reaction to various linear and aromatic dicarboxylic acids. In **Table 7** the results obtained are reported.

Table 7 Applicability of the developed process to various dicarboxylic acids.

Entry	Product	Yield (%)	Selectivity (%)
1	HO ₂ C(CH ₂) ₄ CO ₂ Me	80	90
2	HO ₂ C(CH ₂) ₂ CO ₂ Me	70	92
3	HO ₂ C(CH ₂) ₆ CO ₂ Me	72	87
4	HO ₂ C(CH ₂) ₇ CO ₂ Me	73	89
5	HO ₂ C(CH ₂) ₁₀ CO ₂ Me	40	86
6	<i>ortho</i> -HO ₂ CC ₆ H ₄ CO ₂ Me	0	-
7	<i>para</i> -HO ₂ CC ₆ H ₄ CO ₂ Me	0	-

Reaction conditions: 25 °C, 48 h, methanol = 2 ml/mmol acid, cat. = Al₂O₃ CE 50 mg/mmol acid

By using long chain dicarboxylic acids, slightly lower yields are obtained, whereas the selectivity values remain around 90%. The lower reactivity of long chain dicarboxylic acids can be ascribed to their reduced solubility in methanol. The phthalic acids, that are completely insoluble, were recovered unchanged at the end of the reaction.

In order to further increase the selectivity of the reaction, we studied the process under continuous flow conditions. This reaction system allows to avoid the prolonged contact of the initially formed product, the monoester, with the catalyst, in order to prevent its further transformation into the unwanted diester.

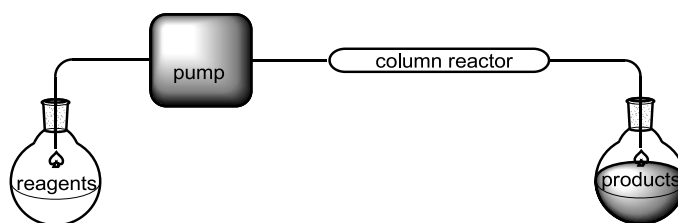


Figure 8 Scheme of the process in continuous flow.

The reagent solution was passed into the column with a flow rate of 1000, 500 or 250 $\mu\text{l}/\text{min}$, selected to have a total residence time of 5, 10 or 20 min respectively. Results are presented in the graphs below (**Figure 9**).

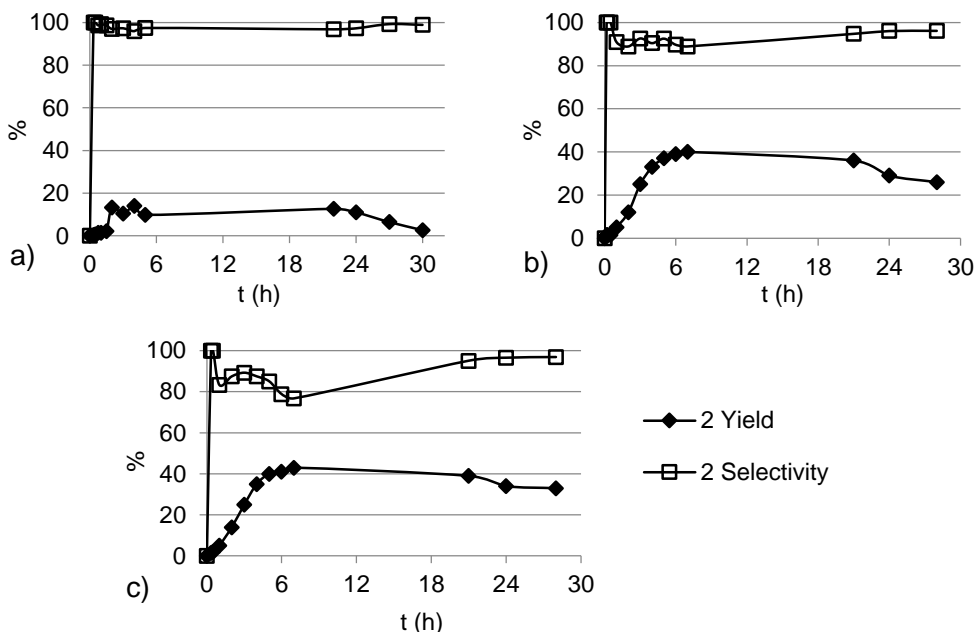


Figure 9 Yield and selectivity of monomethyl adipate obtained in flow condition with flow rate = 1000 (a), 500 (b) or 250 (c) $\mu\text{l}/\text{min}$.

By increasing the retention time (that is, using lower flows) the yield increases, but the selectivity decreases. Under the optimal reaction conditions (flow = 500 $\mu\text{l}/\text{min}$, **graph b**) a yield of 40% together with a good selectivity (90%) were achieved. At longer reaction times, a yield decrease was observed due to the catalyst inhibition by the product itself, which probably remains inside of the catalyst; this also explains why the yield observed is lower compared to that obtained in batch. Further studies are in progress in order to identify better reaction conditions in order to find out an efficient continuous flow process.

Finally, the reaction was carried out using 250 mmol of adipic acid in 500 mL of methanol. After 48 h, the catalyst was recovered by filtration; the reaction mixture was concentrated (300 ml of methanol were recovered) and then put in a refrigerator to favor the precipitation of the adipic acid. After one day the solution was filtrated and dried. The degree of purity of the product obtained is verified by GC analysis (90%). On the base of these results, some green metrics were calculated and compared to those obtained by using other procedures (**Table 8**).

Table 8 Calculated green metrics.

Plan	Yield (%)	AE	E-kernel	E-excess	E-aux	E-total	PMI
This procedure	80	0.89	0.391	0	12.363	12.753	13.753
Nishiguchi et al.^[a]	91	0.81	0.350	23.690	> 24.543	> 48.581	> 49.581
Taya et al.^[b]	> 99	0.85	0.175	0	389.536	389.711	390.711

[a]: Tetrahedron Letters 1996, 37(37), 6733-6736 (butilic ester)
[b]: JACS 1985, 107, 1365-1369

These metrics allow to quantify the efficiency or environmental performance of chemical processes. In particular, they were considered:

- the atom economy (AE):²⁴ it measures the conversion efficiency of a chemical process in terms of all atoms involved and the desired products produced;
- the E-factor:²⁵ it is defined by the ratio of the mass of waste per unit of product and can be decomposed into its contributing E-factors from reaction byproducts, side products from competing side reactions, and unreacted starting materials (E-kernel), excess reagent consumption (E-excess), and auxiliary material consumption (E-auxiliaries);
- the Process Mass Intensity (PMI):²⁶ it is the total mass of materials per mass of product.

The studies chosen for comparison are two of the best procedures reported in literature, in particular they present the selective synthesis of monoesters via transesterification catalyzed by strongly acidic ion-exchange resins in ester/octane mixtures [a] or by reaction with diazomethane using acid alumina as catalyst [b].

These data confirm the more efficiency of the proposed method: the amount of wastes produced is in fact lower than the other reported procedures, as confirmed by AE and E-total values.

2.2.3 Conclusions

The selective protection of dicarboxylic acids, which represents a major challenge for the synthetic chemist since the carboxyl groups are located in a symmetrical position in the molecule, was examined. The process was studied using adipic acid as a model reagent and following an environmentally friendly approach: a solid acid (acid alumina) was used as catalyst, methanol was utilized as esterifying agent and the reaction was conducted at room temperature.

Different aluminas were tested and their activities were correlated to their different proprieties and acidity; the selectivity of the process has been ascribed to a balanced acidity/basicity of the bifunctional alumina catalyst that prevents the esterification of a COOH functional group due to the formation of a carboxylate anion by reaction with the basic sites and favors the esterification of the second COOH group through its interaction with the acid sites coordinating water.

An interesting feature of the reaction is that it is necessary a small amount of water to be able to obtain good yields: the process is inhibited in a completely anhydrous environment whereas high amounts of water favor the hydrolysis process that restores the starting dicarboxylic acid. It has been speculated that the small amount of water could coordinate the acid sites of the alumina and then take active part in the catalytic process.

The reaction has been extended to various linear dicarboxylic acids obtaining good yields and high selectivity; on the contrary, using the phthalic acids (*ortho* and *para*) it has not been possible to obtain the corresponding monoesters having total inactivity of these reagents.

2.2.4 Experimental section

Catalytic reactions under batch conditions. In a stirred batch reactor methanol (10 ml), the dicarboxylic compound (5 mmol) and the heterogeneous catalyst (250 mg of acid Al_2O_3) were stirred at room temperature for 48 hours. Then the solid catalyst was recovered by filtration and the reaction mixture was analyzed by high resolution capillary GC with a fused silica capillary column SE52 (5% Phenyl, 95% Methyl

Polysiloxane, 30m x 25mm) using decane as internal standard. The products were identified by NMR (^1H and ^{13}C).

Catalytic reactions under continuous flow conditions. A steel HPLC column (4.6 x 250 mm) was packed with 3.5 g of the selected catalyst (Al_2O_3 CE). A pump was connected to the reactor allowing a precise control of the flow rate of the adipic acid solution in methanol, 0.1M. The flow rate was selected to have a total residence time of 5, 10 or 20 min. The eluates were analyzed by high resolution capillary GC with a fused silica capillary column SE52 (5% Phenyl, 95% Methyl Polysiloxane, 30 m x 25 mm) using decane as internal standard.

Nitrogen adsorption–desorption measurements were performed at liquid nitrogen temperature (196 °C) with an ASAP2010 apparatus of Micromeritics. The analysis procedure is fully automated and operates with the static volumetric technique. Before each measurement, the samples (0.1 g) were outgassed at 130 °C for 12 min. The N_2 isotherms were used to determine the specific surface areas (S.A.), through the BET equation, and the specific pore volume (V_s) calculated at $p/p^\circ = 0.98$. The Barrett-Joyner-Halenda (BJH) model was used to calculate the pore size distribution.

Infrared spectra in diffuse reflectance (DRIFT-IR) were acquired between 4000 e 400 cm^{-1} on a FT-IR NICOLET Magna-IR™ instrument, with an AVATAR 360 FT-IR E.S.P accessory. The resolution was kept at 4 cm^{-1} and the spectra were measured using KBr (sample mass fraction of 2% in KBr).

The total acidity of the samples was determined by temperature-programmed desorption of ammonia (NH_3 -TPD). Measurements were carried out by an AUTOCHEM 2910 automatic temperature programmed desorption apparatus (Micromeritics). About 100 mg of sample were treated at 673 K in helium flow for 90 min. The temperature was reduced to 373 K and the sample was kept in a flow of NH_3 (1% in helium) for 30 min and then in helium flow (40 ml/min) for 60 min. The amount of desorbed NH_3 was determined by heating the sample at 25 K/min up to 673 K in helium flow (40 ml/min) and a thermal conductivity detector was used.

The total basicity of the samples was determined by temperature-programmed desorption of CO₂ (CO₂-TPD). About 300 mg of sample were treated at 773 K in helium flow for 60 min. The temperature was reduced to 293 K and the sample was kept in a flow of CO₂ for 30 min. The amount of desorbed CO₂ was determined by heating the sample at 10 K/min up to 773 K and then kept at 773 K for 1 h in helium flow.

IR spectral measurements were carried out in an evacuable Pyrex cell with CaF₂ windows. The sample was ground to a fine powder. A total of 10 mg of the sample was pressed at 4 tons, in order to get a self-supporting wafer. The wafers were mounted in the holder of the IR cell and degassed by heating at 373 K and 10⁻⁴ Torr. After cooling to RT pyridine vapour was adsorbed on the samples. The spectra were recorded after degassing the wafers under vacuum at 373 K and 10⁻⁴ Torr for 2 h.

Characterization of products

1) (a) monomethyl adipate

¹H NMR (400.1 MHz, CDCl₃): δ = 8.48 (1H, br), 3.40 (3H, s), 2.10 (4H, m), 1.40 (4H, m). ¹³C NMR (100.5 MHz, CDCl₃): δ = 177.6, 173.7, 51.0, 32.90, 32.87, 23.6, 23.5.

(b) dimethyl adipate

¹H NMR (400.1 MHz, CDCl₃): δ = 3.56 (6H, s), 2.23 (4H, m), 1.56 (4H, m). ¹³C NMR (100.5 MHz, CDCl₃): δ = 173.4, 51.2, 33.4, 24.1.

2) (c) 4-methoxy-4-oxobutanoic acid

¹H NMR (400.1 MHz, CDCl₃): δ = 3.70 (3H, s), 2.65 (4H, m). ¹³C NMR (100.5 MHz, CDCl₃): δ = 177.9, 172.6, 51.9, 28.8, 28.6.

(d) dimethyl succinate

¹H NMR (400.1 MHz, CDCl₃): δ = 3.63 (6H, s), 2.57 (4H, m). ¹³C NMR (100.5 MHz, CDCl₃): δ = 172.6, 51.6, 28.7.

3) (e) 8-methoxy-8-oxooctanoic acid

^1H NMR (300.1 MHz, CDCl_3): δ = 10.43 (1H, br), 3.61 (3H, s), 2.31(4H, m), 1.60 (4H, m), 1.33 (4H, m). ^{13}C NMR (75.4 MHz, CDCl_3): δ = 179.9, 174.3, 51.5, 33.94, 33.93, 28.7, 28.6, 24.7, 24.4.

(f) dimethyl octanedioate

^1H NMR (300.1 MHz, CDCl_3): δ = 3.66 (6H, s), 2.29 (4H, m), 1.62 (4H, m), 1.32 (4H, m). ^{13}C NMR (75.4 MHz, CDCl_3): δ = 174.1, 51.4, 33.9, 28.7, 24.7.

4) (g) 9-methoxy-9-oxononanoic acid

^1H NMR (400.1 MHz, CDCl_3): δ = 3.66 (3H, s), 2.32 (4H, m), 1.61 (4H, m), 1.30 (6H, m). ^{13}C NMR (100.5 MHz, CDCl_3): δ = 179.9, 174.3, 51.5, 34.05, 33.98, 29.01, 28.99, 28.93, 24.9, 24.6.

(h) dimethyl nonanedioate

^1H NMR (300.1 MHz, CDCl_3): δ = 3.40 (6H, s), 2.03 (4H, m), 1.35 (4H, m), 1.05 (6H, m). ^{13}C NMR (75.4 MHz, CDCl_3): δ = 174.2, 51.4, 34.0, 28.9, 28.8, 24.8.

5) (i) 12-methoxy-12-oxododecanoic acid

^1H NMR (400.1 MHz, CDCl_3): δ = 3.65 (3H, s), 2.31 (4H, m), 1.61 (4H, m), 1.27 (12H, m). ^{13}C NMR (100.5 MHz, CDCl_3): δ = 179.6, 174.3, 51.3, 34.1, 34.0, 29.28, 29.27, 29.13, 29.12, 29.08, 28.99, 24.9, 24.6.

(j) dimethyl dodecanedioate

^1H NMR (300.1 MHz, CDCl_3): δ = 3.66 (6H, s), 2.30 (4H, m), 1.61 (4H, m), 1.27 (12H, m). ^{13}C NMR (75.4 MHz, CDCl_3): δ = 174.3, 51.4, 34.1, 29.3, 29.2, 29.1, 24.9.

2.3 Oxidative dehydrogenation of butane to butadiene

2.3.1 Introduction

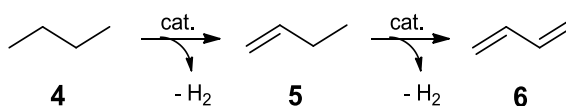
The dehydrogenation of light alkanes into olefins has received growing attention as a substitute process for obtaining olefins.²⁷ In particular, butenes obtained from the dehydrogenation of butane can be used as a feedstock for the production of 1,3-butadiene (1,3-BD), the most important conjugated diene, being the basis of a wide variety of synthetic rubbers, elastomers and polymer resins upon polymerisation by itself or in conjunction with other polymerisable monomers. It is mainly used in the production of styrene-butadiene rubbers, polybutadiene rubbers (which makes up 54% of the global demand), nitrile rubbers and styrene-butadiene latex. Moreover, it is used as a monomer in different plastics; ABS polymers consist of acrylonitrile, styrene and butadiene, and shock-resistant polystyrene contains monomeric butadiene. Synthetic butadiene rubbers are highly important in the production of tires.

Currently, butadiene is produced from steam-cracking as a by-product of ethylene production. Butadiene is extracted from a stream of C4 unsaturated hydrocarbons when cracking saturated hydrocarbons. The C4 stream is isolated and fed to certain butadiene extraction units where butadiene is separated with extractive distillation.²⁸ It is usually made from cracking naphtha; this is a heavy feed that yields high amounts of butadiene.²⁹ Lighter feeds produce only little C4 streams and usually do not have any butadiene extraction units.³⁰ However, it is only recently that ethane (shale-gas derived feed³¹) has become less expensive and is more commonly used as a feed in steam cracking. Using a lighter feed leads to a lower butadiene production and therefore to an increase in price.³⁰ Additionally, nowadays the lack of sufficient butadiene makes it more expensive. While in the beginning of 21st century butadiene cost far less than ethylene, it has now risen to a price higher than 50% of the ethylene price.³² So due to its demand, its decrease in production and increase in price, it can be very interesting to develop alternative routes to produce butadiene.³⁰

Butadiene productions from renewable materials could be one of the alternative routes.³³ A lot of research is done to convert ethanol to butadiene.³⁴ Nowadays it is

possible to produce ethanol via fermentation or syngas³⁵ and so the idea of ethanol being converted to butadiene has gained interest.³⁶

Another route for butadiene production is the conversion of butane. Butane can be obtained from crude oil and Fischer Tröpsch synthesis and is available as feedstock. In order to be economically beneficial, the conversion of butane to butadiene should yield high selectivity and conversion.³⁷ Butane can be converted into 1,3-butadiene by catalytic dehydrogenation. Since this is an endothermic process, in order to shift the equilibrium towards butadiene high temperatures are needed (600 to 700 °C). The strong endothermic character of this reaction is a disadvantage, as well as the coke formation and the regeneration of the catalyst within a short period. Oxidative dehydrogenation (ODH) of butane is a great alternative. The reaction forms H₂O and because of the stability of water the reaction becomes thermodynamically favorable.³⁸ Therefore, a lot of research is done on catalytic oxidative dehydrogenation that seems promising. During the reaction, oxygen initiates dehydrogenation and removes the allylic hydrogens. It is done in two steps: first butane loses hydrogen and the first insaturation is formed (a mixture of 1-butene, *trans*-2-butene and *cis*-2-butene is obtained, usually in 2:1:1 ratio) and then it loses again hydrogen leading to 1,3-butadiene.³⁷



Scheme 2 ODH of butane to butene to 1,3-butadiene.

However, many side reactions with oxygen can take place, usually as these reactions are thermodynamically more favourable than butadiene conversion. Therefore, a high selective catalyst is needed. It is possible to operate with low conversion to get high selectivity; nevertheless, the challenge is to develop a catalyst to perform oxidative dehydrogenation reactions with high yield.

In recent years, a lot of research has been done to develop interesting catalysts for the oxidative dehydrogenation of butane.³⁹ Generally, for the removal of hydrogen by catalytic oxidation a transition metal or its oxide is used. Most of the previous

studies used unsupported catalysts, especially V-Mg-O is often described in literature. Some other well-working catalytic systems use Ni-Mo-O, Mg-Mo-O or Mg-Ni-Sn-O systems. Supported systems usually contain the transition metals Ni or V with SiO₂ or Al₂O₃ as support.⁴⁰ Although a lot is published⁴¹ about TiO₂-based catalysts, there is only little known about the use of TiO₂ alone as catalyst for the oxidative dehydrogenation of butane to butadiene. The aim of this research is to investigate TiO₂ as catalyst, to test and develop it and to seek deeper understanding concerning its catalytic performance.

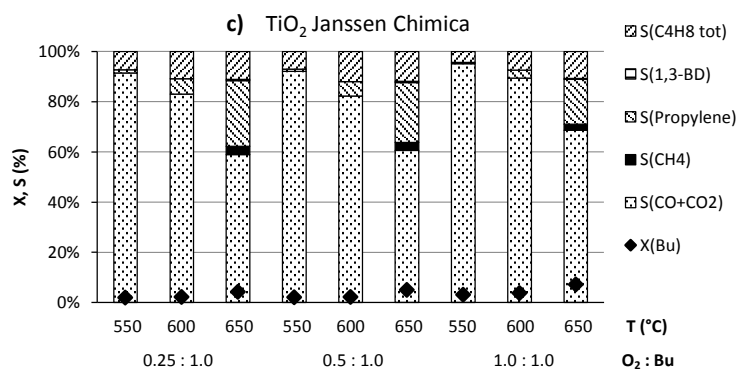
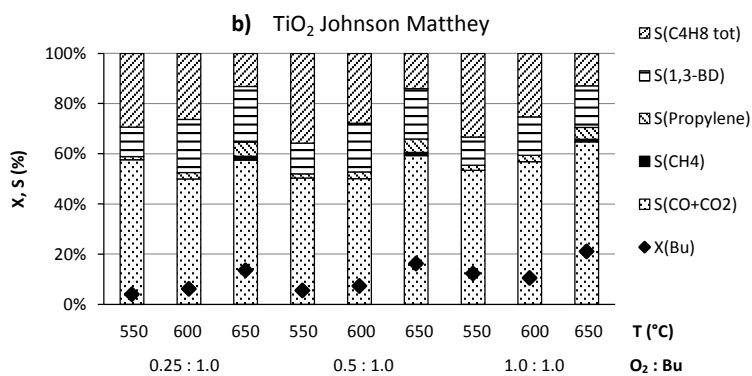
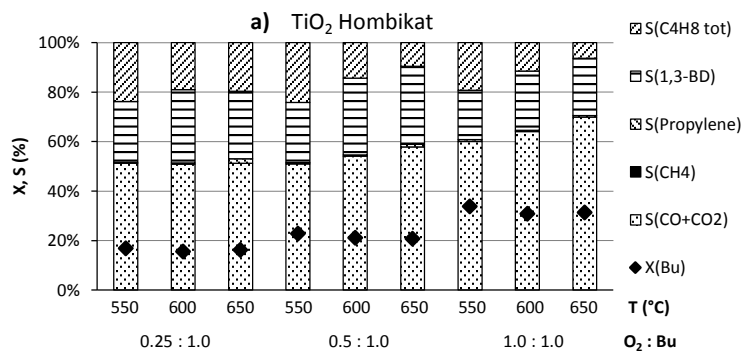
2.3.2 Results and discussion

In a first set of experiments the catalytic activity of TiO₂ from different brands was tested. For all oxidative dehydrogenation reactions an automated six-flow parallel reactor system was used. This reactor consists of six quartz tube reactors where the flow rate and the catalyst can be chosen independently, whereas the gas feed composition and the temperature are the same. The reaction mixture is analyzed by a gas chromatograph and a quadrupole mass spectrometer directly connected to the reactor. For each reaction 100 mg of non-calcined catalyst and a total flow of 50 ml/min were used. The reaction temperatures explored were 550, 600 and 650 °C and the O₂:Bu ratio was varied between 0.25 and 1.0. Results are showed in **Figure 10 a, b and c**. In general, higher temperatures and O₂ flows lead to a higher butane conversion, but in these conditions the total oxidation to CO and CO₂ is favoured so that the selectivity to butenes and 1,3-BD is lower. Hombikat TiO₂ works better for the conversion of butane to butenes and 1,3-butadiene. Conversion varied between 15% and 30% with a selectivity of 1,3-butadiene between 20-30%. The best performance was observed at 600 °C with an O₂:Bu ratio of 0.5:1. In these conditions, butane conversion was 21% with total butenes selectivity of 15% and the 1,3-BD selectivity about 31%. It is important to underline that 1,3-BD selectivity is higher than that of butenes. Usually the catalysts reported in literature show a better selectivity for butenes than to 1,3-butadiene: this behavior is ascribed to the fact that

the first dehydrogenation is easier to be accomplished, and once obtained the mono-unsaturated product, it is easily total combusted to CO and CO₂ instead of being further dehydrogenated to butadiene. On the contrary, both Johnson Matthey and Jansen Chimica TiO₂ have low performances; in fact, the best conversion value reached was only 20 and 7% respectively with low 1,3-BD selectivity and many by-products derived from total combustion.

As confirmed by XRD spectra (**Figure 10d**), all these three TiO₂ are in the anatase phase. So, they were calcined at 550 and 900 °C and tested in the ODH of butane. Only Hombikat showed what was expected: anatase phase at lower temperatures and rutile phase after calcination at higher temperatures⁴². All Johnson Matthey TiO₂ XRD patterns showed a mixture of anatase and rutile, which explains the lower catalytic performance compared to Hombikat. Janssen Chimica showed anatase phase at all calcination temperatures. All experiments with TiO₂ calcined at 550 °C showed results similar to those obtained with the non-calcined materials, while all TiO₂ calcined at 900 °C showed lower conversion and lower selectivity of 1,3-butadiene. Moreover, a lot of combustion was detected and a higher selectivity towards propylene, meaning more cracking, had taken place. This is probably due to a lowering of the surface area of the catalyst after the heating treatment.

As reported in literature, the {101} rutile surface has a lower surface energy and the binding energy of Ti-O in rutile phase is weaker compared to that of the anatase phase. Calculations have been done showing that rutile TiO₂ is more easily reduced than anatase TiO₂. This would imply that rutile TiO₂ will be a better dehydrogenation catalyst; however according to literature anatase TiO₂ is more effective. This is due to the surface area which is much higher per unit for anatase than for rutile. Due to the higher surface area, more oxygen species are exposed and thus anatase is a more effective catalyst.⁴³



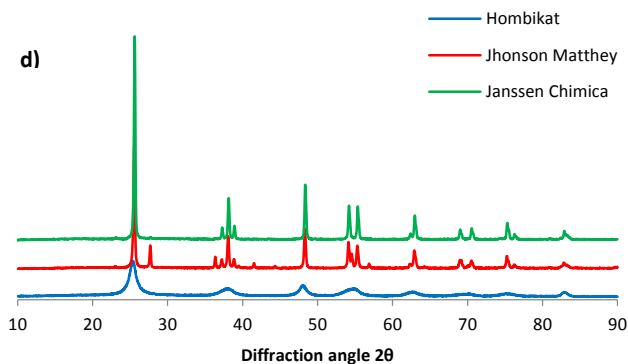


Figure 10 a,b,c) Performance of different brands TiO₂ (not calcined) in ODH reaction of n-butane. Reaction conditions: total flow = 50 ml/min; O₂:butane ratio = 0.25, 0.5 or 1.0; T = 550, 600 or 650 °C. d) XRD patterns of TiO₂ of Hombikat, Johnson Matthey and Janssen Chimica not calcined.

Understanding the Catalytic Mechanism

As TiO₂ Hombikat showed the best performance, it was further used to study the long-term stability in the best reaction conditions (600 °C and O₂:Bu = 0.5) (**Figure 11**). The catalyst showed a steady butane conversion for 24 h (around 20%). In the subsequent hours a slight decrease is observed before reaching another steady state after about 100 h reaction [X(Bu) = 12%]. At the initial state of the reaction, the total butene selectivity drop down as the production of 1,3-butadiene increased. This confirms the two step process: butane is firstly converted to butene which then is converted into 1,3-butadiene. During all the time monitored, 1,3-BD selectivity remains constant (31%) and the butenes selectivity, after the initial decreasing, increases again up to 24% and remains constant during all the 120 h monitored. Moreover, propylene selectivity is only 1% for all the reaction long, confirming that the cracking process is not favored.

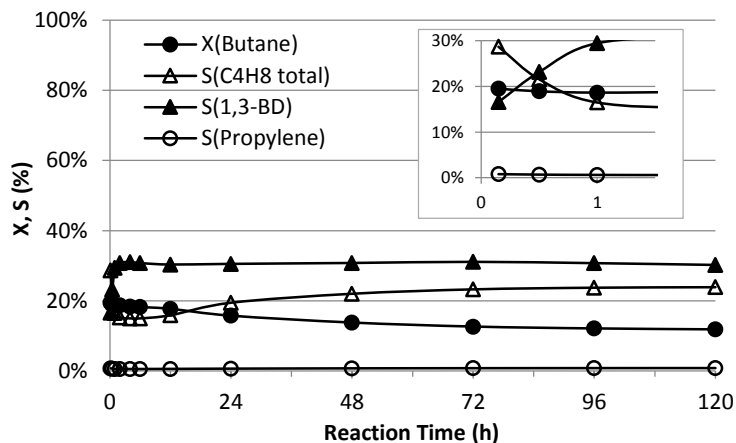


Figure 11 Time on stream activity of TiO₂ Hombikat for ODH. Reaction conditions O₂: Bu = 0.5:1; total flow 50 ml/min; T = 600 °C.

To gain more information about the oxidative dehydrogenation process, several oxygen treatment experiments were done. In a first experiment, the catalyst loaded in the reactor was pre-treated with an O₂ flow at 550 °C for 1 h. Then, the dehydrogenation reaction was performed without any O₂ flow (only Argon was used as carrier gas). At 550 and 600 °C the conversion was <5%, while at 650 °C 15% butane conversion was observed, a value comparable to that obtained under O₂ flow (**Figure 12**). Moreover, without the use of O₂ during the reaction, the decrease in conversion was much more slow. After regeneration of the catalyst under O₂ flow, improved conversion and selectivity was shown, which then decreased again.

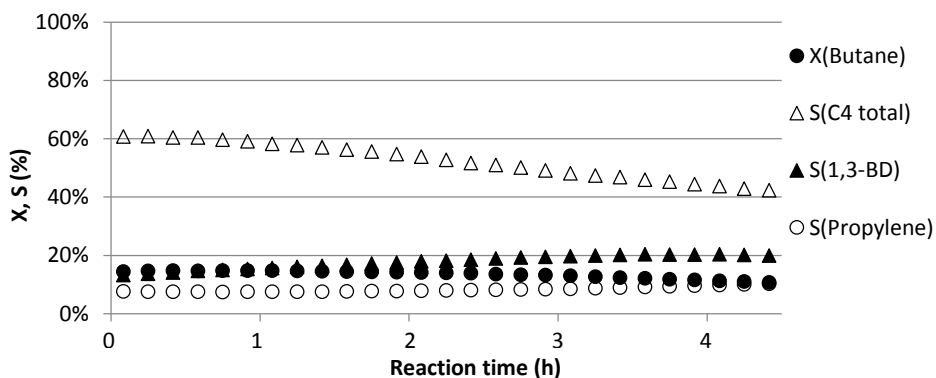


Figure 12 Kinetic curve of non-oxidative dehydrogenation of butane with oxygen pretreatment.

This confirms clearly the oxidative dehydrogenation mechanism: the structure consists of reductive active sites which accommodates oxygen species which are used for the reaction, and H₂O is produced with the removed hydrogens. In addition, 1,3-BD selectivity was around 20%, not so different from that obtained under oxidative condition, while total butenes selectivity was very high (60% at the beginning of the process). It must be noted that the only by-product observed was propylene (<10%), whereas no CO and CO₂ were detected.

Most interestingly was the non-oxidative reaction without an oxygen pretreatment (**Figure 13**). After an increase in selectivity of 1,3-butadiene and a concurring decrease of butenes selectivity, the opposite happens: a decrease of 1,3-butadiene selectivity and an increase in C₄H₈ selectivity. At the beginning of the reaction, high selectivity of butenes (70%) is observed, and thereafter butene is converted to butadiene, thus decreasing butene selectivity.

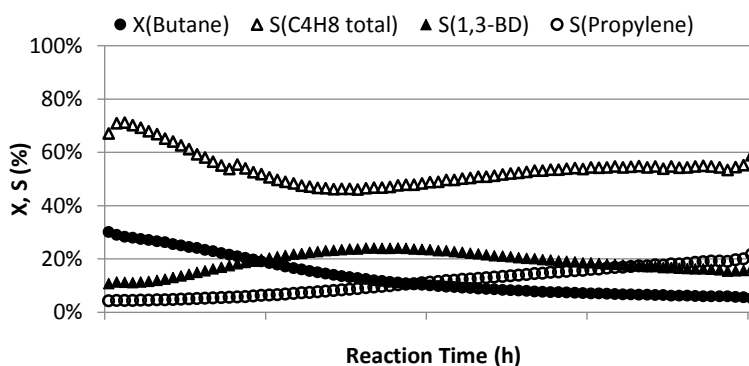


Figure 13 Kinetic curve of ODH of butane without O₂ flow at 650 °C.

From this data, the following explanation can be given based on a Mars-Van-Krevelen type mechanism.⁴⁴ Butane or butene reacts directly with a lattice oxygen species leading to butane or 1,3-butadiene respectively and a vacancy appears in the structure. At these oxygen vacancies the two unpaired electrons are located on two Ti³⁺.⁴⁵ As the catalyst is more and more reduced, replacement of new oxygen species at these active sites it is needed to re-oxidize the cation. This can either be done by adsorption of gaseous O₂ or by network-oxygen diffusivity,^{44,46} however the adsorption of

molecular O_2 is faster than network-oxygen diffusivity.⁴⁶ This is also confirmed by the data from the (non)-oxidative reactions.

Adsorption and reactions of O_2 on anatase TiO_2 is deeply studied.⁴⁵ Electron transfer from the surface to the oxygen molecule is essential for oxygen adsorption. In fact, O_2 does not adsorb on stoichiometric TiO_2 ; excess electrons are required. As titania samples are very often reduced,⁴⁷ excess electrons originating from oxygen vacancies and titanium interstitials are typically present in the material. Both defects were recently shown to exist exclusively in the subsurface region in the case of anatase $\{101\}$ ⁴⁸ which is the majority surface of this TiO_2 being polymorph. Anatase $\{001\}$ surfaces contain fivefold Ti (Ti_{5c}) atoms and two- or threefold oxygen atoms. Whereas $\{101\}$ surfaces exhibit Ti_{5c} with O_{2c} and six fold Ti (Ti_{6c}) atoms with threefold coordinated oxygen atoms. The edges contain fourfold Ti atoms with twofold coordinated oxygen atoms. These edges are highly reactive for gas adsorption.⁴⁷ In fact, gaseous oxygen will adsorb at a Ti_{5c} near an oxygen vacancy, the extra charge (localized on the two Ti^{3+}) is now transferred to O_2 which will form a peroxide species (O_2^{2-} that is energetically more stable than O_2^-). The adsorbed peroxo species functioning as a bridging dimer is put forward as an important intermediate in the oxygen evolution reaction. This phenomenon may also be responsible for the higher catalytic activity of anatase TiO_2 .⁴⁵ It has been also demonstrated that defects are not just a static source of negative charge to enable the formation of adsorbed superoxo or peroxo species. Instead, they actively take part in the reaction with O_2 even though they are located in subsurface layers. Adsorption of molecular oxygen favours the migration of the defects toward the surface. Titanium interstitials can then exothermically react to form TiO_2 -like islands on the surface, whereas oxygen vacancies can accommodate O_2 molecules in the bridging dimer configuration. Hence, both types of reducing intrinsic defects provide energetically favourable pathways for the incorporation of O_2 into anatase TiO_2 .

Moreover, the temperature-programmed reduction (TPR) showed two distinctive peaks (**Figure 14**) at 120 and 505 °C.

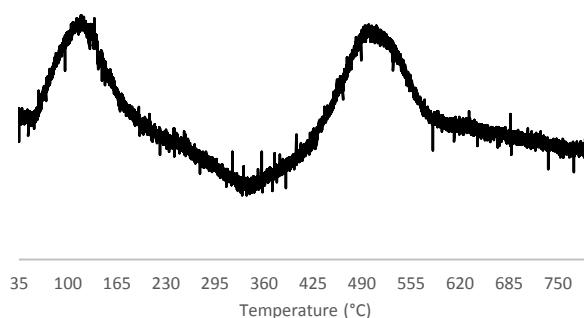
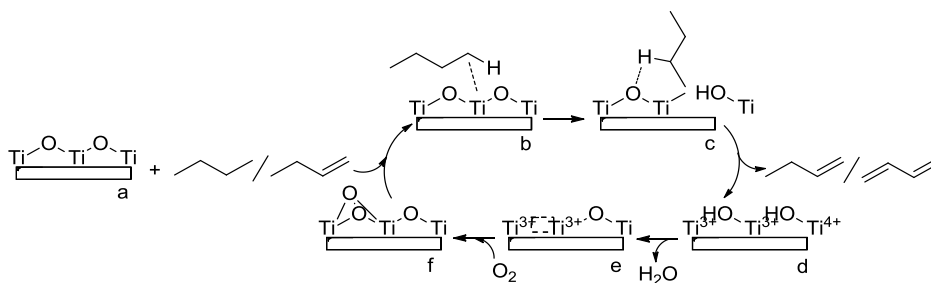


Figure 14 TPR of TiO₂ Hombikat.

This shows the reducibility of TiO₂ in which surface oxygen species are involved in the reduction at lower temperatures and lattice oxygen species are involved in reduction at higher temperatures. According to literature, O₂⁻ species are bound close to and around oxygen vacancies and will desorb around a temperature of 137 °C. Moreover, there are some oxygen atoms adsorbed on the surface and these will all disappear when the surface is heated to more than 300 °C.⁴⁷ As the ODH reaction takes place at temperatures ranging from 550 to 650 °C it indicates that the active oxygen species during ODH are lattice oxygen species. The following mechanism is proposed:



Scheme 3 Proposed mechanism for ODH reaction of n-butane: (a) Anatase TiO₂ surface; (b) C₄H₁₀ adsorbed; (c) dehydrogenation of C₄H₁₀ to C₄H₈; (d) surface after butane desorption (e) oxygen vacancy; (f) gaseous oxygen adsorption forming a peroxo.

Butane is initially adsorbed onto titania surface; the first dehydrogenation occurs leading to C₄H₈ product. This also generates an oxygen vacancy on the catalyst surface, that is filled with the gaseous O₂ used during the reaction. This permits the

regeneration of the catalyst that in this way will be available to further dehydrogenation.

Optimizing TiO₂ as a catalyst

As shown in previous section, TiO₂ from different companies show very different results. Many structural aspects such as particle size or surface area influence the properties and the catalytic performance of TiO₂.⁴⁹ It was investigated if different methods to synthesize TiO₂ would affect their catalytic performance. Synthesizing TiO₂ by a sol-gel method (which is most used) gave low conversion and only 10-15% 1,3-butadiene selectivity. However, many synthesis conditions (acidity of the solution, hydrolysis period etc.) play a role in the shape and morphology of TiO₂. Better performing TiO₂ nanoparticles could have been obtained by prolonging the hydrolysis period at a higher temperature. Synthesizing TiO₂ at room temperature will give more amorphous and oxygen deficient nanoparticles.⁵⁰ Also the water-to-titanium ratio could be optimized as this influences the size and stability of TiO₂ nanoparticles.⁴⁹

Poisoned TiO₂ - Surface Treatment - Different oxides were added to the surface of titanium dioxide to investigate their effect. Two types of treatments were done to synthesize two different structures. Diluted phosphoric acid was added and calcinated at 400 °C to 'poison' the surface, either the active oxygen species in the ODH reaction or the less active oxygen species. The TiP₂O₇, TiOSO₄ and TiMgO₃ samples were calcined at 700 °C giving a structure in which the PO₄, SO₄, MgO respectively are incorporated in the surface network. The XRD patterns show an amorphous structure for the modified TiO₂ and a more crystalline surface for the sample calcined at 700 °C, which seem to confirm that PO₄ groups are stuck to the surface whereas TiP₂O₇ has incorporated the PO₄ groups in its structure. Furthermore according to Marcu et al.,⁵¹ the XRD patterns of titanium pyrophosphate should show three peaks between 20 and 30 °. The XRD pattern in **Figure 15** has a broad bump at 25 ° after its treatment,

showing a structural change between 20 and 30°, however the structure is too amorphous.

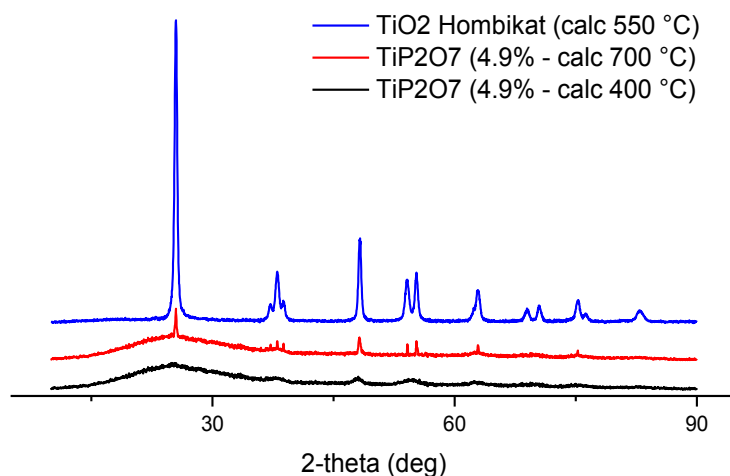


Figure 15 XRD patterns from down to top TiP₂O₇ (4.9%, calcinated 400 °C), TiP₂O₇ (4.9%, calcinated 700 °C) and Hombikat TiO₂ (calcinated 550 °C).

The comparison between TiP₂O₇ and TiO₂ modified with phosphoric acid (**Figure 16**) implies different catalytic performances because of their structure. Modified TiO₂ gives very little conversion, indicating that the PO₄ groups shield the active oxygen which then cannot be used for ODH of butane. On the other hand TiP₂O₇ gives low selectivity but high conversion, which comes from more combustion and cracking products.

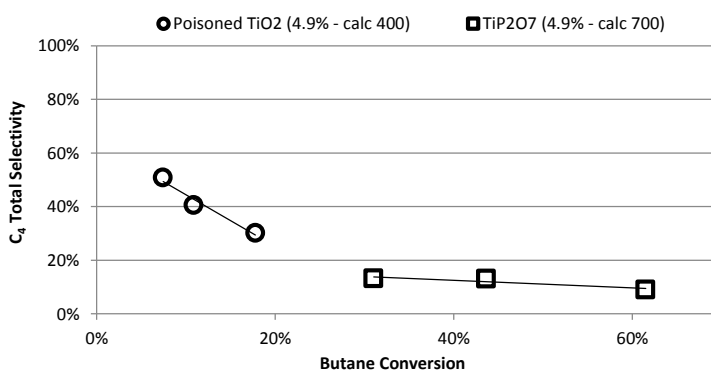


Figure 16 C₄ total selectivity (butene and butadiene) and conversion of the 'modified' TiO₂ with PO₄ and TiP₂O₇. Each dot represents an O₂:Bu condition. From left to right 0.25:1, 0.5:1 and 1:1. T=650 °C.

At lower temperatures (400-600 °C) data of the ODH reaction using modified TiO₂ showed extremely low conversion and inaccurate selectivity; however at 500 °C using an excess of oxygen (O₂:Bu = 2:1) a rather surprising conversion of 32% and total selectivity of 26% was found. At 650 °C the butane conversion was 30% with a total selectivity for butenes and butadiene of 18%.

On the basis of these data it is possible to hypothesise that the PO₄ groups on the surface poison the useful oxygen species used for the ODH reaction. At a temperature of 500 °C the catalytic performance during ODH reaction seems to be better. The graphic (**Figure 17**) shows that TiO₂ Hombikat powder (T = 550 °C) is outperforming the other catalysts: the surface treatment led to less well performing titania based catalysts. In addition, an higher percentage of added groups (4.9%) at high temperatures led to increasing conversion but decreasing selectivity. At lower temperatures conversion was too low for accurate selectivity. According to Marcu et al.,⁵¹ Lewis acidity strongly influences the selectivity of the ODH reaction. Lewis acid sites may absorb the intermediates, or the butenes and 1,3-butadiene, during the reaction as these molecules shows a basic character. Additionally, data shows higher percentage of CH₄ and propylene as well as products of total oxidation. In other words, higher temperature and acidity are promoting cracking and more combustion. TiO₂ functionalized with the lower percentage of acids groups (2.45%) showed not much difference with the unaltered TiO₂, meaning that a little addition of acid groups will have only little influence on the performance of the catalyst. At a temperature of 650 °C TiOSO₄ performed better than TiMgO₃ which performed better than TiP₂O₇ (with a conversion of ~30%). However this is not the same at lower temperatures: TiOSO₄ performs better than TiP₂O₇, and TiMgO₃ did not perform at all. Further research (e.g. acidity of the catalysts) should be done in order to better understand the observed effect of the modification.

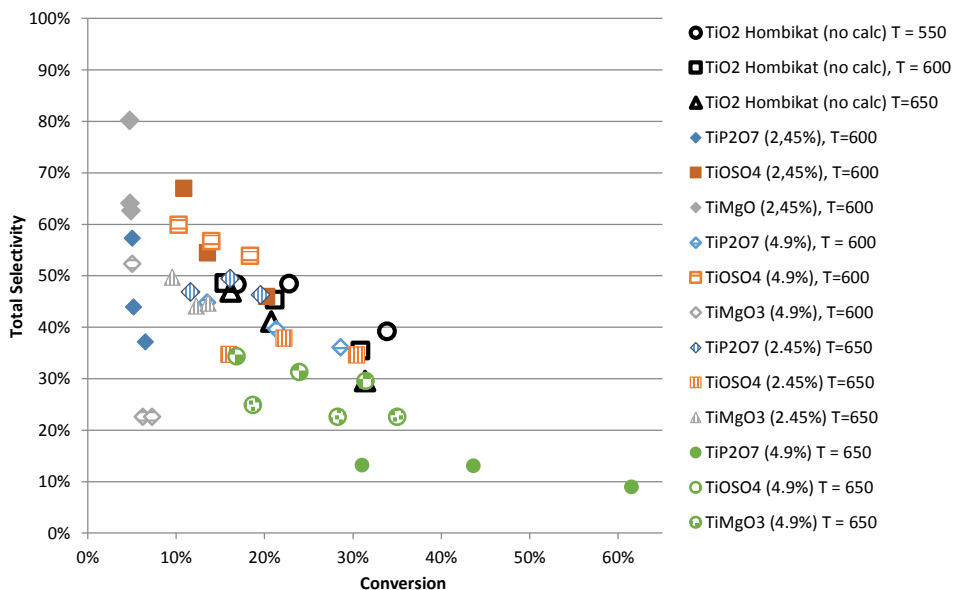


Figure 17 Total selectivity (butene and butadiene) and conversion of the ‘poisoned’ TiO₂ and Hombikat powder. Each dot represents an O₂:Bu condition. From left to right 0.25:1, 0.5:1 and 1:1.

Titanium Silica Nanoparticles – Isolation of titanium oxide species - In order to isolate the titanium oxide species, SiO₂ was used as a support for TiO₂. **Table 9** shows an increase in BET surface area of titanium silica nanoparticles (20:80). TiO₂ Hombikat powder has a mesopores structure whereas TiO₂/SiO₂ contains micropores. It clearly comes forward by calculating the intrinsic activity (**Figure 18**) how the SiO₂ support affected the catalytic performance. Titania silica nanoparticles are stable at higher temperatures and show a maximum yield of 34% per mmol of TiO₂ (650 °C, O₂:Bu = 1:1), whereas TiO₂ Hombikat powder decreases in activity at higher temperatures and shows a maximum yield of only 11% per mmol TiO₂ (650 °C, O₂:Bu = 1:1). Isolating TiO₂ particles and high surface area have a positive effect on the catalytic performance during the ODH reaction of butane.

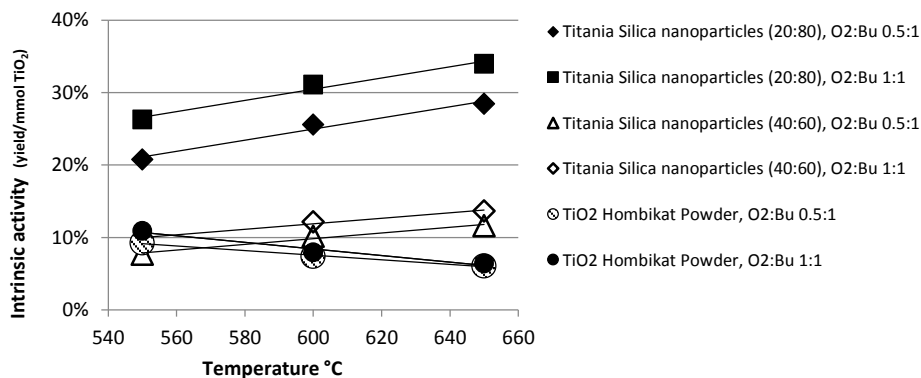


Figure 18 Intrinsic activity (yield/mmol TiO₂) at different temperatures of TiO₂ Hombikat powder and titania silica nanoparticles with the wt% ratios of 20:80 and 40:60.

Table 9 Physic-chemical characteristics of TiO₂ Hombikat M311 and TiO₂/SiO₂ (20:80).

Catalyst	TiO ₂ Hombikat M311 powder	Titanium silica nanoparticles (20:80)
BET specific surface area (m ² g ⁻¹)	369	369
Pore volume (cm ³ g ⁻¹)	0.8	0.8
Pore diameter (nm)	20-30	20-30

2.3.3 Conclusions

In this research titanium dioxide was used as catalyst in the oxidative dehydrogenation of butane to 1,3-butadiene. As anatase TiO₂ (Hombikat) showed good conversion (31%) and total selectivity (39%) it is fundamental to gain a deeper structural understanding. A possible mechanism is proposed: TiO₂ is a reducible oxide and gets reduced as lattice oxygen species are used in the ODH reaction. Replacement of new oxygen species at the active sites is needed to reoxidate the cation. Adsorption of gaseous O₂ will go through a peroxide formation, that can explain the higher catalytic activity of anatase TiO₂, but to gain more prove for this mechanism further research will be done. To optimize TiO₂ as a catalyst, acidic groups were incorporated in its structure. However, this seemed to decrease its performance: in fact, acidity promotes cracking and leads to a very low selectivity. Moreover, isolated TiO₂ particles by using

SiO₂ as support increased the surface area and therefore an increase of intrinsic activity was shown.

High percentage of SiO₂ (20wt%:80wt%) performed best with a yield of 34% per mmol TiO₂, however further research should be done to optimize the Ti:Si ratio.

2.3.4 Experimental section

Materials and Instrumentation. All reactions were carried out in an automated six-flow parallel reactor system, with six quartz tube reactors. The gas feed flow rate and the composition of each catalyst bed can be selected independently, whereas the gas feed composition and the temperature are the same for all six reactors. A back-pressure regulator maintains the feed pressure to the six distributing mass-flow controllers of the individual reactors. A selection valve sequentially selects the product mixture of each reactor and sends it for analysis to a gas chromatograph (Interscience microGC, with FID and TCD) and a quadrupole mass spectrometer (Granville Phillips, Brooks Automation). For structural analysis X-Ray Diffraction (XRD) was used (Miniflex II diffractometer, using Ni-filtered Cu K α radiation). The X-ray tube was operated at 30 kV and 15 mA. The samples were recorded with 2.0 ° (2 θ) steps over a 10-90 ° angular range with a scan rate of 0.025. Temperature programmed reduction measurements (TPR) were done on a Thermo TPDRO 1100 instrument using a thermal conductivity detector (TCD). The samples (0.25 mg) were measured under 5% H₂ in a N₂ flow of 20 ml/min, heating at 5 K/min from 30 to 900 °C. Specific surface areas were measured with the BET method, using a N₂ at 77 K on a Thermo Scientific Surfer instrument. Samples were dried in vacuum (1x10⁻³ mbar) for 3 h at 200 °C prior to the measurement.

Procedure Catalyst Preparation. Unless it is noted, all chemicals were purchased from commercial companies. TiO₂ powder was purchased from Hombikat, Janssen Chimica and Johnson Matthey. The powders were used without calcination, calcination at 550 °C (for 5 h) and calcination at 900 °C (for 5 h). It will be noted when which TiO₂ was used. Additionally, other samples of modified TiO₂ were tested.

Synthesis of Anatase TiO₂ Nanopowder. Titanium isopropoxide (8.2 ml, 27.69 mmol) was diluted in ethanol (40 ml). A mixture of ethanol and water (30 ml/30 ml) was drop wisely added as well as 9 drops of nitric acid (65 wt%). It was heated to 70 °C, a white solution was formed which aged in air for 72 hours after which it was dried in the oven at 120 °C (12 h). Two calcinations were done, one of 300 °C (6 h) and one of 550 °C (6 h).

Synthesis of Anatase Titania-silica Composite Nanoparticles. Two different titania-silica samples were made; one of the ratio Ti:Si 20 wt%:80 wt% and Ti:Si 50 wt%:50 wt%. Nitric acid (55 ml, 2 M) was heated to 50 °C to which TEOS (tetra ethoxysilica) (11.2 ml, 0.0499 mol) and respectively (44.6 ml/0.1996 mol) was added. A white fluid formed and TB (titanium butoxide) (17 ml, 0.0499 mol) was added within half an hour. After stirring for 1.5 hour the 20:80 solution formed a gel and turned from yellow to orange. To the 50:50 solution an extra 6 ml TEOS was added after which a gel was formed as well. Adding an extra 6 ml gave titania silica nanoparticles a ratio of 40 wt%:60 wt%. The gels were put in the oven at 50 °C for 24 hours and dried at 120 °C for 12 hours. Both samples were calcinated at 400 °C (2 h).

Synthesis of Titaniumpyrophosphate / Titaniumoxide Sulfate / Magnesium Titanite. Six samples were prepared; two of titanium pyrophosphate (TiP₂O₇), titanium oxide sulfate (TiOSO₄) and magnesium titanite (TiMgO₃). Different volumes of phosphoric acid, sulfuric acid and magnesium nitrate were added. For each sample a 1 M solution was prepared. Magnesium nitrate (1 M) was prepared with nitric acid (2.5 ml, 2 M) and magnesium oxide (0.1 g). Of every 1 M solution 12.25 mL and 24.50 mL was added to TiO₂ (1 g, Hombikat). This corresponded to 1 'poisoning' group per 2 nm² (2.45%) and respectively 1 group per 1 nm² (4.9%). Stirring at 80 °C a white slurry formed which was dried in air for 72 hours after which it was dried at 120 °C for 20 hours. All samples were calcinated at 700 °C (2.5 h), with the exception of titanium pyrophosphate, of which another sample was calcinated at 400 °C as well.

Procedure Catalytic Experiments. Each reactor was loaded with 100 mg catalyst, additionally anatase TiO₂ (Hombikat) tests had reactors loaded with 100 mg up to 500

mg catalyst. All the samples were pelleted and prepared with a size of 300-400 μm . Reaction Temperature varied between 550 and 650 $^{\circ}\text{C}$, with the exception of TiP_2O_7 tests where lower temperatures (400 to 500 $^{\circ}\text{C}$) were applied as well. Total reaction feed of 50 ml/min was passed through each reactor. Argon was used as a carrier gas. The volumetric ratio of O_2 :butane varied between 0.125:1.0 up to 2.0:1.0.

2.4 Non-oxidative dehydrogenation of butane to 1,3-butadiene

2.4.1 Introduction

As already mentioned (**Chapter 2.3.1**), catalytic dehydrogenation of C2-C5 alkanes offers an attractive alternative for the synthesis of olefins because it utilizes low-cost reactants and can be carried out with high selectivity.⁵² Several types of catalysts are used for ODH of hydrocarbons.⁵³ Noble metal-based catalysts are used for the dehydrogenation reactions⁵⁴ owing to their C-H activation abilities. However, noble metals are also highly active, causing undesired combustion of hydrocarbons into CO_x, significantly decreasing selectivity. Moreover, they deactivate fast during the reaction. These problems may be avoided by modifying the nature of the metallic catalysts.

Platinum is known to be the most effective transition metal for dehydrogenation of light alkanes.⁵⁵ However, in the absence of a promoting element, platinum catalysts exhibit low alkene selectivity and deactivate rapidly due to coke formation.⁵⁶ Here, the Pt-based catalyst are modified by adding a second element (Fe, In, Zn, Ga, and Sn). The catalysts are prepared by wet impregnation on γ -Al₂O₃ support. The loadings of Pt and the second metal were 1wt% each. Their dehydrogenation activities and stabilities are compared with that of Pt/Al₂O₃.

2.4.2 Results and discussion

We tested all catalysts under the same dehydrogenation conditions (100 mg of catalyst, 600 °C, H₂:Bu = 2:1, total flow = 50 ml/min). Pt/Al₂O₃ showed good performance: 31% butanes conversion with 50% selectivity for C₄H₈ products (**Figure 19**). However, the catalyst deactivated fastly during the first hour of reaction by coke deposition.⁵⁷ After the first reaction cycle, the catalyst was regenerated under O₂ flow, reduced and used in further reactions. Nevertheless, we observed significant decrease in butanes conversion in the 2nd cycle of reaction (**Figure 20**). Bimetallic

catalysts were tested using the same reaction conditions. In **Figure 21** their activity at the initial state (10 min) is reported.

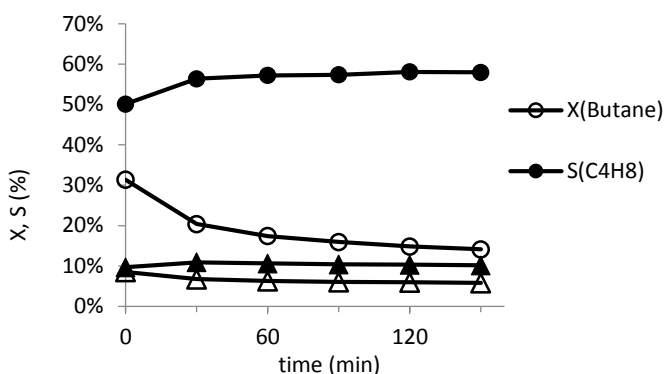


Figure 19 Butane conversion and products selectivity obtained with the Pt/Al₂O₃ catalyst at 600 °C.

Flow rate = 50 ml/min, reaction time = 3 h, H₂:butane ratio = 2:1.

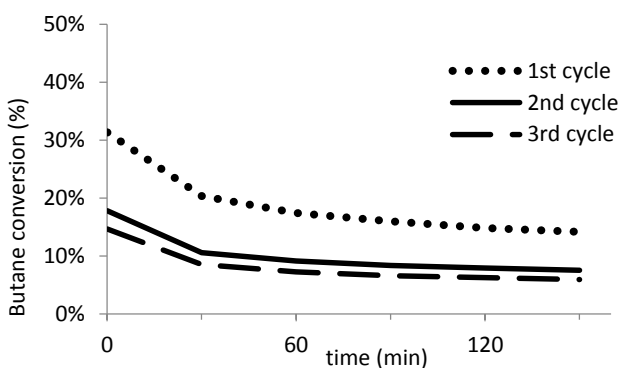


Figure 20 Butane conversion in the first three cycles. Reaction conditions: T = 600 °C, flow rate = 50 ml/min, H₂:butane ratio = 2:1.

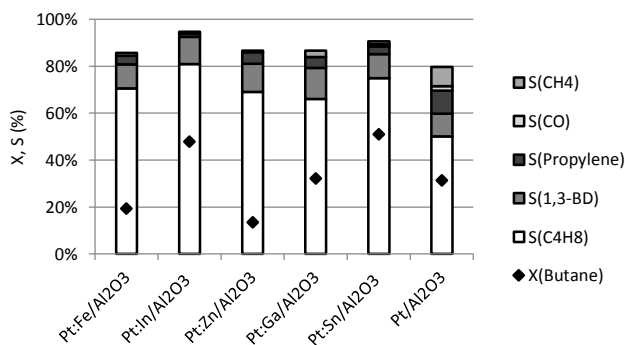


Figure 21 Performance of the Pt-based catalysts at the initial state of the reaction (10 min) at 600 °C, flow rate = 50 ml/min, H₂:butane ratio = 2:1.

Since it is a gas phase reaction, the surface area can determine different catalytic activities as it can influence the adsorption of the gas reagents on the catalyst. In this case, all the catalyst showed different activity, but this behavior can not be ascribed to the different surface area, because, as showed in **Table 10**, their surface areas and pore volumes are very similar.

Table 10 BET surface area of the various Pt-based catalysts supported on Al₂O₃.

Catalyst	Pt/ Al ₂ O ₃	Fe:Pt/ Al ₂ O ₃	Ga:Pt/ Al ₂ O ₃	In:Pt/ Al ₂ O ₃	Sn:Pt/ Al ₂ O ₃	Zn:Pt/ Al ₂ O ₃
BET S.A. (m ² /g)	220	211	209	221	198	176
Pore volume (cm ³ /g)	0.7	0.6	0.7	0.7	0.6	0.6

Both PtFe/Al₂O₃ and PtZn/Al₂O₃, even if butenes selectivity is better than the one obtained with Pt/Al₂O₃, gave the lowest butane conversion (19 and 14% respectively). Using PtGa/Al₂O₃ the same conversion of Pt/Al₂O₃ was reached (32%); moreover, the selectivity was increased and less amount of by-products (propylene, methane and CO) were obtained. The best catalysts in term of conversion and selectivity were PtIn/Al₂O₃ and PtSn/Al₂O₃. In particular, with the first one 48% conversion, 81% C₄H₈ selectivity and 12% 1,3-BD selectivity was observed with only 2% of by-products. On the contrary, with PtSn/Al₂O₃ similar and good conversion and selectivity were obtained (51, 75 and 10%), but more amount of by-products were produced (6%).

The most important aspect to be studied was the possibility of recycling the used catalysts, since Pt/Al₂O₃ showed a significant decrease in butane conversion in the subsequent cycles (from 31 to 15% after only three cycles). So all the used catalysts were regenerated under O₂ flow at 500 °C for 3 h, reduced under H₂ flow at 500 °C for 3 h and finally reused for another cycle of reaction at 600 °C for 3 h. The results are reported in **Figure 22**.

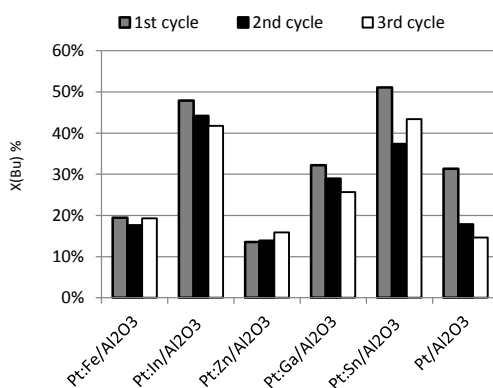


Figure 22 Butane conversion in the first three cycles using all the different Pt-based catalysts prepared.

Reaction conditions: T = 600 °C, flow rate = 50 ml/min, H₂:butane ratio = 2:1.

With all the bimetallic catalysts prepared, the conversion obtained in the 2nd and 3rd cycle is nearly the same of that obtained in the 1st reaction. Considering both butanes conversion and selectivity of the obtained products, the best catalysts were PtSn/Al₂O₃ and PtIn/Al₂O₃. Therefore, further studies were done only by using these two catalysts.

At first, the stability of the catalysts during time was studied. However, despite the use of H₂ flow during the reaction, for all the catalysts a deactivation was observed, probably due to coke deposition on the catalyst itself (**Figure 23**).

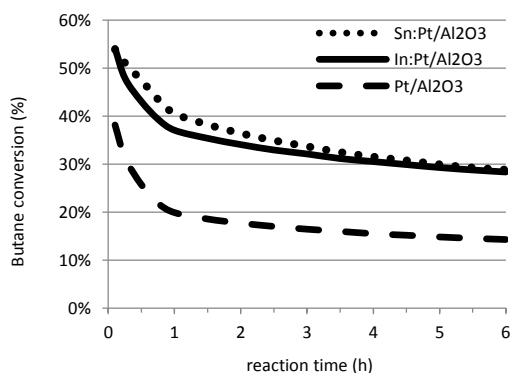


Figure 23 Time on stream activity of bimetallic catalysts for non-ODH. Reaction conditions: T = 600 °C, flow rate = 50 ml/min, H₂:butane ratio = 2:1.

To better understand and compare the performance of different catalysts, it is necessary to compare the selectivity obtained at the same conversion level. So, reaction conditions were changed, such as temperature and catalyst amount, in order to obtain different conversion values. The graph ‘selectivity VS conversion’ (**Figure 24**) shows that the worst results were obtained with the only-Pt catalyst. Moreover, with this catalyst the maximum conversion obtained is only 30%.

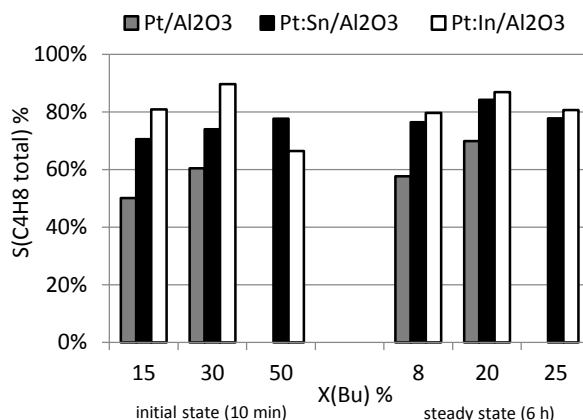


Figure 24 Compared activity of Pt/Al₂O₃, PtSn/Al₂O₃ and PtIn/Al₂O₃ at the same conversion value.

The addition of Sn or In led to better results: the activity of these catalysts is practically the same at the steady state when a stability is reached; while at the very beginning of the reaction the In-catalyst showed slightly better selectivity values.

Then, the influence of the relative amount of the 2nd element and the amount of Pt was studied (**Figure 25**).

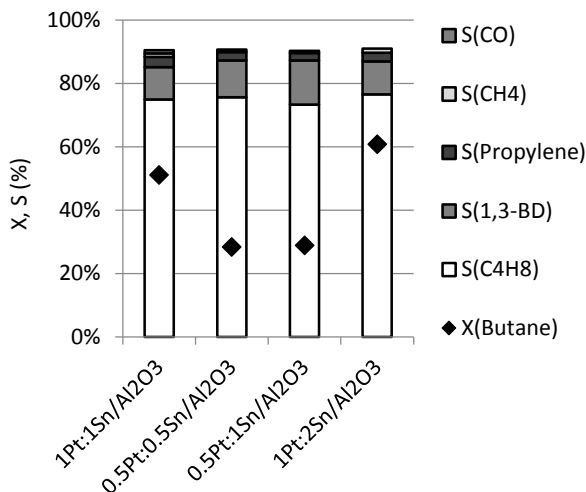


Figure 25 Performance with different Pt/Sn ratio and total amount. Reaction conditions: T = 600 °C, Flow rate = 50 ml/min, H₂:butane ratio = 2:1.

By decreasing the amount of Pt, also the conversion decreased, because Pt is the real active species, while the relative amount of Sn doesn't have any influence on the conversion. Moreover, when the reaction was carried out by using support Al₂O₃, a sample with only Sn (1%Sn/Al₂O₃) or by carrying out the process in the absence of catalyst, no butane conversion was observed.

Why bimetallic catalysts are better than Pt/Al₂O₃? The Pt amount, the catalytically active metal, is the same and, as already mentioned, the surface areas are very similar. Therefore, further characterization were done to understand the different catalytic behavior.

The XRD spectra are practically identical to that of the support because the metal amount is too small to be revealed. On the contrary, the TPR of fresh catalysts in their oxidized and reduced state showed interesting results (**Figure 26**).

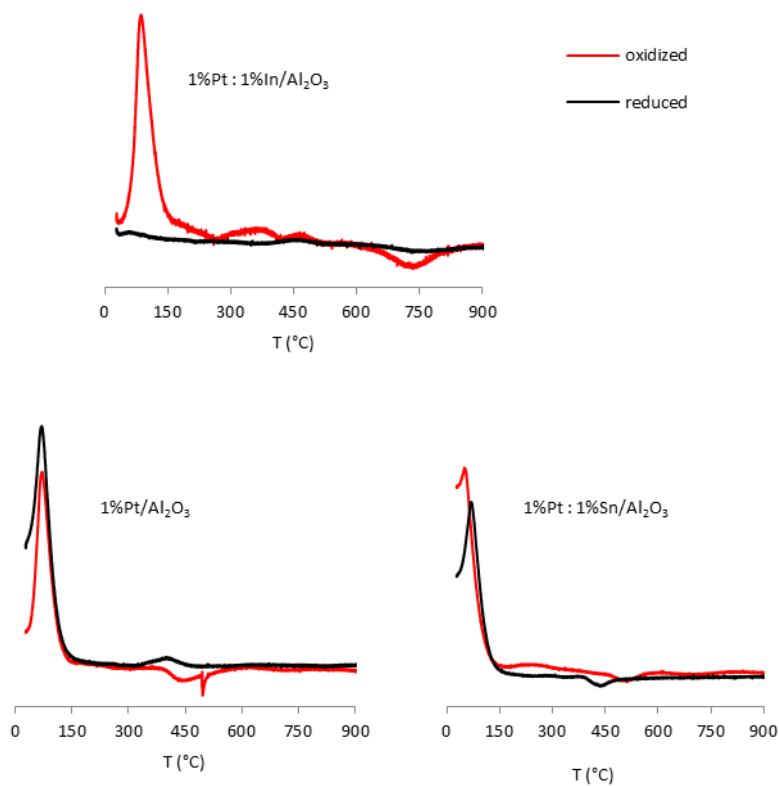


Figure 26 TPR curves of Pt/Al₂O₃, PtIn/Al₂O₃ and PtSn/Al₂O₃ in their oxidized and reduced states.

As expected, the three oxidized catalysts show a peak that corresponds to the reduction of Pt. After reduction, PtIn/Al₂O₃ doesn't present any reduction peak because all metal particles were already in the reduced state. This means that In favours Pt reduction and so the regeneration and recycle of the catalyst itself. We expected to obtain the same result collecting the TPR curve of Pt/Al₂O₃ and PtSn/Al₂O₃ in their reduced form. Surprisingly, they both showed a reduction peak, probably because the Pt reduction is not as favourable as in the presence of In. However, PtSn and PtIn catalyst showed the same result, so that the role of the second metal probably is not linked only to Pt reduction.

In order to get further information, XPS analysis was done on the 1%Pt:1%Sn/Al₂O₃ sample in four different states (**Figure 27**):

- Fresh: catalyst after calcination;
- Reduced: catalysts after H₂ pre-treatment;

- React 5 min: catalysts after 5 minutes of reaction;
- Deactivated: catalyst after 6 hours reaction, when the steady state is reached.

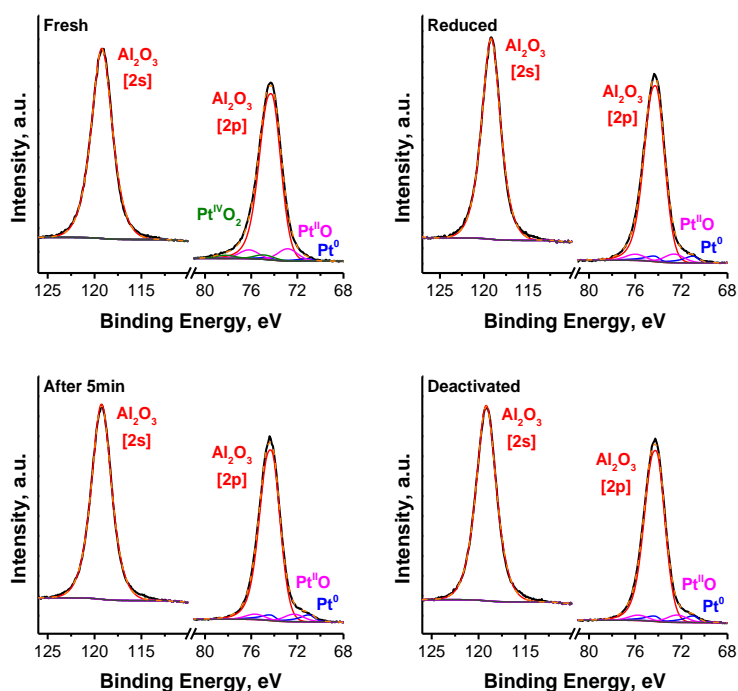


Figure 27 XPS spectra for PtSn/Al₂O₃ in four different states: fresh, reduced, used 5 min, and deactivated catalyst.

From the XPS measurements it came out that Pt is present in different oxidation states depending on the state of the catalyst itself. After calcination at 550 °C for 5 h Pt is main present in its oxidized form, both Pt(II) (64%) and Pt(IV) (23%), while there is only the 13% of Pt(0). After the pre-treatment under H₂ flow at 500 °C for 3 h, Pt is reduced so that Pt(IV) is completely absent and the amount of Pt(II) and Pt(0) is 56 and 44% respectively. During the reaction, no oxidation of the catalyst is observed, due to the H₂ flow used to limit the deactivation of the catalyst itself. This is confirmed by XPS analysis that revealed, on the deactivated catalyst, 48% of Pt(0), 52% of Pt(II) and 0% of Pt(IV). On the contrary, for Sn particles no significant changes are observed. This is a further evidence that the real catalytic specie is Pt.

By analyzing all the results obtained, we can suggest that the role of the 2nd element is probably to prevent the formation of Pt agglomerates (**Figure 28**).

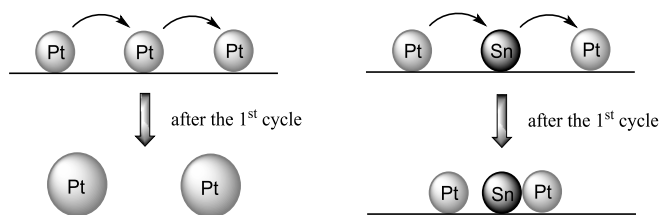


Figure 28 Hypothesis of the metal particles behavior during the catalytic reaction.

Since the catalyst is prepared by impregnation methodology, the metal particles are not inside the structure, but on the surface of the support. For this reason, the high temperature and the flow used during the reaction can allow the catalyst particles to move on the surface of the support. Particles of the same metal can agglomerate in bigger particles when they meet each other. So, the presence of a 2nd different element prevents the formation of bigger Pt particles and in this way the decreasing of the number of catalytic active sites and the changing of their distribution on the solid support, maintaining the catalyst activity unchanged during further reaction cycles.

2.4.3 Conclusions

The catalytic butane dehydrogenation with Pt-based catalysts was investigated. Bimetallic systems were synthesized by wetness impregnation and their catalytic activity was tested in a six-flow parallel reactor, coupled with an online fast GC and a MS. The addition of a 2nd metal particle (In, Sn, Fe, Zn or Ga) has the scope to improve the catalytic activity of the monometallic system Pt/Al₂O₃ and this was further investigated with analytic techniques such as XPS, TPR, and XRD. The best results were obtained with PtSn/Al₂O₃ catalyst that leads to 51% butane conversion and 75% butene selectivity. This improvement is probably due an inhibition of the diffusion of Pt particles on the surface thanks to the presence of the 2nd metal, preventing the formation of bigger metal particles and preserving thereby the catalytic activity of the material.

2.4.4 Experimental section

Catalysts preparation. The monometallic Pt catalyst supported on γ -Al₂O₃ (1wt%Pt/Al₂O₃) was prepared by wetness impregnation: a solution of 60 mg of Pt(NH₃)₄(NO₃)₂ in 1.8 ml of water was added to 3 g of Al₂O₃. The mixture was stirred with a glass stirring rod until it became as homogeneous as possible. Then the catalyst was dried at 120°C for 5 hours and calcined at 550°C for 5 hours.

The bimetallic catalysts were prepared by wetness co-impregnation, using the precursors showed in **Table 11**: a solution of precursor A in 0,9 ml of water was added to a solution of precursor B in 0.9 ml of water. The resulting mixture was added to 3 g of Al₂O₃. The catalysts were then dried at 120°C for 5 hours and calcined at 550°C for 5 hours.

Table 11 Precursors used to synthesize the bimetallic catalysts.

Catalyst	Precursor A	mg A	Precursor B	mg B
1% Pt : 1% Fe	Pt(NH ₃) ₄ (NO ₃) ₂	60	Fe(III)(NO ₃) ₃ *9H ₂ O	217
1% Pt : 1% Ga	Pt(NH ₃) ₄ (NO ₃) ₂	60	Ga(NO ₃) ₃ *xH ₂ O	110
1% Pt : 1% In	Pt(NH ₃) ₄ (NO ₃) ₂	60	In(NO ₃) ₃ *xH ₂ O	79
1% Pt : 1% Sn	Pt(NH ₃) ₄ (NO ₃) ₂	60	SnCl ₂ *2H ₂ O	57
1% Pt : 1% Zn	Pt(NH ₃) ₄ (NO ₃) ₂	60	Zn(NO ₃) ₂ *xH ₂ O	87
0.5% Pt : 0.5% Sn	Pt(NH ₃) ₄ (NO ₃) ₂	30	SnCl ₂ *2H ₂ O	29
0.5% Pt : 1% Sn	Pt(NH ₃) ₄ (NO ₃) ₂	30	SnCl ₂ *2H ₂ O	57
1% Pt : 2% Sn	Pt(NH ₃) ₄ (NO ₃) ₂	60	SnCl ₂ *2H ₂ O	114

Catalysts characterization. Surface area measurements were done using a N₂ at 77 K on a Thermo Scientific Surfer instrument. Samples were dried in vacuum (1x10⁻³ mbar) for 3 h at 200°C prior to the measurement. Powder X-ray diffractograms were obtained on a Miniflex II diffractometer using Ni-filtered Cu K α radiation. The X-ray tube was operated at 30 kV and 15 mA. Temperature programmed reduction (TPR) measurements were done on a Thermo TPDRO 1100 instrument using a thermal

conductivity detector (TCD). TPR was measured under 5 % H₂ in a N₂ flow (20 ml/min), heating at 5 K/min from 30 until 900 °C.

Butane dehydrogenation. Catalytic activity measurements were carried out in a continuous-flow glass reactor directly connected to a GC (Interscience microGC, with FID and TCD) to analyse the reaction mixture. The reactor was loaded with 100 mg catalyst, which was before pelleted and prepared with a size of 300-400 µm. The catalyst was reduced in situ at 500 °C for 3 h under H₂ flow and then used for the catalytic dehydrogenation of butane, performed at 600 °C, using a H₂:Bu ratio about 2:1 and a total flow of 50 ml/min.

3. Supported sulfonic acids

3.1 General introduction

In the last years, many methods have been developed for the transformation of homogeneous catalysts into recyclable heterogeneous ones. In fact, the heterogenization of a catalyst permits to maintain the advantages of the homogeneous catalysis and to avoid the disadvantages. To achieve this goal the catalyst can be either impregnated on to a solid support or chemically bonded to an organic or inorganic support. Many methods have been used for the transformation of many homogeneous catalysts.

The most used are are:⁵⁸

- steric hinderance-occlusion in porous systems (“ship-in-a-bottle”): the host-guest interaction is neither covalent nor ionic. The active catalyst is retained in the matrix by restrictive pore openings and will, in principle, keep all properties of the homogeneous complex in addition to the advantages offered by the heterogeneous system.
- impregnation: one or more catalytically active compounds are impregnated on supporting carrier materials. This method can be chosen to immobilise acids and bases as well as salts, oxides or complexes. The major drawback is leaching of one or more component that leads to irreversible deactivation of the catalyst.
- covalent bond: the immobilisation of organic molecules on inorganic supports by the creation of a chemical bond. This stable bond prevents leaching of the anchored moiety, aspect that makes this method the most suitable for the heterogenization of a catalyst. For this reason it was selected for the synthesis of the catalysts of which activity will be discussed in the next sections. In particular, it was used the tethering method, that consists in the introduction of a suitable linker between the catalyst and the support. This helps the stability of the catalyst itself, but it can also affect the catalytic properties of the active component.

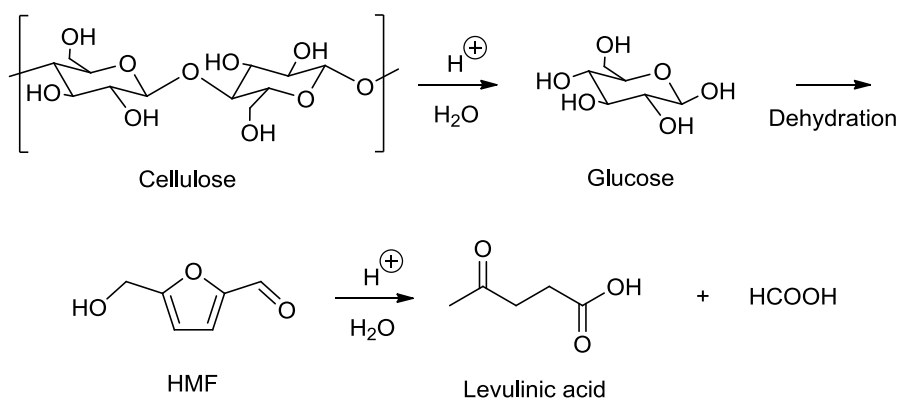
However, the creation of the ideal supported catalyst is far to be accomplished and indeed many problems related to this technology have to be overcome. First of

all, the heterogenization procedure usually causes a decrease in both selectivity and activity of the catalyst: in fact the solid support determines limited diffusion of reactants to the active site and this results in lower reaction rates. The possible lower selectivity too, which often represents a drawback of the heterogeneous system, has to be ascribed to the matrix effect. With its chemical and physical properties the support surface in close proximity of the anchored catalytic site can influence the extent of the reaction and determine lower selectivity. Anyway, with a careful catalyst design and an appropriate support choice based on reaction conditions (solvent, temperature, reactants, ...) it is possible to overcome these drawbacks.

3.2 Levulinic acid esterification

3.2.1 Introduction

In the last ten years the interest in biomass conversion in industrial companies has increased very much, mainly because biomass conversion provides a renewable source of carbon, which can substitute fossil feedstocks.⁵⁹ From lingo-cellulosic biomass it is possible to extract levulinic acid (LA) (**Scheme 4**),⁶⁰ which is an important chemical platform. In fact, it is a versatile building block for chemicals and materials.⁶¹



Scheme 4 Scheme for the dehydration of lingo-cellulosic derived sugars into levulinic acid.

Levulinic acid offers one of the largest families of value-added derivatives. These include (**Figure 29**):

- Gamma-valerolactone (GVL)
- Methyltetrahydrofuran (MeTHF)
- Methyl Butanediol (MeBDO)
- Alpha-methylene-gamma-valerolactone (alpha-mGVL)
- Delta-amino levulinic acid (DALA)
- Levulinic acid esters (LA-esters)
- Diphenolic acid (DPA)

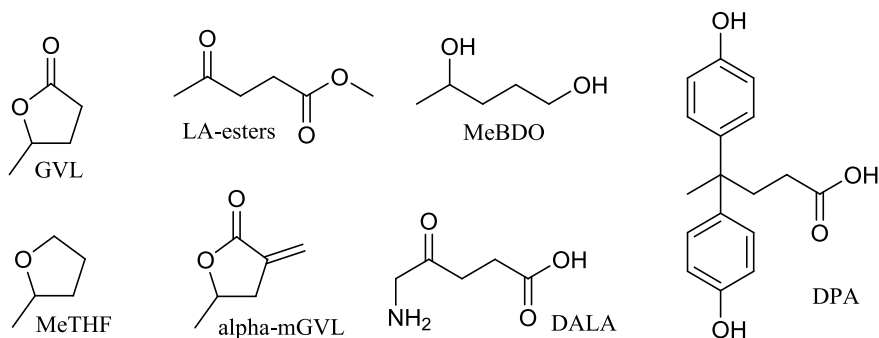


Figure 29 Scheme of the principal derivatives of levulinic acid.

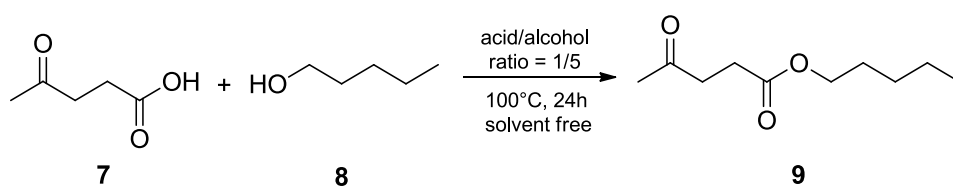
Levulinic acid esters are sold today as niche fruity flavor and fragrance ingredients. Ethyl levulinate is a potential replacement for valencene, a flavor currently extracted from oranges and used in most beverages. The increasing demand for green solvents has put levulinic acid esters on the agenda of many chemical companies. Because other ester solvents, e.g. ethyl acetate, are known to be harmful for humans and the environment, levulinic acid esters are a great cost-competitive alternative. Ethyl levulinate has been also tested as an additive for transportation fuels to improve emissions of nitrogen oxides in high compression diesel engines.⁶²

Due to their importance, new strategies have been developed for the production of these derivative compounds.⁶³ In earlier studies, levulinate esters were mainly produced from LA in the presence of mineral acids, which leads to a high yield of corresponding products.⁶⁴ However, some drawbacks were exposed, such as catalyst recycling, product separation, environmental problems, and reaction conditions. Consequently, the development of green, efficient, and recyclable solid acid catalysts is welcome. The commonly used solid acids include heteropolyacids, sulfated metal oxides (such as $\text{SO}_4^{2-}/\text{TiO}_2$ and $\text{SO}_4^{2-}/\text{ZrO}_2$), zeolite molecular sieves, hydrotalcite-like compounds, and so on.⁶⁵ The merits of these catalysts are the easy recovery, high activity and easy activation, which provide a real basis for wide application in acid-catalyzed reactions. Nevertheless, the conditions reported do not represent an ideal green process: in fact, a huge excess of alcohol is often used, together with high temperatures and long reaction times. Here we present an alternative strategy in which

the heterogeneous catalyst selected represents the key to improve the eco compatibility for the synthesis of levulinic acid esters.

3.2.2 Results and discussion

In this experiment the influence of different kind of Lewis and Bronsted solid acid catalysts on the reaction between an alcohol and levulinic acid to form the corresponding ester was tested.



Scheme 5 Scheme of the esterification of levulinic acid with pentanol.

The reaction was carried out using the condition usually reported in literature: 100 °C, 24 h, levulinic acid/alcohol ratio = 1/5 and solvent free conditions (or, better, the use of the alcohol as solvent-reagent). 1-Pentanol was selected as model alcohol in order to be able to work at high temperatures. Results are reported in **Table 12**.

Table 12 Activity of different solid acid catalyst in the esterification reaction of levulinic acid.

Entry	Catalyst	Catalyst acidity	Acid Conversion (%)	Ester Yield (%)	Ester Selectivity (%)
1 ^[a]	ZrO(OH) ₂ / calc. 300°C		60	58	97
2 ^[a]	ZrO(OH) ₂ / calc. 500°C		78	76	98
3 ^[a]	ZrO(OH) ₂ / calc. 700°C		61	56	92
4 ^[a]	Zeolite MFI		54	53	98
5 ^[a]	Zeolite HSZ		45	43	96
6 ^[b]	SiO ₂ -(CH ₂) ₃ -SO ₃ H	0.51 mmolH ⁺ /g	96	94	98
7 ^[c]	Aquivion supported on silica	0.012 mmolH ⁺ /g	98	88	88

[a]: cat = 10% wt / mmol levulinic acid
[b]: cat = 1% H⁺ / mmol levulinic acid
[c]: cat = 0.01% H⁺ / mmol levulinic acid

Bronsted acid catalysts did not result the most suitable for this kind of reaction: zeolites HSZ and MFI presented the worst levulinic acid conversion values, only 54 and 45% respectively. With ZrO(OH)₂ the activity was better, but the conversion still not complete. Silica supported sulfonic acid (**entry 6**) showed the highest catalytic activity with 96% levulinic acid conversion reached in only 2 h reaction and almost total selectivity.

Then the reagents ratio was evaluated (**Table 13**).

Table 13 Results obtained by using different amount of alcohol.

Entry	Acid/alcohol ratio	Acid Conversion (%)	Ester Yiled (%)	Ester Selectivity (%)
1	1/5	96	94	98
2	1/2	95	93	98
3	1/1	96	94	98

All the reactions were carried out at 100 °C and monitored for 2 h. By varying the amount of alcohol, the conversions and the selectivities do not change: this is a very

important result because allows the use of a stoichiometric amount of alcohol, making the process more eco-friendly (less waste is produced) and cheaper.

The reaction conditions were further optimized studying the effect of the temperature. So, a series of experiment were conducted using the sulfonated catalyst (1%), an equimolecular amount of reagents under solvent free conditions, changing the temperature between 50 and 100 °C. Results are reported in **Table 14**.

Table 14 Results obtained by using different reaction temperatures.

Entry	Temperature (°C)	Acid Conversion (%)	Ester Yield (%)	Ester Selectivity (%)
1	100	96	94	98
2	75	95	93	98
3	50	79	77	98

In all cases, the selectivity towards the esterification product is total. The reaction at 50 °C (**entry 3**) was monitored for 24 h: after 7 hours of reaction a maximum was reached (79% conversion and 77% yield), but this result is not better than the one obtain at 75 °C. By increasing the temperature to 100 °C no improvement was obtained.

Finally, other silica supported sulfonic acid were synthesized to check the influence of the linker on the catalytic activity (**Table 15**). For comparison, a commercial Lewis solid acid (Amberlyst 15) was tested.

Table 15 Activity of different solid sulfonic catalysts in the esterification reaction of levulinic acid.

Entry	Sulfonated catalyst	Catalyst acidity (mmol H ⁺ /g)	Acid Conversion (%)	Ester Yield (%)	Ester Selectivity (%)
1	SiO ₂ -(CH ₂) ₃ -SO ₃ H	0.51	95	93	98
2	SiO ₂ -C ₆ H ₄ -SO ₃ H	0.65	92	90	98
3	SiO ₂ -(CH ₂) ₃ OC ₆ H ₄ -SO ₃ H	0.73	94	84	98
4	Amberlyst 15	4.7	52	31	98
5	Aquivion supported on silica	0.012	76	74	98
6 ^[a]	SiO ₂ -(CH ₂) ₃ -SO ₃ H	0.51	96	94	98

[a]: dry conditions

Despite what reported in literature,^{63d} the commercial sulfonic acid Amberlyst 15 (**entry 4**) is not as efficient as the others catalysts tested.

Concerning the supported sulphonic acids, by changing the linker between the silica support and the SO₃H group, the catalytic activity doesn't change. Furthermore, dry conditions were evaluated (**entry 6**): the reaction was carried out using dry 1-pentanol and putting molecular sieves in the round bottom flask in which the reaction was carried out; in this way the water produced during the reaction could be removed and the ester formation favored. However, results obtained in these conditions are identical to what obtained in non-dry conditions, so that all this procedure becomes useless.

The last parameter studied was the catalyst amount (**Table 16**).

Table 16 Results obtained by using different amount of catalyst.

Entry	Catalyst amount	Acid Conversion (%)	Ester Yield (%)	Ester Selectivity (%)
1	5%	95	85	89
2	1%	95	93	98
3	0.1%	36	35	98
4	0.01%	15	14	98

As expected, decreasing the amount of catalyst used, the acid conversion noticeably decreased. Even extending the reaction time to 24 h, only 58 and 38% conversion was obtained with 0.1 and 0.01% catalyst respectively. In any case, the selectivities were very high (98%). On the other hand, using a higher amount of catalyst, the conversion is high but the selectivity of the process worsens.

Moreover, we ensured the heterogeneous role of the catalyst by performing the Sheldon test and monitoring no further conversion on the filtrate.⁶⁶ The recyclability of the catalyst was then evaluated. The catalyst was recovered by filtration, washed with ethyl acetate, dried and reused for a further esterification reaction. Results are reported in **Table 17**.

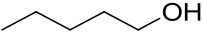
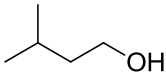
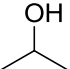
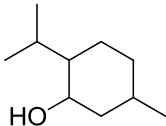
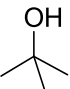
Table 17 Activity of the supported sulfonic acid catalyst in five successive cycles.

Cycle	Acid Conversion (%)	Ester Yield (%)	Ester Selectivity (%)
1 st	95	93	98
2 nd	95	93	98
3 rd	93	91	98
4 th	94	92	98
5 th	92	90	98
6 th	93	91	98

The catalyst can be recovered by filtration and reused at least for 6 cycles, obtaining optimum values of conversion and selectivities.

Finally, the reaction, in the optimized conditions found, was extended to other alcohols.

Table 18 Esterification reaction of levulinic acid with different alcohols.

Entry	Alcohol	Acid Conversion (%)	Ester Yield (%)	Ester Selectivity (%)	Time (h)
1		95	93	98	2
2		80	79	99	5
3		60	59	99	2
4		77	76	99	2
5		0	0	0	24

As expected, the best performances were obtained with the primary alcohols (**entries 1 and 2**), giving 93 and 79% yield respectively. Despite the minor reactivity, very good results are obtained also with secondary alcohols (**entries 3 and 4**, 59 and 76% yield). In particular, it is important to underline that with menthol the chirality of the

reagent is maintained in the product and not altered during the reaction, indicating that the procedure proposed is efficient for the esterification and the mild conditions used permit to preserve the structure of the initial reagents. Unlikely, by using a tertiary alcohol no conversion of levulinic acid is observed (**entry 5**). Finally, in all cases reported the selectivity towards the esterification product is total and this confirms the efficiency of the method.

3.2.3 Conclusions

Silica supported sulfonic acids evidence a higher activity in the esterification of levulinic acid compared with other solid acid catalysts. Esterification can be carried out under mild conditions (100 °C, 2 h) giving excellent yields with various primary and secondary alcohols and total selectivity. Moreover, the selected catalyst allowed the use of stoichiometric amount of reagents, making the process more eco-friendly (less waste is produced) and cheaper. Finally, the recycle of the catalyst was evaluated: the solid material was recovered and reused maintaining the same activity for at least six cycles.

3.2.4 Experimental section

In a stirred batch reactor levulinic acid, petanol and the heterogeneous catalyst were stirred for 24 hours. The acid/alcohol ratio, as well as the reaction temperature and the amount of the catalyst were changed as described in the previous section (**Chapter 3.2.3**) Then the solid catalyst was recovered by filtration and the reaction mixture was analyzed by high resolution capillary GC with a fused silica capillary column SE52 (5% Phenyl, 95% Methyl Polysiloxane, 30m x 25mm). The products were identified by NMR.

3.3 Friedel-Crafts acylation reaction

3.3.1 Introduction

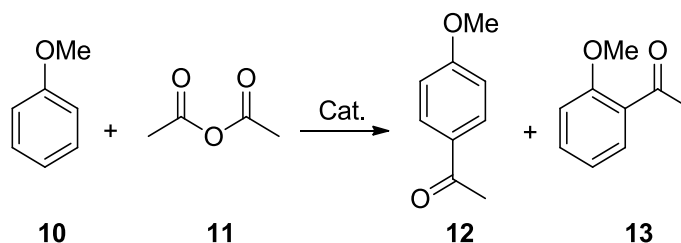
Since the first paper reported by Friedel and Crafts, the acylation of aromatic compounds has undoubtedly become one of the most investigated synthetic reactions.⁶⁷ The considerable practical value of the aromatic ketones pushed indeed a great interest towards the study of electrophilic acylation and the optimization of related synthetic processes.⁶⁸ These products are particularly interesting building blocks for fragrance and pharmaceutical industries.⁶⁹ Electrophilic acylation reactions are usually catalyzed by Lewis acids (ZnCl_2 , AlCl_3 and FeCl_3) or strong protic acids (HF and H_2SO_4). The use of Lewis acids or corrosive mineral acids is however associated with a great number of environmental and economic issues. In most cases, reactions require stoichiometric amounts of catalyst and troublesome work-up procedures. Moreover, these processes ultimately release a huge quantity of anions (especially chlorides) in aqueous medium. For these reasons, during the past decade, the development of more eco-compatible Friedel-Crafts acylation reactions has become a fundamental goal of green chemistry.⁷⁰

Different materials have been studied as heterogeneous catalysts for Friedel-Crafts acylations, including zeolites,⁷¹ metal oxides⁷² and heteropoly acids.⁷³ In recent years this strategy was further developed leading to the design of hybrid organic–inorganic mesoporous silicas functionalized with sulfonic acids, combining therefore the strength of a strong Bronsted acid with the elevated surface area of mesoporous materials.^{74,75,76} The present section reports the evaluation of synthetic aspects of the acylation of anisole with acetic anhydride in order to expand the viability of this catalytic process.

3.3.2 Results and discussion

Four different supported sulfonic acids were prepared, namely silica supported propanesulfonic acid [$\text{SiO}_2\text{-(CH}_2\text{)}_3\text{-SO}_3\text{H}$], MCM-41 supported propanesulfonic acid [$\text{MCM-41-(CH}_2\text{)}_3\text{-SO}_3\text{H}$], silica supported ethylphenylsulfonic acid [$\text{SiO}_2\text{-(CH}_2\text{)}_2\text{-}$

C₆H₄-SO₃H] and silica supported (2-trifluoromethyl)-perfluoroethanesulfonic acid [SiO₂-CF₂-CF-(CF₃)-SO₃H]. The catalytic activity of these materials has been evaluated mixing anisole and acetic anhydride as model reagents for 90 minutes at 120 °C with 10 mol% of the heterogeneous catalyst (**Scheme 6**). Employing a 3:1 acetic anhydride/anisole molar ratio it is possible to obtain the best performances in terms of yield and selectivity toward the desired product (4-methoxyacetophenone, **12**), according to our previous findings.⁷⁷ This reaction leads also to the production of small amount of 2-methoxyacetophenone **13**.



Scheme 6 Acylation of anisole with acetic anhydride.

Results reported in Table 18 show that 4-methoxyacetophenone is the main product of these reactions (**entries 1-4**). The amorphous silica supported propanesulfonic acid is the less active catalyst (15% conversion, 12% yield, **entry 1**) among the solid acids. These findings are in agreement with the hypothesis that the efficiency of the catalyst is proportional to its acidity.^{77,78} Gratifyingly, the MCM-41-(CH₂)₃-SO₃H catalyst allows the formation of desired ketone **3** in 52% yield (**entry 2**). Orderly supported propanesulfonic acids are stronger acids than alkylsulfonic ones synthesized by tethering the active species on silica due to a positive cooperative effect between proximal catalytic sites.⁷⁹ In this case the high surface area of the MCM-41 support may play too an important role. Best catalytic performances were achieved using the silica supported ethylphenylsulfonic acid (73% conversion; 68% yield, **entry 3**) and the silica supported (2-trifluoromethyl)-perfluoroethanesulfonic acid (75% conversion; 71% yield, **entry 4**). We decided to study the scope of the reaction employing the former catalyst instead of the latter as it is cheaper, safer and easier to prepare.

Table 19 Reaction of anisole with acetic anhydride, catalyzed by silica supported sulfonic acids.

Entry	Catalyst	Surface acidity (mmol g ⁻¹)	Surface area (m ² g ⁻¹)	10 Conversion (%)	12 Yield (%) ^[a]
1	SiO ₂ -(CH ₂) ₃ -SO ₃ H	0.51	470	15	12
2	MCM-41-(CH ₂) ₃ -SO ₃ H	2.53	970	60	52
3	SiO ₂ -(CH ₂) ₂ -C ₆ H ₄ -SO ₃ H	1.14	293	73	68
4	SiO ₂ -CF ₂ -CF-(CF ₃)-SO ₃ H	1.85	282	75	71 ^[b]

Reaction conditions: **10** (1.0 mmol), **11** (3.0 mmol), and solid catalyst (10% mol) were stirred at 120°C for 90 minutes;

[a]: Yields were determined by GC analysis of the crude reaction mixture using dodecane as external standard;

[b]: see ref. 77.

Reactions were then performed screening different alkyl anhydrides in order to evaluate the effect of the acylating reagent. These reactions were carried out under mild conditions (100 °C halving the catalyst amount) to better recognize reactivity trends by limiting the conversion of anisole. Reactions were carried out for 1 hour using a 3:1 molar excess of anhydride respect to anisole and 5% mol of SiO₂-(CH₂)₂-(C₆H₄)-SO₃H catalyst. **Figure 30** clearly show that the reactivity of the differently substituted anhydrides with anisole correlates with the length of their alkyl chain.

Both the conversion of anisole and the yield of the aromatic ketone increase together with the number of carbon atoms of the anhydride and best results were observed using valeric anhydride (60% yield and 73% conversion). Then, the reactivity slightly decreases by further increasing the length of the alkyl chains: this behavior may be attributed to a positive hydrophobic effect, which could increase the reactivity up to a certain extent but is eventually outmatched by steric factors.

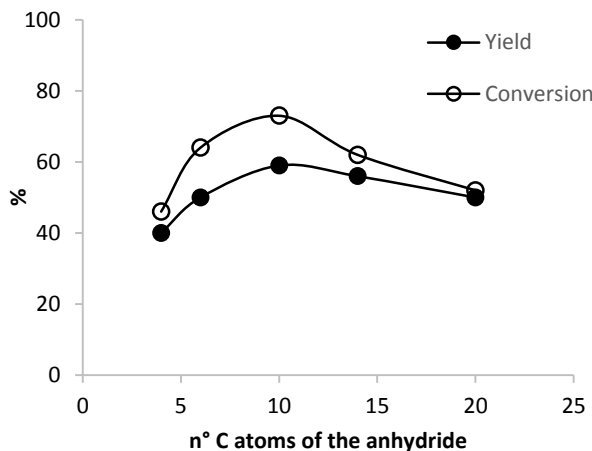
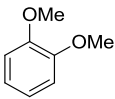
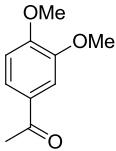
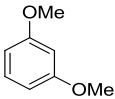
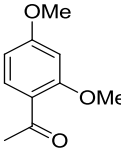
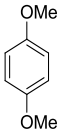
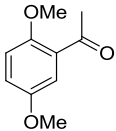
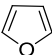
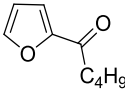
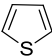
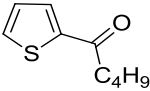
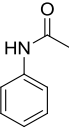
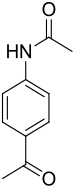


Figure 30 Acylation of anisole with different anhydrides.

We next examined the effect of the aromatic partner. Experimental results reported in **Table 20** confirm the general applicability of this silica-supported catalyst in these acylation reactions. 1,2- and 1,3-dimethoxybenzene (**entries 1 and 2**) gave the desired product in 77% and 75% yield respectively. 1,4-dimethoxybenzene proved less reactive than its regioisomers (**entry 3**, 20% conversion) but displayed remarkable selectivity towards *ortho*-acylation (90%). A lower yield was obtained using acetanilide as substrate (10%, **entry 4**). The slight solubility of acetanilide in acetic anhydride may be responsible for its low reactivity. Electron rich heterocycles, as furane and tiophene, could be efficiently acylated (**entries 4 and 5**). In these cases, reactions could be carried at room temperature, in order to prevent therefore their competitive polymerization. Under these remarkably mild conditions they smoothly react with valeric anhydride, which proved to be a stronger acylating agent than acetic anhydride, delivering mono-substituted products in 50 and 69% yield respectively. These results show the feasibility of the acylation of heteroaromatics by means of a supported sulfonic acid catalyst. We next investigated the possible recycle of the solid catalyst. As mentioned in the introduction, this point represents one of the most complicated issues of heterogeneous Friedel-Crafts acylations as supported (sulfonic) acids usually lose their activity after the first run. It has been proposed that the deactivation of these materials is attributable to the formation of ionic species that strongly interact with the Bronsted sites of the catalyst.⁷⁵

Table 20 Friedel-Crafts acylation of aromatics.

Entry	Substrate	Product	Conv. (%)	Yield (%) ^[a]
1			90	77
2			95	75
3			20	18
4 ^[b]			100	50
5 ^[b]			100	69
6			15	10

Reaction conditions: substrate / acetic anhydride molar ratio 1:3, SiO₂-(CH₂)₂-(C₆H₄)-SO₃H: 5% mol, T = 120 °C, 1.5 h;

[a]: Isolated yield after flash chromatography. Eluent: Hexane / Ethyl Acetate;

[b]: Reaction performed with valeric anhydride, T = 22 °C.

In our case too, while the hot filtration test has excluded both leaching and coexistence of homogeneous catalysis,⁸⁰ the supported sulfonic acid loses its activity after the first use. The presence of adsorbed poisoning compounds was indirectly confirmed by the intense yellow color assumed by the solid acid at the end of the reaction (**Figure 31b**). Several attempts to regenerate the catalyst by washing with various solvents as ethanol, ethyl acetate and water did not provide any positive outcome. The possible

oxidation of the adsorbed compounds with concentrated hydrogen peroxide proved similarly fruitless. Nevertheless we eventually founded a method to restore a certain activity by washing the solid with a 2 N solution of HCl or HNO₃. The catalyst was further washed with distilled water to eliminate traces of mineral acids and subsequently dried at 100 °C for 2 hours. Upon this treatment the catalyst retrieved its original white color (**Figure 31c**) and the catalytic activity was partially restored (~40% yield). While the deactivation of heterogeneous catalysts remains a recurrent problem in Friedel-Crafts acylations, present results may open new chances to address this issue in the future.



Figure 31 a) as prepared catalyst; b) used catalyst; c) recovered catalyst washed with HCl_{aq} 2 N.

3.3.3 Conclusions

Silica supported sulfonic acids evidence a higher activity in acylation reactions compared with other homogeneous and heterogeneous sulfonated acid catalysts. Acylations can be carried out with a variety of anhydrides and aromatics leading to the formation of a variety of aromatic ketones as shown by GC measurements. The present findings could be considered to be promising for the development of novel catalysts able to reach even higher yield and selectivity values and afford pure compounds intermediates.

3.3.4 Experimental Section

General All the reagents were used as received without further purifications. Solvents were distilled under nitrogen and dried before use. Before functionalization the siliceous supports were dried at 300 °C for 5 hours. The amorphous silica used was the commercial Kieselgel 60 (KG-60) purchased from Merck. Gas-chromatographic analyses were accomplished on a Trace GC Thermo Finnigan instrument with a fused silica capillary column SPB-20 from Supelco (30 m x 0.25 mm). N₂ adsorption-desorption isotherms, obtained at 77 K on a Micromeritics PulseChemiSorb 2705, were used to determine specific surface areas (S.A.BET). Before each measurement the samples were outgassed at 383 K for 1 h.

Silica supported propanesulfonic acid⁷⁵ Amorphous silica (8 g) has been refluxed with 4-hydroxy-1-butanesulfonic acid β -sultone (1.8 ml; 15 mmol) under stirring for 6 hours in toluene (120 ml). The resulting solid was then filtered off and washed with toluene (3 x 20 ml) and acetone (3 x 20 ml).

MCM-41 supported propanesulfonic acid⁷⁶ C16TACl solution in water (20.9 ml; 25 wt%) was added to a solution of NH₄OH (31.7 ml; 30 wt%) and the mixture was stirred for 30 min in a closed polyethylene bottle. A mixture of bis[3-(triethoxysilyl)propyl]tetrasulfide (TESPT) (1.49 ml; 3.0 mmol) and tetraethyl orthosilicate (TEOS) (3.12 ml; 13.4 mmol) was slowly added to the base/surfactant solution kept under gentle stirring. Stirring was maintained for 30 min and resulting solutions were then aged at 80°C for 4 days in their closed polyethylene bottle. The resulting white powder was collected by filtration, washed thoroughly with water and air-dried under ambient conditions. The solid material (2.5 g) was then stirred for 48 h in a refluxing solution of concentrated HCl (37 wt%, 10 g) and methanol (70 g) to remove the surfactant. To exchange the ion of the surfactant, the sample was stirred in a refluxing solution of NaCl (1 g) in ethanol (100 g). The solid material was filtered off, washed with water (3 x 50 ml), methanol (3 x 25 ml) and ethyl acetate (2 x 25 ml). The solvent-extracted sample (2.5 g) was kept under vacuum at 150 °C for 2 days and then treated in refluxing CH₂Cl₂ (150 ml) with Br₂ (1.3 mL; 25 mmol) for 4 h.

The product was isolated on a Buchner funnel and washed with dichloromethane (3 X 25 ml).

Silica supported ethylphenylsulfonic acid⁸¹ Amorphous silica (8.0 g) was refluxed under stirring for 24 hours with trimethoxy(2-phenylethyl)silane (1.8 ml; 8.3 mmol) in toluene (120 ml), filtered and washed with toluene. The supported phenyl group was sulfonated by refluxing the functionalized material with chlorosulfonic acid (10 ml; 150 mmol) under stirring for 4 hours in 1,2-dichloroethane (60 ml). The solid material was then recovered by filtration and washed carefully with 1,2-dichloroethane (3 x 20 ml), acetone (3 x 20 ml) and water (3 x 50 ml).

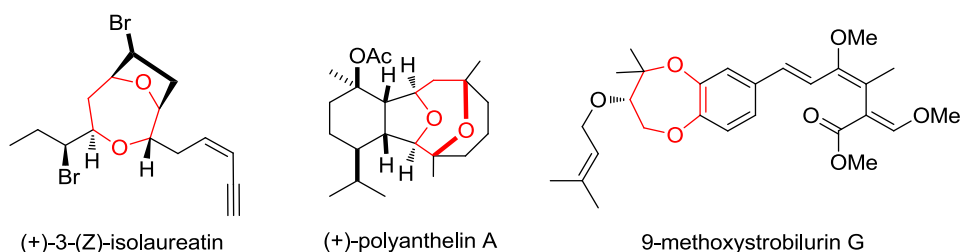
Silica supported (2-trifluoromethyl)-perfluoroethanesulfonic acid⁷⁵ Amorphous silica (8 g) has been refluxed with 1,2,2-trifluoro-2-hydroxy-1-(trifluoromethyl) ethanesulfonic acid β -sultone (3,45 g; 15 mmol) under stirring for 6 hours in toluene (120 ml). The solid was then filtered off and washed with toluene (3 x 20 ml) and acetone (3 x 20 ml). The surface acidity and surface area of all catalysts presented in **Table 18** were determined by a reported titration method⁸² and B.E.T. method respectively.

General procedure for acylation reactions Anisole (1, 0.108 ml, 1.0 mmol) was added under stirring at room temperature to a mixture of acetic anhydride **2** (0.286 ml, 3.0 mmol) and solid catalyst (0.10 mmol). The mixture was then stirred for 90 minutes at 120 °C, diluted with ethanol, filtered and the remaining solid was further washed with ethanol (3 x 5 ml). The filtrate was analyzed by GC using dodecane as external standard.

3.4 Reaction of α,β -Unsaturated Carbonyls with Epoxides

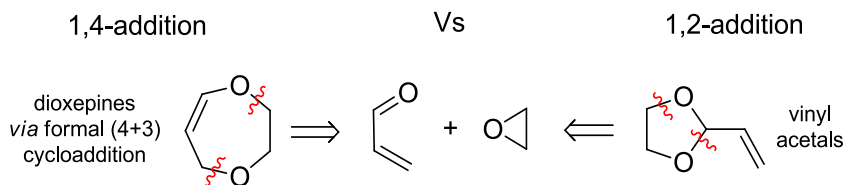
3.4.1 Introduction

Catalytic cycloadditions are a powerful synthetic tool for the straightforward construction of complex polycyclic frameworks from readily available precursors.⁸³ Regarding medium-sized rings, their broad domain of applications pushed the development of a variety of elegant methods to access seven-membered cyclic cores by either a (4 + 3) or a (5 + 2) strategy.⁸³ While extremely efficient protocols exist to form carbocycles, the incorporation of heteroatoms within the ring remains synthetically challenging.⁸⁴ 1,4-Dioxepines are well-known for their biological properties (**Scheme 7**),⁸⁵ and their preparation usually requires substrate prefunctionalization and multistep syntheses, ultimately affecting the panel of readily accessible motifs and the environmental cost of the process.⁸⁶



Scheme 7 1,4-Dioxepine Core in Natural Products.

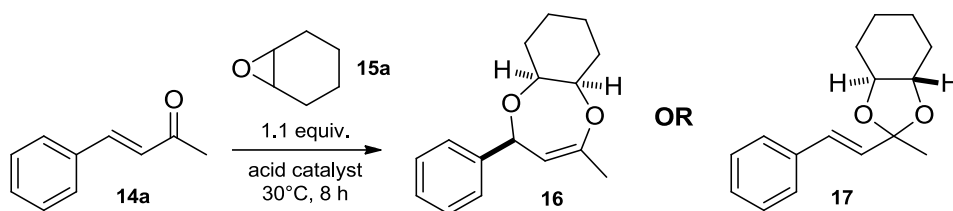
Recently introduced has been the possibility to synthesize these heterocycles by formal cycloaddition between an α,β -unsaturated carbonyl compound and an epoxide in the presence of a Lewis acid as homogeneous catalyst (**Scheme 8**, left).⁸⁷ As part of our ongoing interest toward the development of eco-friendly synthetic processes,⁸⁸ we wished to develop a catalytic synthesis of dioxepines via formal (4 + 3) cycloaddition using heterogeneous acid catalysts. On the basis of our studies, we report herein that products of these reactions are vinyl acetals rather than the originally proposed dioxepines (**Scheme 8**, right).



Scheme 8 Comparison of Possible Outcomes Reacting Epoxides with α,β -Unsaturated Carbonyls.

3.4.2 Results and discussion

As a model reaction, we attempted the synthesis of the reported dioxepine **17**⁸⁷ by stirring 3 mmol of ketone **14a** with 1.1 equiv. of cyclohexene oxide **15a** at 30 °C for 8 h in the presence of a catalytic amount of various solid acids, such as zeolites, clays and supported sulfonic acids (**Scheme 9**).



Scheme 9 1,4- vs 1,2-Addition in the Reaction of Epoxide **15a** with α,β -Unsaturated Ketone **14a**.

Epoxide **15a** was slowly added to the reaction mixture (0.55 mmol/h) to minimize its decomposition under acidic conditions, since in these acidic mediums, the epoxide readily polymerizes already at 30 °C. Upon optimization of reaction parameters, we were then delighted to observe formation of the product described as **17** as a single diastereomer in 68% yield using zeolite HY-360 as catalyst. No reaction took place in the absence of the catalyst, and lower yields were achieved increasing the pace of epoxide addition. The product is relatively sensitive to moisture, slowly decomposing to a mixture of starting ketone and trans-1,2- cyclohexandiol. A comparable selectivity toward the product (62%) was achieved using BF_3 etherate as catalyst.⁸⁷ The heterocycle that we synthesized reproduced all the spectroscopic data reported for dioxepine **17** (^1H and ^{13}C NMR, IR, and MS; **Figure 32** presents relevant captions

of key ^1H and ^{13}C NMR resonances). We were, however, puzzled by the attribution of the surprisingly large coupling constant of 15.9 Hz observed in the ^1H NMR to the interaction between the benzylic and vinylic protons of **17** (highlighted in purple and yellow, respectively), and by the downfield chemical shift of the benzylic carbon (129.0 ppm, purple) and the upfield shift of the quaternary enol (107.2 ppm, cyan). We then decided to model the four possible diastereomers of **17** via DFT and calculate their ^1H and ^{13}C NMR spectra to compare them with experimental ones and thus rationalize the outcome of these reactions.⁸⁹ Optimizations were performed at the M06 level using the IGLO-III basis set, essentially a triple- ζ one especially designed for NMR simulations, and with chloroform as an implicit solvent via the CPCM approach. None of the calculated spectra matched the experimental ones. Regarding the proton NMR, a large coupling constant (15.9 Hz) observed between the benzyl (purple) and the vinyl (yellow) protons suggests a structure with a relatively small dihedral angle among them. However, in all cases, the calculated coupling constants remain below 10 Hz, in striking contrast with the experimental value of 15.9 Hz. Considering the carbon NMR, the calculated resonances of the sp^3 benzylic carbons of **17** are always considerably below 100 ppm (purple, 81.0 ppm for the diastereomer of **Figure 32**), while the quaternary sp^2 enol provided in all cases the most downfielded signal of the whole molecule (cyan, 174.9 ppm for the diastereomer of **Figure 32**).

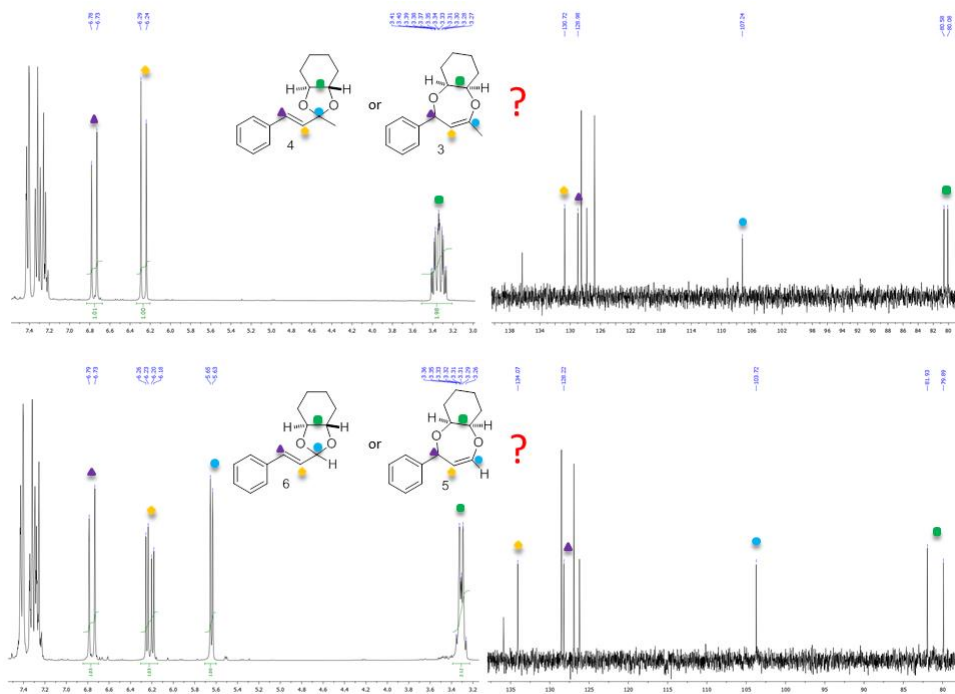
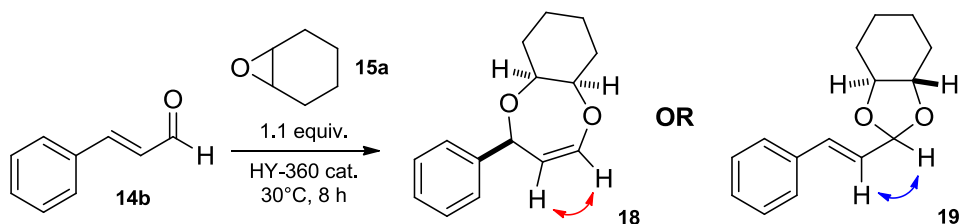


Figure 32 Position of relevant experimental ^1H and ^{13}C resonances of the product between cyclohexene oxide and benzylidenacetone (**16**, **17**, above) and cinnamaldehyde (**18**, **19**, below).

We then considered the structure of acetal **17**, which could, in principle, form in acidic conditions between the epoxide and the carbonyl group of the α,β -unsaturated partner, leaving the C–C double bond untouched. In fact, it is known that in acidic mediums, the reaction of epoxides with saturated ketones and aldehydes delivers the corresponding acetals.⁹⁰ In this case, a clean correlation between calculated and experimental NMR spectra immediately appeared. The trans relation between vinylic protons of the styryl fragment (purple and yellow) evenly matched the experimentally measured large coupling constant among them (calculated $J = 17.0$ Hz). In **17**, the calculated resonance of the benzylidenic carbon appears in the range expected for sp^2 -hybridized species (purple in **Figure 32**, calculated resonance of 139.1 ppm) and the quaternary carbon provides a signal (107.2 ppm) in the region expected for acetals (cyan, calculated shift of 116.3 ppm). Besides these spectroscopic features, acetal **17** is thermodynamically more stable than dioxepine **16** by 6.9 kcal/mol in ΔG . Try as we might, efforts to crystallize these oily products at low temperature to perform X-

ray diffraction proved fruitless. As the originally published method reported that unsaturated aldehydes too could be efficient substrates, we decided to perform the reaction with cinnamaldehyde and cyclohexene oxide to determine the actual structure of the heterocyclic product (**Scheme 10**).



Scheme 10 1,4- vs 1,2-Addition in the reaction of epoxide **15a** with cinnamaldehyde **14b** with Colored Arrows Highlighting Key Difference in Their ^1H NMR Couplings.

If dioxepine **18** forms, it should provide a *cis*-vinyl coupling constant in the ^1H NMR spectrum (red arrow in **Scheme 10**), and a much smaller, aliphatic J should appear in the case of formation of **19** (blue arrow). Gratifyingly, by performing the reaction with HY-360 zeolite as catalyst, the heterocyclic product can be retrieved in 84% yield. A similar result, 77%, was achieved with BF_3 etherate as homogeneous catalyst. The observed positions of relevant NMR resonances are presented in the lower part of **Figure 32**. Expectedly, the quaternary carbon of **17** has been replaced by a C–H group and this hydrogen (highlighted in cyan) couples with the vinyl proton (highlighted in yellow). The experimental coupling constant is 6.3 Hz. This is in perfect agreement with the structure of acetal **19**, whereas it could not match that of the desired dioxepine **18**. All the other resonances parallel those presented above for acetal **17**. To exclude that the outcome of these reactions was dictated by the use of a cyclic epoxide, we replaced it with isobutene oxide. The reaction was less efficient with our heterogeneous catalyst (26% yield) than with a homogeneous Lewis acid (65% with BF_3 etherate). Nonetheless, the product (**Table 21, entry 3**) displayed the same NMR features discussed above for its peers. The reaction of an α,β -unsaturated ketone with styrene or dodecene oxide provided the same reactivity (**entries 4 and 5**, 29 and 40% yield, respectively). NMR resonances consistent with the structure of vinyl acetals were similarly observed reacting **15a** with either 4-chloro- and 4-methoxybenzylidene

acetone (**entries 6 and 7**, 83 and 12% yield, respectively) or aliphatic β -ionone (**entry 8**, 55% yield).

Table 21 Extension of the reaction to other α,β -insaturated compounds and epoxides.

Entry	α,β -insaturated compound	Epoxide	Yield (%)
1			68
2			84
3			26
4			29
5			40
6			83
7			12
8			55

3.4.3 Conclusions

On the basis of all of these spectroscopic and computational data, we thus propose to reassign the structure of these heterocyclic molecules as vinyl acetals rather than 1,4-dioxepines. The reaction of α,β -unsaturated carbonyls with epoxides in the presence of an acid catalyst would not provide the product of a formal (4 + 3) cycloaddition but leaves instead conjugated C=C double bonds untouched.

3.4.4 Experimental section

General Procedure To a round-bottom flask containing 200 mg of zeolite HY-360 was added a solution of the α,β -unsaturated carbonyl compound (3 mmol) in dichloromethane (5 ml), and the resulting mixture was stirred at 30 °C. A solution of the epoxide (3.3 mmol, 1.1 equiv.) in dichloromethane (5 ml) was then slowly added during 6 h via syringe pump (0.55 mmol/h). Upon completion of the addition, the mixture was maintained under stirring for another 2 h. The crude reaction mixture was then filtered, concentrated under reduced pressure, and eventually purified by flash column chromatography on silica gel (1:10 ethyl acetate:hexane).

Characterization of products

1) 2-Methyl-(E)-2-styrylhexahydrobenzo[d][1,3]dioxole

^1H NMR (300.1 MHz, CDCl_3): δ 7.41 (2H, d, $J = 7.1$ Hz), 7.32 (2H, t, $J = 7.1$ Hz), 7.23 (1H, t, $J = 7.1$ Hz), 6.76 (1H, d, $J = 15.9$ Hz), 6.27 (1H, d, $J = 15.9$ Hz), 3.38 (1H, ddd, $J = 9.9, 8.8, 3.7$ Hz), 3.30 (1H, ddd, $J = 9.9, 8.8, 3.7$ Hz), 2.15 (2H, t, $J = 9.8$ Hz), 1.82 (2H, d, $J = 9.7$ Hz), 1.59 (3H, s), 1.49 (2H, m), 1.29 (2H, m); ^{13}C NMR (75.4 MHz, CDCl_3): δ 136.3, 130.7, 129.0, 128.5, 127.8, 126.8, 107.2, 80.6, 80.1, 28.9, 28.7, 26.2, 23.7; IR (neat): 2953, 2795, 1502, 1496, 1398, 1267, 1188, 1123, 1078, 984, 839, 758, 689, 650 cm^{-1} ; HRMS (ESI⁺) calcd. for $\text{C}_{16}\text{H}_{21}\text{O}_2$ [$\text{M} + \text{H}$]⁺, 245.1536; found: 245.1542.

2) (E)-2-Styrylhexahydrobenzo[d][1,3]dioxole.

^1H NMR (300.1 MHz, CDCl_3): δ 7.42 (2H, d, $J = 8.3$ Hz), 7.30 (3H, m), 6.75 (1H, d, $J = 15.9$ Hz), 6.22 (1H, dd, $J = 15.9, 6.3$ Hz), 5.64 (1H, d, $J = 6.3$ Hz), 3.32 (2H, m), 2.19 (2H, m), 1.84 (2H, d, $J = 8.9$ Hz), 1.51 (2H, m), 1.31 (2H, m); ^{13}C NMR (75.4 MHz, CDCl_3): δ 135.9, 134.1, 128.5, 128.2, 126.9, 126.2, 103.7, 81.9, 79.9, 28.9, 28.7, 23.74, 23.70; IR (neat): 2932, 2863, 1448, 1397, 1380, 1278, 1205, 1127, 1080, 1048, 920, 870, 758, 697 cm^{-1} ; HRMS (ESI $^+$) calcd. for $\text{C}_{15}\text{H}_{19}\text{O}_2$ [$\text{M} + \text{H}$] $^+$, 231.1380; found: 231.1373.

3) 2,4,4-Trimethyl-(E)-2-styryl-1,3-dioxolane.

^1H NMR (400.1 MHz, CDCl_3): δ 7.40 (2H, d, $J = 7.2$ Hz), 7.32 (2H, t, $J = 7.4$ Hz), 7.25 (1H, t, $J = 7.2$ Hz), 6.72 (1H, d, $J = 16.0$ Hz), 6.21 (1H, d, $J = 16.0$ Hz), 3.78 (1H, d, $J = 8.1$ Hz), 3.69 (1H, d, $J = 8.1$ Hz), 1.56 (3H, s), 1.35 (3H, s), 1.34 (3H, s); ^{13}C NMR (100.5 MHz, CDCl_3): δ 136.4, 131.4, 129.2, 128.6, 127.8, 126.7, 108.2, 79.6, 75.2, 27.5, 27.0, 26.0; IR (neat): 2948, 2823, 1497, 1481, 1384, 1263, 1198, 1121, 1077, 997, 823, 763, 674, 643 cm^{-1} ; HRMS (ESI $^+$) calcd. for $\text{C}_{14}\text{H}_{19}\text{O}_2$ [$\text{M} + \text{H}$] $^+$, 219.1380; found: 219.1385.

4) (E)-2-(4-Chlorostyryl)-2-methyl-4-phenyl-1,3-dioxolane.

^1H NMR (300.1 MHz, CDCl_3): δ 7.39–7.24 (9H, m), 6.76 (1H, d, $J = 16.1$ Hz), 6.34 (1H, d, $J = 16.1$ Hz), 5.13 (1H, dd, $J = 8.9, 5.9$ Hz), 4.36 (1H, dd, $J = 8.9, 5.9$ Hz), 3.74 (1H, t), 1.65 (3H, s); ^{13}C NMR (75.4 MHz, CDCl_3): δ 138.1, 134.8, 133.6, 131.2, 128.8, 128.6, 128.2, 128.0, 126.6, 126.4, 108.8, 78.7, 71.8, 25.8; IR (neat): 2941, 2937, 2811, 1768, 1729, 1505, 1483, 1386, 1260, 1199, 1111, 1071, 995, 819, 760, 677 cm^{-1} ; HRMS (ESI $^+$) calcd. for $\text{C}_{18}\text{H}_{17}\text{O}_2\text{ClNa}$ [$\text{M} + \text{Na}$] $^+$, 323.0809; found: 323.0803.

5) 4-Decyl-2-methyl-2-(E)-styryl-1,3-dioxolane.

Two diastereomeric forms denoted as A and B in a 6:4 ratio. A: ^1H NMR (300 MHz, CDCl_3): δ 7.40 (2H, d, $J = 7.7$ Hz), 7.32 (2H, t, $J = 7.3$ Hz), 7.25 (1H, t, $J = 7$ Hz), 6.69 (1H, d, $J = 15.9$ Hz), 6.15 (1H, d, $J = 15.9$ Hz), 4.09 (1H, m), 4.01 (1H, m), 3.57

(1H, t, J = 6.9 Hz), 1.54 (3H, s), 1.26 (18H, m), 0.88 (3H, t, J = 6.8 Hz); ¹³C NMR (75.4 MHz, CDCl₃): δ 136.3, 130.3, 129.3, 128.5, 127.8, 126.7, 107.6, 76.1, 69.6, 33.36, 31.9, 29.71, 29.65, 29.60, 29.56, 29.52, 29.3, 26.0, 25.7. B: ¹H NMR (300 MHz, CDCl₃): δ 7.40 (2H, d, J = 7.2 Hz), 7.32 (2H, t, J = 7.5 Hz), 7.24 (1H, t, J = 7.2 Hz), 6.72 (1H, d, J = 16.0 Hz), 6.23 (1H, d, J = 16.0 Hz), 4.12 (2H, m), 3.51 (1H, t, J = 7.4 Hz), 1.54 (3H, s), 1.26 (18H, m), 0.88 (3H, t, J = 6.8 Hz); ¹³C NMR (75.4 MHz, CDCl₃): δ 136.4, 131.2, 129.4, 128.6, 127.8, 126.8, 107.7, 76.7, 69.9, 33.3, 31.9, 29.71, 29.66, 29.60, 29.56, 29.53, 29.3, 26.0, 25.7; IR (neat): 2940, 2815, 1502, 1485, 1383, 1264, 1194, 1113, 1069, 999, 824, 763, 676 cm⁻¹; HRMS (ESI⁺) calcd. for C₂₂H₃₇O₂ [M + H]⁺, 331.2632; found: 331.2636.

6) (E)-2-(4-Chlorostyryl)-2-methylhexahydrobenzo[d][1,3]dioxole.
¹H NMR (300.1 MHz, CDCl₃): δ 7.36 (2H, d, J = 8.5 Hz), 7.30 (2H, d, J = 8.5 Hz), 6.73 (1H, d, J = 15.9 Hz), 6.26 (1H, d, J = 15.9 Hz), 3.39 (1H, ddd, J = 12.4, 8.9, 3.8 Hz), 3.31 (1H, ddd, J = 12.4, 8.9, 3.8 Hz), 2.157 (2H, dd, J = 12.7, 9.5 Hz), 1.84 (2H, d, J = 9.1 Hz), 1.60 (3H, s), 1.49 (2H, m), 1.32 (2H, m); ¹³C NMR (75.4 MHz, CDCl₃): δ 134.9, 133.4, 131.4, 128.7, 128.0, 127.8, 107.1, 80.6, 80.2, 28.9, 28.7, 26.1, 23.7; IR (neat): 2943, 2808, 1774, 1731, 1502, 1488, 1392, 1264, 1192, 1113, 1073, 1000, 822, 764, 678 cm⁻¹; HRMS (ESI⁺) calcd. For C₁₆H₂₀O₂Cl [M + H]⁺, 279.1146; found: 279.1152.

7) (E)-2-(4-Methoxystyryl)-2-methylhexahydrobenzo[d][1,3]dioxole.
¹H NMR (300.1 MHz, CDCl₃): δ 7.35 (2H, d, J = 8.7 Hz), 6.85 (2H, d, J = 8.7 Hz), 6.70 (1H, d, J = 15.9 Hz), 6.13 (1H, d, J = 15.9 Hz), 3.80 (3H, s), 3.37 (1H, ddd, J = 12.5, 8.8, 3.7 Hz), 3.29 (1H, ddd, J = 12.5, 8.8, 3.7 Hz), 2.15 (2H, t, J = 9.7 Hz), 1.81 (2H, d, J = 9.8 Hz), 1.58 (3H, s), 1.48 (2H, m), 1.29 (2H, m); ¹³C NMR (75.4 MHz, CDCl₃): δ 159.4, 129.1, 128.6, 128.5, 128.0, 113.9, 107.4, 80.5, 80.0, 55.3, 28.9, 28.7, 26.3, 23.8; IR (neat): 2940, 2818, 1611, 1589, 1512, 1491, 1397, 1265, 1189, 1115, 1074, 992, 825, 761, 673 cm⁻¹; HRMS (ESI⁺) calcd. for C₁₇H₂₃O₃ [M + H]⁺, 275.1642; found: 275.1639.

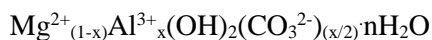
8) (E)-2-Methyl-2-(2-(2,6,6-trimethylcyclohex-1-en-1-yl)vinyl)hexahydrobenzo[d][1,3]dioxole.

^1H NMR (400.1 MHz, CDCl_3): δ 6.26 (1H, d, $J = 16$ Hz), 5.49 (1H, d, $J = 16$ Hz), 3.33 (1H, ddd, $J = 12.5, 8.7, 3.7$ Hz), 3.27 (1H, ddd, $J = 12.5, 8.8, 3.7$ Hz), 2.14 (2H, t, $J = 9.5$ Hz), 1.97 (2H, t, $J = 6.1$ Hz), 1.81 (2H, dd, $J = 9.0$ Hz), 1.67 (3H, s), 1.60 (2H, m), 1.53 (3H, s), 1.45 (4H, m), 1.29 (2H, m), 0.99 (3H, s), 0.98 (3H, s); ^{13}C NMR (100.5 MHz, CDCl_3): δ 136.5, 134.7, 128.6, 127.2, 107.4, 80.6, 79.9, 39.4, 33.9, 32.6, 29.1, 28.8, 28.7, 28.7, 26.2, 23.8, 23.8, 21.3, 19.3; IR (neat): 2822, 1609, 1582, 1519, 1487, 1402, 1263, 1193, 1110, 1079, 989, 831, 744, 680 cm^{-1} ; HRMS (ESI $^+$) calcd. for $\text{C}_{19}\text{H}_{31}\text{O}_2$ $[\text{M} + \text{H}]^+$, 291.2317; found: 291.2312.

4. Hydrotalcites

4.1 General introduction

Hydrotalcites (HTs) are hydroxy carbonates of magnesium and aluminum with lamellar structure and general formula



Part of the Mg^{2+} ions is replaced by Al^{3+} ions, resulting in positively charged cation layers. Charge-balancing anions and water molecules are situated in the interlayers between the stacked cation layers.⁹¹

These mixed hydroxides are commercially called hydrotalcites because fundamental structural studies have been conducted on a specific model called precisely hydrotalcite and whose formula is $\text{Mg}_6\text{Al}_2(\text{OH})_{16}\text{CO}_3\cdot\text{H}_2\text{O}$.

Many metal ions M^{2+} and M^{3+} having an ionic radius not too different from that of Mg^{2+} can be accommodated in the layer cation (such as, for example, Fe^{3+} , Cr^{3+} , Ca^{2+} and Ti^{4+}). This means that it is now possible to prepare a wide range of "Hydrotalcite-like anionic clays" that present extremely diversified catalytic activities.⁹²

Hydrotalcites behave as solid basic compounds. It should be underlined that in a hydrated material basic active sites consist mainly of structural hydroxide anions. On the contrary, in completely dehydrated materials (calcined) there are ion pairs $\text{O}^{2-}\text{---}\text{M}^{n+}$, which act as strong Lewis bases.⁹³ The basicity of this material is influenced by the calcination temperature (typically at 673-773 K) and by its composition, in particular by the Mg/Al ratio. For example Corma et al. have shown that the total number of basic sites increases with the decrease of the ratio Mg/Al.⁹⁴ It should be stressed that this dependence is not always linear.⁹⁵ The anionic clays, as hydrotalcites are, give rise to two endothermic transformations when subjected to heating. The first manifests itself at 370-570 K and corresponds to the loss of water localized in the interlayer zones. The second occurs at 620-750 K and corresponds to the loss of interlayer anions (CO_3^{2-}) and the loss of hydroxide ions from the layer of brucite. This phenomenon has, as consequence, the production of mixed oxides.

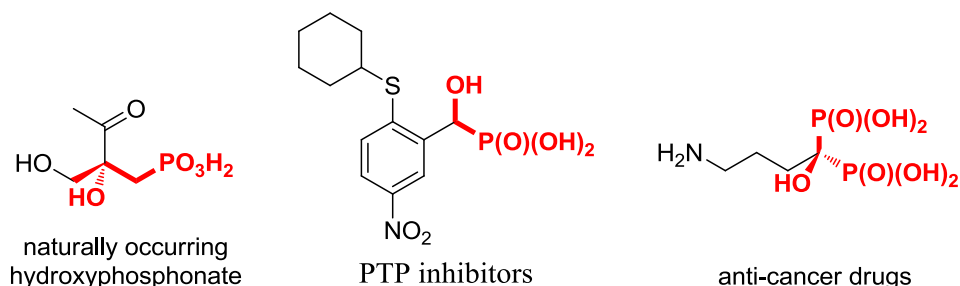
Hydrotalcites offer unique basic properties that make them very attractive for catalytic applications:⁹⁶

- high surface area;
- homogeneous distribution of the elements;
- synergistic effect between the elements that can generate, for example, sites with very high basicity;
- memory effect that can lead to the reconstruction of the original structure if put in contact with appropriate water solutions.

4.2 Phosphite Addition on Carbonyl Groups

4.2.1 Introduction

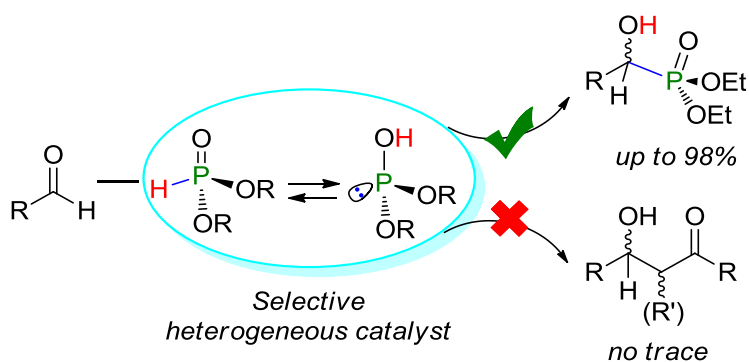
Hydroxyphosphonic acids derivatives are an important class of compounds and their structure could be found in a variety of natural and synthetic functional molecules. They can mediate a variety of biologic processes.⁹⁷ Organophosphonates are known for their ability to act as inhibitors of human enzymes.⁹⁸ They could be used as insecticides,⁹⁹ operating through similar molecular mechanisms on invertebrates. Through suitable modifications, these molecules can mediate plant growth regulator factors,¹⁰⁰ serve as prodrugs,¹⁰¹ show anti-bacterial¹⁰² and anti-viral activity.¹⁰³



Scheme 11 Examples of natural and synthetic bioactive hydroxyphosphonates.

Scheme 11 presents a selection of α -hydroxyphosphonates. These molecules are mainly prepared from the corresponding dialkyl phosphites $(RO)_2P(O)H$. The latter are versatile scaffolds that undergo a wide variety of reactions. Beside free-radical processes,¹⁰⁴ their phosphorus atom could act either as a nucleophilic or electrophilic center.¹⁰⁵ Under homogeneous conditions, it has been possible to use strong bases to catalyse the addition of dialkyl phosphites on carbonyl groups. A brief list¹⁰⁶ includes piperazines, MoO_2Cl_2 , cinchona-functionalized thioureas, and suitable aluminium complexes. In most cases, however, these catalysts are best suited for aromatic aldehydes or ketones because their pronounced basicity could easily trigger undesired self-condensation of the electrophilic reagent. On the other hand, the use of cheap and easily recoverable heterogeneous catalysts represents a cornerstone of green chemistry. They are a tool to minimize wastes and increase the sustainability of

chemical processes. Several inorganic solid bases too have been used to trigger C-P bond formation.¹⁰⁷ However, stoichiometric amounts of promoter were required and, furthermore, the possibility to easily recover and reuse these materials has not been reported. In a more elaborated strategy, solid-supported organo- and organometallic catalyst were tested for this reaction. Selected examples¹⁰⁸ include guanidines- and phosphazenes-tethered polystyrenes and nafion-supported vanadium oxides. However, in all cases the scope of the reaction is limited to non-enolizable aldehydes, mostly aromatic ones.¹⁰⁹ Keeping in mind these studies, we wondered to develop a complementary alternative merging advantages of existing strategies. We propose herein a novel method for the synthesis of α -hydroxyphosphonates by exploiting a cheap, easily recoverable and recyclable hydrotalcite (HT) as catalyst.¹¹⁰ Under mild and solvent-free conditions the basicity of the catalyst ensures almost quantitative yields of desired products. Furthermore, no traces of condensation products are detected, allowing the use of aliphatic, enolizable aldehydes in these reactions (**Scheme 12**).

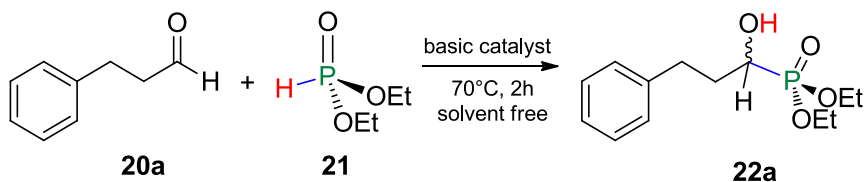


Scheme 12 Reactivity of hydrotalcites as catalyst for the synthesis of α -hydroxyphosphonates.

4.2.2 Results and discussion

Catalysts reported in this study are commercially available hydrotalcites of the PURAL family. In a first series of experiments, we tested whether hydrotalcites might catalyze the hydrophosphonation of an aliphatic aldehyde. Gratifyingly, we soon

realized their activity upon preliminary screening of reaction conditions. In a typical essay (**Scheme 13**), 1 mmol of 3-phenylpropanal **20a** reacts with 1.5 mmol of diethylphosphite **21** in the presence of 50 mg of hydrotalcite as catalyst. Complete selectivity towards **22a** and 80% conversion of **20a** were observed using MG30 as basic catalyst by warming the mixture at 70°C for two hours. The desired product **22a** forms quantitatively using MG70 as catalyst, despite its lower surface area (180 vs 250 m²/g respectively). The increased activity of MG70 is likely due to its more pronounced basicity, which results from a higher magnesium content (vide infra). Remarkably, we did not detect any trace of byproducts due to self-condensation of **20a** by both GC and NMR. Beside the easily recoverable solid base, this solvent-free route affords just the desired product and the recoverable, unreacted phosphites originally in excess.



Scheme 13 General reaction scheme.

For sake of comparison we performed the reaction with triethylamine as traditional homogeneous catalyst. **Figure 33** compares the yield of **22a** monitored through time among different catalytic systems. We were pleased that the reaction with 50 mg of triethylamine proved significantly slower (pink line) than those performed with solid catalysts.

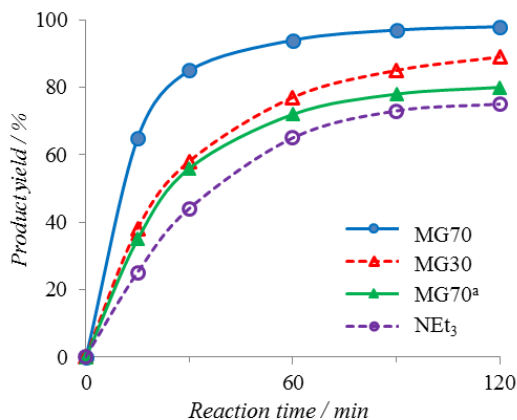


Figure 33 Yield of **22a** versus time using homogeneous (NEt₃) and heterogeneous (hydrotalcites MG70 and MG30) catalysts. Condition as Scheme 3, 1.5 equiv. of phosphite. a: with 1.0 equiv. of phosphite.

Product **22a** forms in 95% and 77% yield within 60 minutes using MG70 and MG30 respectively (blue and red lines). On the contrary, the yield sunk to 65% with triethylamine (violet line). By warming up to 120 minutes, MG70 ensures quantitative conversion of the substrate, while the yield of **22a** is 89% using MG30. The yield of the reaction with their homogeneous peer reaches a plateau below 80%. Furthermore, conversion of substrates eventually stops with triethylamine after two hours. The plot shown in **Figure 33** suggests therefore that solid basic hydrotalcites are more effective catalysts for this reaction than a homogeneous base as triethylamine. The selectivity towards **22a** remains complete reducing the molar excess of **21**. Reactions become however slower when the concentration of the latter fades. The conversion reaches 80% after two hours of warming in this case (green line). Therefore, while the molar excess of the phosphite increases the apparent rate of the reaction, the catalyst itself ensures the complete selectivity towards the desired product. No reaction took place in the absence of the catalyst and lower yields are achieved working at lower temperatures. We ensured the heterogeneous role of the catalyst by performing the Sheldon test and monitoring no further conversion on the filtrate.⁶⁶ We then investigated the possibility to recover and reuse the heterogeneous catalyst (**Table 22**).

Table 22 Reuse of the solid catalyst.

Cycle ^[a]	Yield of 22a (%) ^[b]	Cycle ^[a]	Yield of 22a (%) ^[b]
1 st	98	4 th	97
2 nd	98	5 th	97
3 rd	97	6 th	96

[a]: Reactions on 1 mmol scale, 1.5 equiv. of **21**.
[b]: isolated yields.

At the end of each reaction, the hydrotalcite was retrieved by filtration. Remarkably, it can be directly reused without any treatment. We were pleased that the catalyst efficiency is furthermore fully preserved at least for the first six cycles. These results suggest that the heterogeneous material acts catalytically at the molecular level in these reactions. Together with the mild operating conditions adopted, the possibility to easily recover and recycle the MG70 catalyst clearly witnesses the synthetic viability of our method. We then studied the scope of the reaction to test its general applicability. Results are summarized in **Table 23**.

Table 23 Scope of the reaction.

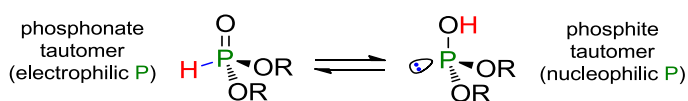
Entry ^[a]	R ₁	R ₂	Yield of 3 (%) ^[b]
1	Ph(CH ₂) ₂ (20a)	H	98
2	(CH ₃) ₂ CH (20b)	H	94
3	(CH ₃) ₂ CHCH ₂ (20c)	H	95
4	Cyclohexyl (20d)	H	98
5	Ph (20e)	H	98
6	4-OMePh (20f)	H	96
7	4-ClPh (20g)	H	95
8	benzo[d][1,3]dioxol (20h)	H	98
9	PhCH=CH (20i)	H	78
10	CH ₃ CH=CH (20j)	H	96
11	-(CH ₂) ₅ - (20k)		80

12 ^[c]	-(CH ₂) ₄ - (20l)		72
13 ^[c]	CH ₃ CH ₂ (20m)	CH ₃	63
14 ^[c]	CH ₃ (20n)	CH ₃	68

[a]: Reactions on 1 mmol scale, 1.5 equiv. of **21**.
 [b]: Isolated yield.
 [c]: The reaction was performed for 6 h.

Beside aldehyde **20a** (**entry 1**, 98%), other aliphatic aldehydes could be readily coupled, delivering corresponding products with excellent yields (**entries 2-4**, 94-98%). In all cases, the selectivity towards **22** is complete, and the desired product could be easily purified by column chromatography together with remaining traces of unreacted starting material. Almost complete conversions within 2 hours were observed with both linear and cyclic aldehydes (**entries 1-3** and **4** respectively). We then switched to aromatic ones (**entries 5-8**). MG70 remained an efficient catalyst for benzaldehyde (**20e**, **entry 5**, 98% yield). Aryl groups could feature electron-donating substituents and their less electrophilic carbonyl remain highly reactive (**entry 6** and **8**, 96 and 98% yield respectively). A withdrawing chlorine atom is similarly tolerated by the catalyst (**entry 7**, 95%). The evenly balanced basicity of hydrotalcite catalysts efficiently preserved other functional groups, leaving them suitable for further functionalization. Beside the acetal group of aldehyde, the solid base left untouched C-C double bonds of α , β -unsaturated aldehydes (**entries 9** and **10**). The presence of a conjugated aryl ring resulted in a slightly reduced conversion, **22i** being retrieved in 78% yield after 2 hours. Crotyl aldehyde **22j** smoothly delivered instead 96% of **22j** in the presence of MG70 as catalyst. As expected, ketones were less reactive substrates for this reaction, requiring usually longer reaction times to fully convert (up to 48 hours warming). This might correlate with the increased steric hindrance of their carbonyl group. Cyclic derivatives were more reactive than linear ones, as witnessed by the reaction of cyclohexanone **20k**, which delivered 80% of **22k** in 2 hours (**entry 11**). The reaction with cyclopentanone (**entry 12**) afforded the product in 72 % yield after 6 h. Conversion was slightly lower by using acetone and 2-butanone, the corresponding products being obtained in 68 % and 63 % yield, respectively. It is important to underline that in all cases the reaction did not produce any aldol

condensation products, even in trace amounts. No traces of other organic byproducts were indeed observed examining crude mixtures via both GC and ^1H -NMR. These features are usually not observed employing stronger bases as catalysts, either homogeneous or heterogeneous. We then wondered to gain insights on the remarkable efficiency and complete selectivity of hydrotalcites as catalysts in these reactions. As mentioned in the introduction, phosphites could display orthogonal reactivity.^{104,106} Their multi-purpose nature is caused by the tautomeric equilibrium between their two extreme forms (**Scheme 14**). Upon intensive studies, consensus exists that the phosphonate form is largely predominant (left, $\text{R} = \text{H}$).¹⁰⁵ The same stability trend occurs considering esters and diesters derivatives. However, it is often postulated the involvement of the less stable phosphite tautomer form in many synthetically relevant reactions (right).^{106,108} In the presence of a suitable catalyst, the tautomeric equilibrium could be therefore shifted by trapping a formal nucleophilic phosphorous atom.



Scheme 14 Tautomeric equilibrium of phosphonates.

Recently, low-temperature NMR analyses demonstrated that a suitable base could stabilize the phosphite tautomer.¹¹¹ We performed ^1H and ^{31}P -NMR studies on samples prepared mixing diethylphosphite with different bases (**Figure 34**).

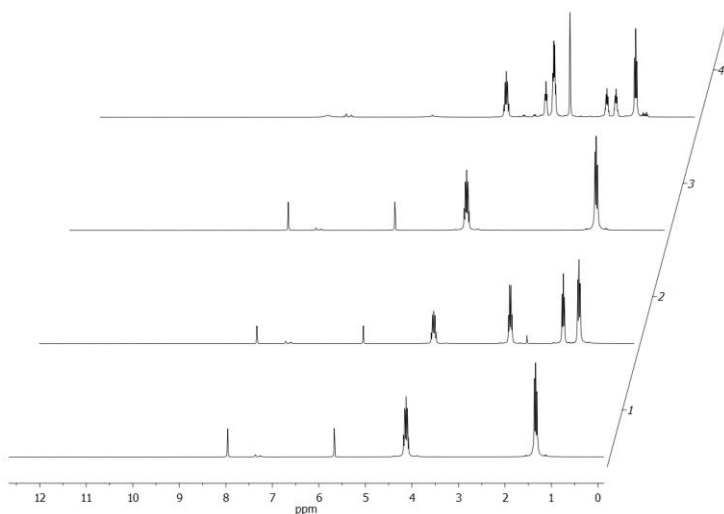


Figure 34 ^1H NMR (400MHz, CDCl_3): 1. diethyl phosphite - 2. diethyl phosphite + NEt_3 - 3. diethyl phosphite + MG70 - 4. diethyl phosphite + methyl-TBD.

The NMR spectra were recorded using a coaxial tube filled with DMSO-d_6 to lock samples and to avoid influences of the solvent on resonances of non-deuterated molecules. Diethyl phosphite was mixed with three different bases. The spectra of sample 1. shows resonances of the reagent alone for sake of comparison. The diagnostic doublet of its P-H group resonate at $\delta = 6.88$ ppm ($J = 688$ Hz). Spectra 2. and 3. contains equimolar amount of triethylamine and hydrotalcite MG70 respectively. They do not show any difference compared to the spectrum 1.. The diagnostic doublet mentioned above do not shift significantly and its resolution measured at half-width is similarly unchanged. This likely indicates that the interaction between the P-H group of diethyl phosphite and these bases do not shift significantly the tautomeric equilibrium of the latter within NMR timescales. Sample 4. provides a different picture. The presence of an equimolar amount of a strong guanidine base (Me-TBD) heavily impacted on observed signals from the reagent. Resonances of the P-H group almost disappeared, two very broad and weak peaks only being barely observed (slopes around 8.0 and 5.9 ppm respectively). Resonances of ethyl groups too were shifted in this case. They moved upfield by 0.1 ppm. From these experimental data, we can conclude that within NMR timescale, the phosphonate form almost disappears in the presence of a strong guanidine base. On

the contrary, no traces of the more elusive phosphite tautomer were detected in the presence of either homogeneous triethylamine or heterogeneous MG70.

The same trend was observed through IR measures (**Figure 35**).

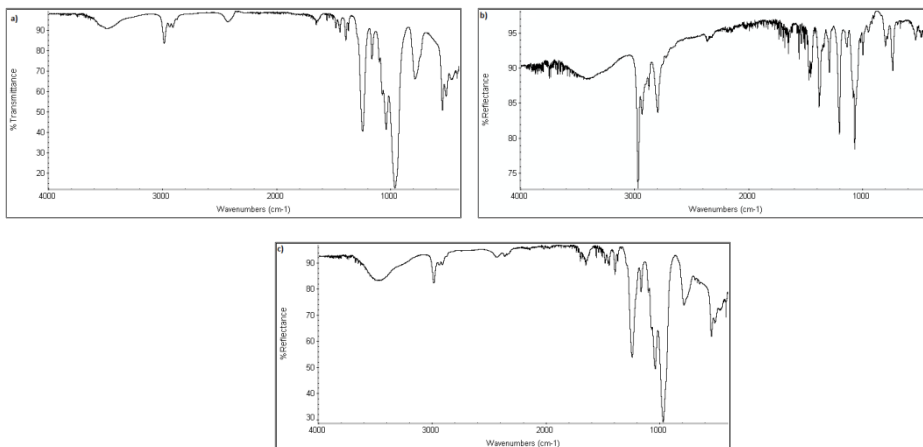
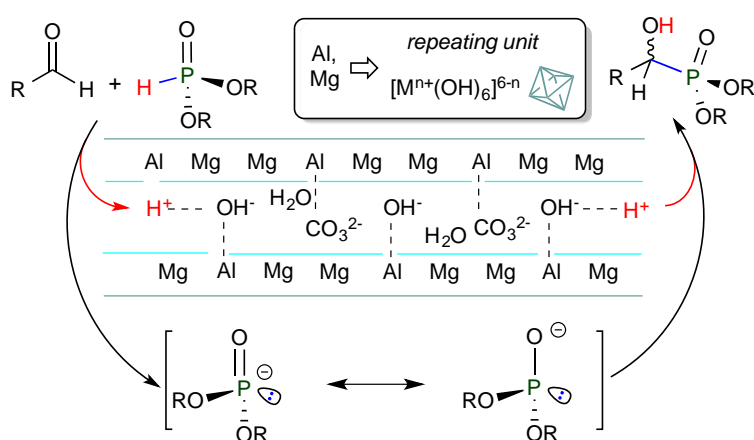


Figure 35 IR spectra of diethyl phosphite (a), triethylamine (b) and a mixture diethyl phosphite/triethylamine = 1/1 (c).

In this case is the band of the P-H bond remains visible ($\nu \approx 2400 \text{ cm}^{-1}$), in analogy to results observed by NMR.

These results let us speculate that the solid catalyst might represent a subtly tuned material that evenly balance its basicity, still ensuring a high reactivity without hampering the selectivity of the process. This could be due to the particular composition and structure of hydrotalcites.¹¹⁰ These materials are mixed hydroxyl carbonates of magnesium and aluminium. They can have different Mg/Al ratios and their basicity correlates with the content of the former. We confirmed this hypothesis by sequential adsorption and desorption of CO₂.¹¹⁰ Values for MG30 and MG70 were 0.095 and 0.158 mmol/g respectively. This confirms that the latter has a higher concentration of basic sites. MG30 provided three small desorption peaks at 122, 163 and 193 °C. MG70 showed a small signal at 135 °C and an intense one at 188 °C. These results suggest that the strength of their basic sites is similar. A comparable result was observed by analyzing a fivefold recycled MG70 catalyst (0.159 mmol/g, peaks at 134 and 206 188 °C). This confirms the robustness of the material.

Regarding the structure of HT, metal atoms are surrounded by hydroxyl groups that fill their coordination sphere. The resulting polyhedral assemble in sheets to provide a lamellar structure to the whole material. These layers are overall positively charged as part of magnesium ions are replaced by aluminium ones, and do not display therefore a strong basic character. Layers are thinly spaced, by less than 4 Å. They are filled by water molecules and charge-balancing anions, mostly carbonate ones, which represent the actual basic sites of the material, somehow shielded by the inorganic structure itself (**Scheme 15**).



Scheme 15 Possible hydrotalcite-promoted activation of phosphorus reagents.

Reasoning on the structure of these material¹¹⁰ and on literature studies,¹¹² it is credible to propose that basic sites on hydrotalcites, likely located in interlayers among metallic lamellae, could act as a catalyst and promote a shift in the tautomeric equilibrium of a proximal diorganophosphite molecule (**Scheme 15**). It is not possible to rule out that cationic charged layers too might cooperate in catalysis, by acting as acid sites that subtly increase the polarization of carbonyl groups. A similar ditopic behavior has been for instance observed with clays.¹¹³ The magnitude of these effects is most likely small, but remains sufficient to trigger the desired reaction without allowing any undesired side-reactivity. It is indeed worth noting that aliphatic aldehydes are generally prone to condensation reactions under both basic and acid conditions.

4.2.3 Conclusions

It is reported a simple catalytic method for the synthesis of α -hydroxyphosphonates under mild condition. Commercially available hydrotalcites have proved cheap and easily recoverable heterogeneous catalysts for an efficient C-P bond formation via selective addition of phosphites on the carbonyl group of aldehydes and ketones. Reactions afford desired products in good to excellent yield and do not require the presence of a solvent. Furthermore, nearly stoichiometric amounts of reagents could be used as the catalyst does not cause the condensation of the carbonyl derivatives, even employing aliphatic aldehydes.

4.2.4 Experimental Section

The desired carbonyl derivative (1.0 mmol), diethyl phosphite (1.5 mmol), and hydrotalcite MG70 (50mg) were sequentially added to a round bottom flask under air. The mixture was then stirred at 70°C for 2h, diluted with EtOAc (10 ml) and filtered to recover the basic catalyst. The desired product was then purified by flash column chromatography over silica gel using an EtOAc/hexane mixture as eluent.

Characterization of products

1) diethyl (1-hydroxy-3-phenylpropyl)phosphonate

^1H NMR (400 MHz, CDCl_3): δ = 1.30-1.36 (m, 6H), 2.02-2.10 (m, 2H), 2.76 (dt, 1H, J = 13.8, 8.3 Hz), 2.96-3.03 (m, 1H), 3.85-3.90 (m, 1H), 4.12-4.23 (m, 4H), 7.18-7.31 (m, 5H). ^{13}C NMR (100.5 MHz, CDCl_3): δ = 16.47 (d, J = 4.6 Hz), 16.52 (d, J = 4.8 Hz), 31.7 (d, J = 14.1 Hz), 33.0, 62.7 (d, J = 7.1 Hz), 62.5 (d, J = 7.1 Hz), 66.8 (d, J = 161.4 Hz), 125.9, 128.4, 128.6, 141.5. ^{31}P NMR (162 MHz, CDCl_3): δ = 25.3.

2) diethyl (1-hydroxy-2-methylpropyl)phosphonate

^1H NMR (400 MHz, CDCl_3): δ = 1.06 (d, 6H, J = 6.7 Hz), 1.33 (t, 6H, J = 7.1 Hz), 2.08 (hept, 1H, J = 6.7 Hz), 2.53 (br, OH), 3.64 (d, 1H, J = 6.1 Hz), 4.17 (m, 4H). ^{13}C NMR (100.5 MHz, CDCl_3): δ = 16.5 (d, J = 5.6 Hz), 17.7 (d, J = 7.6 Hz), 19.8 (d, J = 9.4 Hz), 30.1 (d, J = 2.2 Hz), 62.4 (d, J = 3.0 Hz), 62.5 (d, J = 3.1 Hz), 73.1 (d, J = 155.9 Hz). ^{31}P NMR (162 MHz, CDCl_3): δ = 25.1.

3) diethyl (1-hydroxy-3-methylbutyl)phosphonate

^1H NMR (400 MHz, CDCl_3): δ = 0.91 (d, 3H, J = 6.5 Hz), 0.96 (d, 3H, J = 6.7 Hz), 1.33 (t, 6H, J = 7.0 Hz), 1.46 (m, 1H), 1.68 (m, 1H), 1.92 (m, 1H), 3.94 (ddd, 1H, J = 11.1, 5.1, 3.0 Hz), 4.16 (m, 4H). ^{13}C NMR (100.5 MHz, CDCl_3): δ = 16.5 (d, J = 5.5 Hz), 21.1, 23.5, 24.1 (d, J = 14.3 Hz), 39.9, 62.57 (d, J = 5.8 Hz), 62.64 (d, J = 6.9 Hz), 66.1 (d, J = 158.8 Hz). ^{31}P NMR (162 MHz, CDCl_3): δ = 25.9.

4) diethyl (cyclohexyl(hydroxy)methyl)phosphonate

^1H NMR (400 MHz, CDCl_3): δ = 1.13-1.28 (m, 4H), 1.34 (t, 6H, J = 7.1 Hz), 1.66 (d, 1H, J = 11.3 Hz), 1.76 (d, 4H, J = 7.4 Hz), 2.01 (d, 1H, J = 11.6 Hz), 3.06 (d, 1H, J = 28.5 Hz), 3.67 (q, 1h, J = 5.9 Hz) 4.13-4.22 (m, 4H). ^{13}C NMR (100.5 MHz, CDCl_3): δ = 16.5 (d, J = 5.6), 26.0, 26.2 (d, J = 2.6 Hz), 27.9 (d, J = 7.4 Hz), 29.9 (d, J = 8.7 Hz), 39.7 (d, J = 2.2 Hz), 62.4 (m), 72.6 (d, J = 156.0 Hz). ^{31}P NMR (162 MHz, CDCl_3): δ = 25.1.

5) diethyl (hydroxy(phenyl)methyl)phosphonate

^1H NMR (400 MHz, CDCl_3): δ = 1.19-1.29 (m, 6H), 3.94-4.10 (m, 4H), 5.02 (dd, 1H, J = 10.8, 4.4 Hz), 7.30-7.38 (m, 3H), 7.49 (d, 2H, J = 7.5 Hz). ^{13}C NMR (100.5 MHz, CDCl_3): δ = 16.4, 63.1 (d, J = 7.3 Hz), 63.3 (d, J = 7.3 Hz), 70.9 (d, J = 158.9 Hz), 127.1 (d, J = 5.6 Hz), 128.1, 128.3, 136.6. ^{31}P NMR (162 MHz, CDCl_3): δ = 21.4.

6) diethyl (hydroxy(4-methoxyphenyl)methyl)phosphonate

^1H NMR (400 MHz, CDCl_3): δ = 1.22 (t, 3H, J = 7.1 Hz), 1.28 (t, 3H, J = 7.1 Hz), 3.51 (br, 1H), 3.81 (s, 3H), 3.98-4.09 (m, 4H), 4.95 (d, 1H, J = 9.9 Hz), 6.90 (d, 2H, J = 8.6 Hz), 7.41 (dd, 2H, J = 8.7, 2.2 Hz). ^{13}C NMR (100.5 MHz, CDCl_3): δ = 16.3 (d, J = 2.4 Hz), 16.4 (d, J = 2.4 Hz), 55.1, 62.9 (d, J = 7.3 Hz), 63.2 (d, J = 7.3 Hz), 70.2

(d, J = 161.1 Hz), 113.6 (d, J = 2.22 Hz), 128.4 (d, J = 6.1 Hz), 128.7 (d, J = 1.9 Hz), 129.3 (d, J = 2.9 Hz). ^{31}P NMR (162 MHz, CDCl_3): δ = 21.6.

7) diethyl ((4-chlorophenyl)(hydroxy)methyl)phosphonate

^1H NMR (400 MHz, CDCl_3): δ = 1.23 (t, 3H, J = 7.1 Hz), 1.27 (t, 3H, J = 7.1 Hz), 4.01-4.10 (m, 4H), 5.00 (dd, 1H, J = 10.9, 5.0 Hz), 7.32 (d, 2H, J = 8.4 Hz), 7.42 (dd, 2H, J = 8.5, 2.2 Hz). ^{13}C NMR (100.5 MHz, CDCl_3): δ = 16.3 (d, J = 5.7 Hz), 63.1 (d, J = 7.4 Hz), 63.5 (d, J = 7.2 Hz), 70.0 (d, J = 159.8 Hz), 128.3, 128.3, 128.3, 128.4, 133.7 (d, J = 4.0 Hz), 135.2 (d, J = 2.0 Hz). ^{31}P NMR (162 MHz, CDCl_3): δ = 20.7.

8) diethyl (benzo[d][1,3]dioxol-5-yl)(hydroxy)methyl)phosphonate

^1H NMR (400 MHz, CDCl_3): δ = 1.24 (t, 3H, J = 8.1 Hz), 1.29 (t, 3H, J = 8.1 Hz), 3.98-4.10 (m, 4H), 4.32 (br, 1H), 4.92 (d, 1H, J = 10.1 Hz), 5.96 (s, 2H), 6.78 (d, 1H, J = 7.9 Hz), 6.93 (d, 1H, J = 7.9 Hz), 7.03 (s, 1H). ^{13}C NMR (100.5 MHz, CDCl_3): δ = 16.4 (d, J = 5.5 Hz), 63.0 (d, J = 7.3 Hz), 63.4 (d, J = 7.0 Hz), 70.6 (d, J = 161.2 Hz), 101.1, 107.8 (d, J = 5.2 Hz), 108. (d, J = 2.2 Hz), 120.8 (d, J = 7.2 Hz), 130.6, 147.4 (d, J = 3.1 Hz), 147.6 (d, J = 2.3 Hz). ^{31}P NMR (162 MHz, CDCl_3): δ = 21.4.

9) diethyl (1-hydroxy-3-phenylallyl)phosphonate

^1H NMR (400 MHz, CDCl_3): δ = 1.30-1.35 (m, 6H), 4.16-4.23 (m, 4H), 4.68 (dd, 1H, J = 12.9, 5.9 Hz), 6.33 (m, 1H), 6.79 (ddd, 1H, J = 15.9, 4.8, 1.4 Hz), 7.25 (d, 1H, J = 6.8 Hz), 7.31 (t, 2H, J = 7.4 Hz), 7.40 (d, 2H, J = 7.5 Hz). ^{13}C NMR (100.5 MHz, CDCl_3): δ = 16.5 (d, J = 5.5), 63.1 (d, J = 7.3 Hz), 63.3 (d, J = 7.2 Hz), 69.5 (d, J = 161.0 Hz), 123.9 (d, J = 4.4 Hz), 126.6 (d, J = 1.8 Hz), 127.9, 128.6, 132.2, 132.4, 136.4 (d, J = 2.9 Hz). ^{31}P NMR (162 MHz, CDCl_3): δ = 21.6.

10) diethyl-(1-hydroxybut-2-en-1-yl)phosphonate

^1H NMR (400 MHz, CDCl_3): δ = 1.31 (m, 6H), 1.73 (m, 3H), 4.11 (m, 4H), 4.34 (m, 1H), 5.14 (br, OH), 5.59 (m, 1H), 5.86 (m, 1H). ^{13}C NMR (100.5 MHz, CDCl_3): δ = 16.4 (d, J = 5.5 Hz), 17.8, 62.9 (d, J = 7.50 Hz), 63.0 (d, J = 7.47 Hz), 69.3 (d, J = 161.5), 125.5 (d, J = 3.6 Hz), 130.0 (d, J = 13.5). ^{31}P NMR (162 MHz, CDCl_3): δ = 22.5.

11) diethyl (1-hydroxycyclohexyl)phosphonate

^1H NMR (400 MHz, CDCl_3): δ = 1.18-1.25 (m, 1H), 1.34 (t, 6H, J = 7.0 Hz), 1.57 (m, 2H), 1.66-1.75 (m, 5H), 1.83-1.87 (m, 2H), 4.14-4.21 (m, 4H). ^{13}C NMR (100.5 MHz, CDCl_3): δ = 16.5 (d, J = 5.5 Hz), 20.0 (d, J = 11.0 Hz), 25.3, 31.5 (d, J = 2.7 Hz), 62.6 (d, J = 7.5 Hz), 71.1 (d, J = 164.8 Hz). ^{31}P NMR (162 MHz, CDCl_3): δ = 26.7.

12) diethyl (2-hydroxybutan-2-yl)phosphonate

^1H NMR (400 MHz, CDCl_3): δ = 0.99 (t, 3H, J = 7.5 Hz), 1.32 (t, 6H, J = 7.2 Hz), 1.39 (s, 3H), 1.68-1.88 (m, 2H), 1.93 (s, 1H), 4.12-4.20 (m, 4H). ^{13}C NMR (100.5 MHz, CDCl_3): δ = 6.9, 7.0, 16.5 (d, J = 5.5 Hz), 21.2 (d, J = 4.3 Hz), 29.9 (d, J = 5.3 Hz), 62.6 (d, J = 7.9 Hz), 62.7 (d, J = 7.9 Hz), 72.0 (d, J = 161.0 Hz). ^{31}P NMR (162 MHz, CDCl_3): δ = 27.6.

13) diethyl (2-hydroxypropan-2-yl)phosphonate

^1H NMR (400 MHz, CDCl_3): δ = 1.37 (t, 6H, J = 7.1 Hz), 1.44 (s, 3H), 1.48 (s, 3H), 4.15-4.22 (m, 4H). ^{13}C NMR (100.5 MHz, CDCl_3): δ = 16.5 (d, J = 5.5 Hz), 25.0 (d, J = 4.7 Hz), 62.8 (d, J = 7.4 Hz), 69.9 (d, J = 162.8 Hz). ^{31}P NMR (162 MHz, CDCl_3): δ = 27.4.

14) diethyl (1-hydroxycyclopentyl)phosphonate

^1H NMR (400 MHz, CDCl_3): δ = 1.37 (t, 6H, J = 7.1 Hz), 1.71-1.91 (m, 6H), 2.07-2.12 (m, 2H), 4.18-4.25 (m, 4H). ^{13}C NMR (100.5 MHz, CDCl_3): δ = 16.6 (d, J = 5.6 Hz), 24.0, 24.2, 36.7 (d, J = 7.9 Hz), 62.7 (d, J = 7.2 Hz), 79.2 (d, J = 168.3 Hz). ^{31}P NMR (162 MHz, CDCl_3): δ = 27.0.

4.3 Allylation reaction of β -dicarbonyl compounds

4.3.1 Introduction

The formation of new C-C bonds is a fundamental reaction in organic synthesis. An important class of such reactions is represented by the allylation of β -dicarbonyl compounds.¹¹⁴ Generally, this reaction is carried out using allyl halides as allyl substrate and transition metals as catalysts. For the enantioselective version (AAA - Asymmetric Allylic Alkylation) various bidentate ligands C2 and C1-symmetric in combination with metals were used as catalysts getting excellent enantiomeric excesses.¹¹⁵

In recent years, given the increasingly pressing need to develop synthetic processes environmentally friendly, many research groups have studied the possibility of using allyl acetate or allyl alcohols as allyl substrate, with excellent results in terms of yield and selectivity. However, most of these reactions provides the use of metal-based homogeneous catalysts.¹¹⁶

In literature it is reported the use of some heterogeneous catalysts for promoting reactions of allylation of 1,3-dicarbonyl compounds. For example a functionalized silica with pendants diamine and complexed with palladium as catalyst was employed for the allylation of ethyl 3-oxo butanoate with methyl allyl carbonate,¹¹⁷ but the catalytic activity decreases when the catalyst is recovered and reused. A catalyst based on palladium "imprisoned" in an organic polymer has been used in reactions of this type with good results;¹¹⁸ the polymer based on palladium still requires four successive reactions for its preparation, although the authors report that can be reused without observing metal leaching in solution.

4.3.2 Results and discussion

In a preliminary series of experiments the activity of various solid base catalysts in combinations with different allyl substrates was evaluated. The allylation of benzoylacetone was carried out for 24 hours in toluene, a green eco-compatible solvent that permit to carry out the reaction in a quite large range of temperatures

(until 120 °C). The reaction temperature was changed depending on the boiling point of the allyl substrate used. The catalysts used were both commercially available solid bases and catalysts prepared by the tethering methodology. For a preliminary study, for each mmol of the 1,3-dicarbonyl compound 100 mg or 10%/mol of catalyst were used for the solid bases or the prepared catalysts respectively. The obtained results are shown in **Table 24**.

Table 24 Catalytic activity of various heterogeneous basic catalysts in the allylation reaction of benzoylacetone.

Reaction scheme: Benzoylacetone (23) + Allyl substrate (24) $\xrightarrow{24 \text{ h, toluene}}$ Allylated product (25)

Entry	X	T	Catalyst	Yield
1	Cl	25°C	HT MG30	-
2	Cl	25°C	HT MG70	-
3	Cl	25°C	mixed oxide SiO ₂ /CuO	-
4	Cl	25°C	SiO ₂ -TBD	-
5	Cl	40°C	mixed oxide SiO ₂ /CuO	-
6	Br	25°C	HT MG70	-
7	Br	25°C	mixed oxide SiO ₂ /CuO	-
8	Br	25°C	Pd/C(5%)	-
9	Br	70°C	HT MG70	40%
10	Br	70°C	HT MG30	13%
11	Br	70°C	Pd/C(5%)	-
12	Br	70°C	SiO ₂ -TBD	3%
13	Br	70°C	-	-
14	CH ₃ COO-	25°C	Pd/C(5%)	-
15	CH ₃ COO-	100°C	Pd/C(5%)	-
16	CH ₃ COO-	100°C	HT MG70	-

The data reported show that only by using hydrotalcites, basic clays, it was possible to isolate the desired product **25** in acceptable yields and with total selectivity (there is no formation at all of the product resulting from a double allylation), while the TBD

supported on silica proved to be practically inert and with Pd/C or mixed oxide no conversion at all is observed.

The difference between HT-MG30 and HT-MG70 resides in a different Mg/Al ratio: hydrotalcite MG30 has a MgO/Al₂O₃ of 30/70, while the MG70 is richer of magnesium oxide (MgO/Al₂O₃ = 70/30). The fact that the MG70 is a most efficient catalyst than MG30 can be due to a high number of hydroxyl groups, responsible for the catalytic activity, thanks to the higher content of magnesium. It should be underlined that the reaction carried out in the same conditions but in the absence of catalyst, has led to the total recovery of the starting reagents.

Tests were carried out also with various allyl substrates, in order to make the process more economical, using both allyl chloride and allyl acetate: unfortunately in both cases the catalyst resulted inactive.

In order to obtain higher yields while maintaining the excellent level of selectivity, parameter's reaction were optimized. For this purpose we decided to use a factorial design in order to investigate all the possible combinations of the levels of the factors and to evaluate, through statistical tests, the significance of the factors on the reaction yield.¹¹⁹

In order to streamline the program, only two parameters have been taken into consideration, namely the temperature and the reaction time, and the tests for the optimization of the experimental conditions were planned by performing the experiments provided by a full factorial design with 2 factors and 3 levels (number of experiments = 3²). The 3 levels examined are shown in **Table 25** and in **Table 26** the matrix of experiments is reported.

Table 25 Factorial design for the optimization of the reaction temperature and the reaction time.

Temperature (°C)		Time (h)	
Level	Value	Level	Value
-1	70	-1	6
0	85	0	15
+1	100	+1	24

Table 26 Matrix of the experiments conducted for the optimization of the reaction temperature and the reaction time.

Experiment	Parameter	
	T	t
1	-1	-1
2	0	-1
3	+1	-1
4	-1	0
5	0	0
6	+1	0
7	-1	+1
8	0	+1
9	+1	+1

Each test was replicated twice and the reactions were performed in random order using the *Carousel reaction system*, a system that allows to carry out multiple reactions at the same temperature and with the same stirring. It should be noted that for reactions carried out under heterogeneous conditions it is very important to have a stirring comparable for the various tests performed, as also the agitation (number of revolutions per minute) influence the catalytic process since it allows a greater or lesser dispersion of the heterogeneous catalyst into the reaction mixture. The results obtained are reported in **Table 27**.

Table 27 Yields obtained with the factorial design.

Entry	Time (h)	Temperature (°C)	Yield (%)	
			1 st exp	2 nd exp
1	6	70	30	33
2	15	70	34	38
3	24	70	39	44
4	6	85	39	38
5	15	85	42	46
6	24	85	41	36
7	6	100	31	32
8	15	100	38	37
9	24	100	48	53

With the data collected by the factorial design, we proceeded to an analysis of variance using ANOVA with 2-way interactions and then to a multiple regression in order to obtain a function of the response illustrating the weight of various factors on the reaction yield.

The analysis of significance was assessed at the 5%, and are therefore significant results both individual factors and the interaction time-temperature profile. It is therefore inferred that each factor considered is significant for the optimization of the reaction yield. In order to consider which are the factors that contribute most to the response function of the experimental design study, it was decided to apply a multiple regression analysis with the study of the factors backward. It was initially considered each factor (T and t), the interactions between factors (T x t) and auto-interactions (T x T and t x t): after each test, the less significant factor was discarded and the test is repeated until obtaining only the relevant factors, which were found to be temperature, the interaction time-temperature and the auto-interaction temperature-temperature.

Table 28 Results obtained with the multiple regression analysis

Multiple Regression Analysis				
Dependent variable: Yield				
		Standard	T	
Parameter	Estimate	Error	Statistic	P-Value
T	0.764517	0.0842171	9.07792	0.0000
T x t	0.00660451	0.00162671	4.06005	0.0010
T x T	-0.00463299	0.000905284	-5.11772	0.0001

The following response function of the factorial design studied was then obtained:

$$\text{Yield} = 0.764517 * T + 0.00660451 * T \times t - 0.00463299 * T \times T$$

From the response surface of **Figure 36** it can be observed that the quadratic term of the temperature present in the response function generates a curvature of the surface, with the maximum within the range studied in experimental design, then the

temperature rise beyond the point of maximum results in a gradual decrease in yield. The effect is observable at both low and high time values.

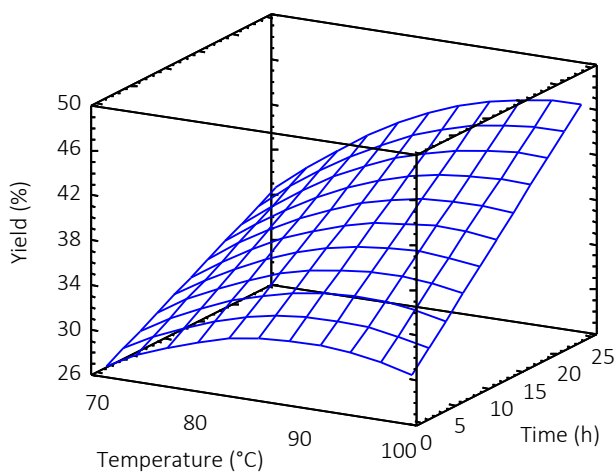


Figure 36 Response surface.

On the contrary, as can be observed in **Figure 37**, the linear term of the time in the function of response generates a linear increase of the reaction yield, effect more and more pronounced as the temperature increases, until reaching the upper end of the time domain studied in the factorial. It can therefore be noted that the effect of the interaction between time and temperature is critical: in fact, for short times there is no discrimination on the temperature, since the same yields are obtained, while when time increases the yield grows faster with increasing temperatures.

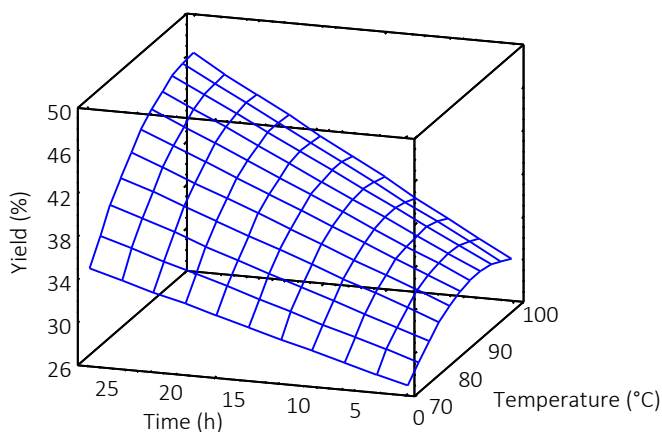


Figure 37 Response surfaces.

Finally, by studying the derivative of the function of the response it was found that the maximum yield of the reaction in the range studied is 46% at the temperature of 99 °C for 24 hours. It was therefore examined the idea to maintain a fixed temperature as its point of maximum fall in the range already studied, and to extend the domain of the times beyond 24 hours imposed in the original plan in order to ensure the predictability of function response, which suggests the possibility of a further increase in reaction yield.

On the basis of these results the reaction was conducted in toluene in the presence of hydrotalcite MG70 at 100 °C to evaluate the influence of reaction time on the process. The model reaction was monitored during more than 190 hours; the results are reported in **Figure 38**.

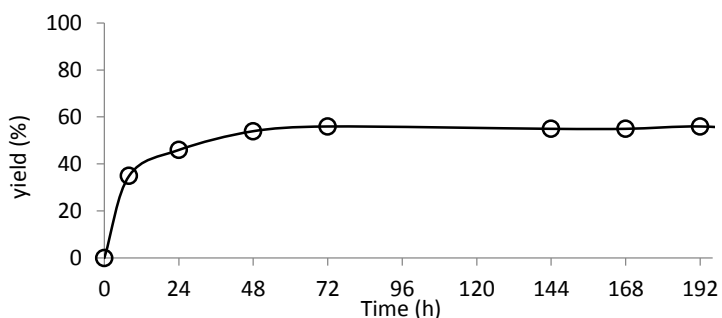


Figure 38 Yield of the monoalkylation product in function of the reaction time.

After 24 hours the reaction proceeds even leading to a maximum yield after about 72 hours, after which time no further increases are observed; the selectivity of the reaction remains very high (> 99%) during all the 72 hours.

Optimized the reaction conditions, it was evaluated the possibility of recycling the heterogeneous catalyst. At the end of the reaction (at 100 °C for 72 hours), the hydrotalcite MG70 was separated by filtration, washed with ethyl acetate, dried in air and reused with a new batch. Unfortunately the yield obtained dropped down to about 5%. Probably HBr, the other product of the reaction, remains inside the catalyst blocking its catalytic activity. So, the used catalyst was suspended in a NaOH solution 0.1 M for one hour, washed properly, dried and reused. A yield of 51% yield was restored. The recycle was repeated for additionally five times and the results obtained are reported in **Table 29**.

Table 29 Recycling of the heterogeneous catalyst.

Cycle	Yield (%)	Cycle	Yield (%)
1 st	53	4 th	52
2 nd	51	5 th	51
3 rd	52	6 th	51

With the NaOH washing, the catalyst can be utilised for six cycles obtaining the same values concerning the yield end the selectivity. It is important to underline that the reaction between benzoylacetone and allyl bromide catalyzed by NaOH, a basic compound that could be able to deprotonate the dicarbonyl compound and to favor the formation of the desired product, affords only the decarboxylated product **26** if carried out at 100 °C and gives no conversion at all if conducted at room temperature.

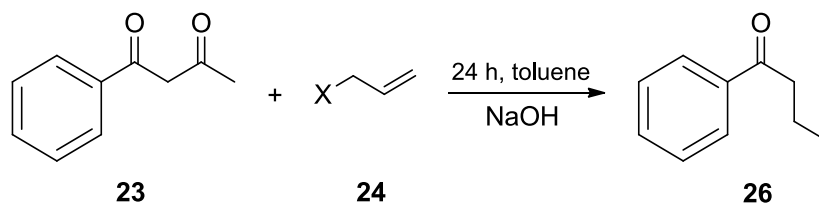


Figure 39 Allylation reaction of benzoylacetone in presence of NaOH.

Since it was observed that the catalyst is inhibited by the evolution of HBr during the reaction, we have carried out the process with amount of catalyst higher than the 100 mg utilized in the preliminary studies of the reaction. The results are reported in **Table 30**.

Table 30 Product yield by using different amount of catalyst.

Entry	Mg cat./mmol reagent	Yield (%)	Selectivity (%)
1	100	51	100
2	150	58	100
3	200	70	100
4	300	94	94
5	400	84	84

As expected, the conversion of benzoylacetone increases with the increasing of the amount of the catalyst. However, the use of a too much amount of catalyst results in a not total selectivity of the desired product of allylation because the decarboxylated product **26** is also obtained. The best results are observed using 200 mg of catalyst per mmol of reagent, condition that allows a 70% yield with 100% selectivity.

Finally, the influence of the solvent was evaluated. The reaction was carried out at 100 °C for 72 h using 200 mg of catalyst and in absence of solvent. These conditions permitted to improve the performances by leading to 90% of yield of the allylation product after only 24 h reaction, with total selectivity (in presence of toluene after 24 h the yield was only about 50%).

4.3.2 Conclusions

In conclusion, the problem of selective allylation of β -dicarbonyl compounds, which represents an important methodology for the formation of new carbon-carbon bonds, has been faced using a solid basic catalyst and using benzoylacetone and allyl bromide as model reagents.

Parameter reaction such as temperature and reaction time were optimized by using a factorial design with 2 factors and 3 levels: by means of a function of the response 100 °C and 24 hours of reaction were identified as ideal conditions. After the optimisation of other reaction parameters, the proposed procedure (solvent free, 100 °C, 72 h, hydrotalcite MG70) allows to obtain the product with a good yield combined with high level of selectivity. Further studies will carry out to extend the method to other dicarboxylic compounds.

4.3.3 Experimental section

For each allylation reaction benzoylacetone (2 mmol, 0.32 g) and allyl bromide (2 mmol, 0.17 ml) were mixed in 5 ml of toluene and finally 200 mg of solid catalyst MG70 were added. The temperature and the time for each reaction were varied following the factorial design and the matrix of the experiments described in table 24 and 25. The reaction mixture was then filtered on Buckner funnel and the catalyst washed with ethyl acetate. The yield was determined by the method of the internal standard by using the gas chromatography. The desired product was then purified by flash column chromatography over silica gel using an EtOAc/hexane mixture (98:2) as eluent.

Characterization of products

1) 2-allyl-1-phenylbutane-1,3-dione

^1H NMR (400 MHz, CDCl_3): δ = 2.17 (s, 3H), 2.77 (m, 2H), 4.56 (t, 1H, J = 7.2 Hz), 5.08 (m, 2H), 5.78 (ddt, 1H, J = 17.0, 10.0 Hz), 7.51 (t, 2H, J = 7.6 Hz), 7.62 (t, 1H, J = 7.6 Hz), 8.01 (d, 2H, J = 7.6 Hz); ^{13}C NMR (100.5 MHz, CDCl_3): δ = 28.2, 33.0, 62.7, 117.5, 127.5, 128.1, 128.7, 128.9, 133.8, 134.4, 136.4, 198.8, 203.6.

2) 1-phenylpent-4-en-1-one

^1H NMR (400 MHz, CDCl_3): δ = 2.51 (dt, 2H, J = 13.6, 6.7 Hz), 3.09 (t, 2H, J = 7.4 Hz), 5.02 (dd, 1H, J = 10.2, 1.5 Hz), 5.09 (dd, 1H, J = 17.1, 1.6 Hz), 5.9 (ddt, 1H, J = 16.8, 10.1, 6.5 Hz), 7.5 (t, 2H, J = 7.4 Hz), 7.6 (t, 1H, J = 7.3 Hz), 8.0 (d, 2H, J = 7.1 Hz); ^{13}C NMR (100.5 MHz, CDCl_3): δ = 28.2, 37.8, 115.3, 128.0, 128.6, 133.0, 137.0, 137.3.

References

1. Brundtland Report, *World Commission on Environment and Development*, **1987**.
2. R. A. Sheldon, *Green Chem.*, **2008**, 10, 359-360.
3. P. T. Anastas, L. G. Heine, T. C. Williamson, *Green Chemical Syntheses and Processes: Introduction*. In *Green Chemical Syntheses and Processes*, American Chemical Society: Washington, DC, **2000**; Chapter 1.
4. P. T. Anastas, J. C. Warner, *Green Chemistry: Theory and Practice*; Oxford University Press: New York, **1998**, p.30.
5. P. T. Anastas, M. M. Kirchhoff, *Accounts Chem. Res.* **2002**, 35 (9), 686-694.
6. P. T. Anastas, M. M. Kirchhoff, T. C. Williamson, *Appl. Catal. A: Gen.* **2001**, 221 (1-2), 3-13.
7. (a) A. Dijkstra, A. Marino-González, A. M. Payeras, W. C. E. Arends, R. A. Sheldon, *J. Am. Chem. Soc.* **2001**, 123, 6826-6833. (b) E. B. Mubofu, J. H. Clark, D. J. Macquarrie, *Green Chem.* **2001**, 3 (1), 23-25. (c) C. J. Adams, M. J. Earle, K. R. Seddon, *Chem. Commun.* **1999**, 1043-1044. (d) E. L. Dias, M. Brookhart, P. S. White, *J. Am. Chem. Soc.* **2001**, 123, 2442-2443. (e) W. F. Hoelderich, *Appl. Catal. A: Gen.* **2000**, 194-195, 487-496. (f) S. I. Murahashi, N. Komiya, Y. Oda, T. Kuwabara, T. Naota, *J. Org. Chem.* **2000**, 65, 9186-9193.
8. T. J. Collins, S. W. Gordon-Wylie, M. J. Bartos, C. P. Horwitz, C. G. Woomer, S. A. Williams, R. E. Patterson, L. D. Vuocolo, S. A. Paterno, S. A. Strazisar, D. K. Peraino, C. A. Dudash, *The design of green oxidants*. In *Green Chemistry: Frontiers in Benign Chemical Syntheses and Processes*, Oxford University Press: New York, **1998**, Chapter 3.
9. J. H. Clark, *Pure Appl. Chem.*, **2001**, 73, 103-111.
10. (a) H. W. Kouwenhoven, H. van Bekkum, In *Handbook of Heterogeneous Catalysis*; G. Ertl, H. Knözinger, J. Weitkamp, Eds. VCH: Weinheim, **1997**; Vol. 5, 2358; (b) G. Sartori, R. Maggi, *Chem. Rev.* **2006**, 106, 1077-1104.
11. G. Sartori, R. Maggi, V. Santacrose, *Catalytic Friedel-Crafts Acylation Reactions* in *Arene Chemistry: Reaction Mechanisms and Methods for*

- Aromatic Compounds*”, **2015**, Jacques Mortier Editor, John Wiley & Sons, 1st Edition, 58-82.
12. Horsley, J. A. *Chemtech* **1997**, 27, 45.
 13. J. R. H. Ross, *Heterogeneous Catalysis - Fundamentals and Applications*, Elsevier, **2012**, 56-63.
 14. C. Doornkamp, V. Ponc, *J. Mol. Catal. A: Chem.* **2000**, 162, 19-32.
 15. G. Sartori, R. Ballini, F. Bigi, G. Bosica, R. Maggi, P. Righi, *Chem. Rev.*, **2004**, 104, 199-250.
 16. M. Minami, S. Kai, JP 04,182,452 (**1992**) (*Chem. Abstr.*, **1993**, 118, 124071y).
 17. S. M. Levonis, L. F. Bonarghi, T. A. Houston, *Aust. J. Chem.*, **2007**, 60, 821-823.
 18. A. M. Klibanov, *Acc. Chem. Res.*, **1990**, 23, 114-120.
 19. A. Sharma, S. Chattopadhyay, V. R. Mamdapur, *Biotechnol. Lett.*, **1995**, 17, 939-942.
 20. J. Zerda, G. Barak, Y. Sasson, *Tetrahedron*, **1989**, 45, 1533-1536.
 21. (a) H. Ogawa, Y. Ichimura, T. Chihara, S. Teratani, K. Taya, *Bull. Chem. Soc. Jpn.* **1986**, 59, 2481-2483; (b) H. Ogawa, T. Chihara, K. Taya, *J. Am. Chem. Soc.* **1985**, 107, 1365-1369; T. Chihara, *J. Chem. Soc., Chem. Commun.*, **1980**, 1215-1216; (c) H. Ogawa, N. Hiraga, T. Chihara, S. Teratani, K. Taya, *Bull. Chem. Soc. Jpn.*, **1988**, 61, 2383-2386; (d) H. Ogawa, T. Chihara, S. Teratani, K. Taya, *Chem. Commun.*, **1986**, 1337-1338.
 22. (a) M. Saito, S. Fujisaki, Y. Ishii, T. Nishiguchi, *Tetrahedron Lett.* **1996**, 37, 6733-6736; (b) T. Nishiguchi, Y. Ishii, S. Fujisaki, *J. Chem. Soc., Perkin Trans. I* **1999**, 3023-3027.
 23. Barton and Ollis (2007).
 24. A.P. Dicks and A. Hent, *Green Chemistry Metrics*, Springer Briefs in Green Chemistry for Sustainability, **2015**, 17-43.
 25. J. Andraos, *Org. Process Res. Dev.* **2009**, 13, 161-185.
 26. C. Jimenez-Gonzalez, C. S. Ponder, Q. B. Broxterman, J. B. Manley, *Org. Process Res. Dev.* **2011**, 15, 912-917.

27. (a) F. Cavani, N. Ballarini, A. Cericola, *Catal. Today*, **2007**, 127, 113-131; (b) M.M. Bhasin, J.H. McCain, B.V. Vora, T. Imai, P.R. Pujadó, *Appl. Catal. A: Gen.* **2001**, 221, 397-419; (c) J. McGregor, Z. Huang, E.P.J. Parrott, J.A. Zeitler, K.L. Nguyen, J.M. Rawson, A. Carley, T.W. Hansen, J. Tessonier, D.S. Su, D. Teschner, E.M. Vass, A. Knop-Gericke, R. Scholgl, L.F. Gladden, *J. Catal.* **2010**, 269, 329-339.
28. C. White, *Chem.-Biol. Interact.* **2007**, 166 (1-3), 10-14.
29. L. Rodríguez, D. Romoreo, D. Rodríguez, J. Sánchez, F. Domínguez, G. Arteaga, *Appl. Catal. A: Gen.* **2010**, 373, 66-70.
30. J. Burla, R. Fehnel, P. Louie, P. Terpeluk, *Two-step Production of 1,3-butadiene from ethanol*. Senior Design Reports (CBE), **2012**, Penn Libraries, University of Pennsylvania.
31. P. C. A. Bruijninx, B. M. Weckhuysen, *Angew. Chem. Int. Edit.* **2013**, 52 (46), 11980-11987.
32. D. Seddon, *The High Price of Butadiene*. Duncan Seddon & Associated PTY. LTD., **2012**, Retrieved, April 15th 2015, from <http://www.duncanseddon.com/>.
33. E. V. Makshina, M. Dusselier, W. Janssens, J. Degreève, P. A. Jacobs, B. F. Sels, *Chem. Soc. Rev.*, **2014**, 43, 7917-7953.
34. (a) C. Angelici, B. M. Weckhuysen, P. C. A. Bruijninx, *ChemSusChem* **2013**, 6(9), 1595-1614; (b) E.V. Makshina, W. Janssens, B.F. Sels, P.A. Jacobs, *Catalysis Today* **2012**, 198, 338-344; (c) M. D. Jones, C. G. Keir, C. Di Iulio, R. A. M. Robertson, C. V. Williams, D. C. Apperley, *Catal. Sci. Technol.*, **2011**, 1, 267-272.
35. G. Meixiang, L. Zongzhang, Z. Minhua, T. Lui, *Catal. Lett.* **2014**, 144 (12), 2071-2079.
36. M. D. Jones, *Chemistry Central Journal*, **2014**, 8 (53), 1-5.
37. D. Milne, D. Glasser, D. Hildebrandt, B. Hausberger, *Ind. Eng. Chem. Res.*, **2006**, 45, 2661-2671.
38. L. M. Madeira, M. F. Portela, *Catal Rev.* **2002**, 44 (2), 247-286.
39. (a) N. Madaan, R. Haufe, N. R. Shiju, G. Rothenberg, *Top Catal.*, **2014**, 57, 1400-1406; (b) W. Yan, Q. Y. Kouk, K. Lou, Y. Liu, A. Borgna, *Catal. Commun.* **2014**,

- 46, 208-212; (c) H. Seo, J. K. Lee, U. G. Hong, G. Park, Y. Yoo, J. Lee, H. Chang, I. K. Son, *Catal. Commun.* **2014**, 47, 22-27.
40. A. S. Barnard, L. A. Curtiss, *Nano Lett.*, **2005**, 5 (7), 1261-1266.
41. (a) R. Benjaram, K. Atallah, *Catal. Rev.* **2005**, 47, 257-296; (b) A. Khodakov, B. Olthof, A. T. Bell, E. Iglesia, *J. Catal.* **1999**, 181, 205-216; (c) A. H. Shahbazi Kootenaiea, J. Towfighia, A. Khodadadib, Y. Mortazavib, *Appl. Surf. Sci.* **2014**, 298, 26-35.
42. (a) R. Austin, S. F. Lim, *PNAS*, **2008**, 105 (45), 17217-17221; (b) Y. Hwua, Y. D. Yaoa, N. F. Chenga, C. Y. Tungb, H. M. Linb, *Nanostruct. Mater.* **1997**, 9 (1-8), 355-358.
43. M. Batzill, *Energy Environ. Sci.*, **2011**, 4, 3275-3286.
44. J. M. P. Martirez, S. Kim, E. H. Morales, B. T. Diroll, M. Cargnello, T. R. Gordon, C. B. Murray, D. A. Bonnell, A. M. Rappe, *J. Am. Chem. Soc.*, **2015**, 137 (8), 2939-2947.
45. (a) Y. Li, U. Aschauer, J. Chen, A. Selloni, *Acc. Chem. Res.*, **2014**, 47 (11), 3361-3368; (b) A. Selloni, *Nature Materials*, **2008**, 7, 613-615.
46. J. C. Mikkelsen, *Appl. Phys. Lett.* **1984**, 45, 1187-1189.
47. (a) U. Diebold, *Surf. Sci. Rep.* **2003**, 48 (5-8), 53-229; (b) H. G. Yang, C. H. Sun, S. Z. Qiao, J. Zou, G. Liu, S. C. Smith, H. M. Chen, G. Q. Lu, *Nature*, **2008**, 453, 638-642; (c) Y. Xia, K. Zhu, T. C. Kaspar, Y. Du, B. Birmingham, K. T. Park, Z. Zhang, *Phys. Chem. Lett.*, **2013**, 4, 2958-2963.
48. (a) H. Cheng, A. Selloni, *Phys. Rev. B*, **2009**, 79, 92101; (b) H. Cheng, A. Selloni, *J. Chem. Phys.*, **2009**, 131, 54703; (c) Y. He, O. Dulub, H. Cheng, A. Selloni, U. Diebold, *Phys. Rev. Lett.*, **2009**, 102, 106105.
49. (a) S. Mahshid, M. Sasani Ghamsari, M. Askari, N. Afshar, S. Lahuti, *Semicond. Phys. Quantum Electron. Optoelectron.* **2006**, 9 (2), 65-68; (b) X. Chen, S. S. Mao, *Chem. Rev.*, **2007**, 107 (7), 2891-2959.
50. M. Pal, G. A. Serrano, P. Santiago, U. Pal, *J. Phys. Chem. C*, **2007**, 111, 96-102.
51. I. Marcu, I. Sandulesca, J. M. Millet, *J. Mol. Catal.* **2003**, 203, 241-250.
52. (a) D.E. Resasco, *Encyclopedia of Catalysis 3*, **2002**, 49; (b) J.C. Bricker, *Top. Catal.* **2012**, 55, 1309-1314.

53. (a) A. Dinse, R. Schomaecker, A. T. Bell, *Phys. Chem. Ch. Ph.* **2009**, 11, 6119-6124; (b) E. V. Ramos-Fernandez, N. J. Geels, N. R. Shiju, G. Rothenberg, *Green Chem.* **2014**, 16, 3358-3363; (c) N. R. Shiju, M. Anilkumar, S. P. Gokhale, B. S. Rao, C. V. V. Satyanarayana, *Catal. Sci. Technol.* **2011**, 1, 1262-1270.
54. (a) S. M. Stagg, C. A. Querini, W. E. Alvarez, D. E. Resasco, *J. Catal.* **1997**, 168, 75-94; (b) S. A. Bocanegra, Sergio R. de Miguel, Irina Borbath, Jozsef L. Margitfalvi, Osvaldo A. Scelza, *J. Mol. Catal. A: Chem.* **2009**, 301, 52-60; (c) A. D. Ballarini, C. G. Ricci, S. R. de Miguel, O. A. Scelza, *Catal. Today*, **2008**, (133-135), 28-34.
55. (a) P. Sun, G. Siddiqi, M. Chi, A.T. Bell, *J. Catal.* **2010**, 274, 192-199; (b) E.L. Jablonski, A.A. Castro, O.A. Scelza, S.R. de Miguel, *Appl. Catal. A: Gen.* **1999**, 183, 189-198.
56. (a) R.D. Cortright, J.M. Hill, J.A. Dumesic, *Catal. Today*, **2000**, 55, 213-223; (b) J. Salmones, J.-A. Wang, J.A. Galicia, G. Aguilar-Rios, *J. Mol. Catal. A: Chem.* **2002**, 184, 203-213.
57. B. M. Nagarajaa, C.-H. Shinb, K.-D. Junga, *Appl. Catal. A: Gen.* **2013**, 467, 211-223.
58. D.C. Sherrington, A.P. Kybett, *Supported Catalysts and Their Applications*, The Royal Society of Chemistry **2001**, 76-80.
59. (a) P. Gallezot, *Chem. Soc. Rev.*, **2012**, 41, 1538-1558; (b) P. McKendry, *Bioresource Technology*, **2002**, 83, 37-46; (c) R. Beerthuis, G. Rothenberg, N. R. Shiju, *Green Chem.*, **2015**, 17, 1341-1361; (d) M. J. Climent, A. Corma, S. Iborra, *Green Chem.*, **2014**, 16, 516-547.
60. R. O. M. A. de Souza, L. S. M. Miranda, R. Luque, *Green Chem.*, **2014**, 16, 2386-2405.
61. A. Corma, S. Iborra, A. Velty, *Chem. Rev.*, **2007**, 107, 2411-2502.
62. <http://www.gfbiochemicals.com>
63. (a) J. Zhang, S. B. Wu, B. Li, H. D. Zhang, *ChemCatChem*, **2012**, 4, 1230-1237; (b) C.R. Patil, P.S. Niphadkar, V.V. Bokade, P.N. Joshi, *Catal. Commun.* **2014**, 43, 188-191; (c) K. Y. Nandiwale, V. V. Bokade, *Chem. Eng. Technol.* **2015**, 38,

- 246-252; (d) D.R. Fernandes, A.S. Rocha, E.F. Mai, Claudio J.A. Mota, V. Teixeira da Silva, *Appl. Catal. A: Gen.* **2012**, (425-426), 199-204.
64. H. J. Bart, J. Reidetschläger, K. Schatka, A. Lehmann, *Ind. Eng. Chem. Res.* **1994**, 33, 21-25.
65. (a) L. Penga, L. Lina, J. Zhanga, J. Shia, S. Liub, *Appl. Catal. A: Gen.* **2011**, 397, 259-265; (b) G. Pasquale, P. Vázquez, G. Romanelli, G. Baronetti, *Catal. Commun.* **2012**, 18, 115-118.
66. H. E. B. Lempers, R. A. Sheldon, *J. Catal.* **1998**, 175, 62-69.
67. (a) C. Friedel, J. M. Crafts, *C. R. Hebd. Seances Acad. Sci.* **1877**, 84, 1450; (b) G. A. Olah, *Friedel-Crafts Chemistry*, John Wiley & Sons: New York, **1973**.
68. H. G. Franck, *Industrial aromatic chemistry*, Springer: Berlin, **1988**.
69. (a) K. Bauer, D. Garbe, H. Surberg, *Common Fragrance and Flavor Materials*, WHC: Weinheim, **1990**; (b) N.P. Buu-Hoi, N. D. Xuong, P.C. Jain, V. T. Suu, *Spasmolytic ketones derived from benzofuran* in *C. R. Acad. Sci.* **1961**, Vol. 253, 1075-1076.
70. G. Sartori, R. Maggi, *Advances in Friedel-Crafts Acylation Reactions Catalytic and Green Processes*, CRC Press: Boca Raton, **2010**.
71. B. Chiche, A. Finiels, C. Gauthier, P. Geneste, J. Graille, D. Pioch, *J. Org. Chem.* **1986**, 51, 2128-2130.
72. A. Corma, *Chem. Rev.* **1995**, 95, 559-614.
73. I. V. Kozhevnikov, *Appl. Catal. A: Gen.* **2003**, 256, 3-18.
74. (a) J. A. Melero, R. van Grieken, G. Morales, V. Nuño, *Catal. Commun.* **2004**, 5, 131-136.
75. M. Alvaro, A. Corma, D. Das, V. Fornés, H. García, *J. Catal.*, **2005**, 231, 48-55.
76. O. Kwon, S. Park, G. Seo, *Chem. Commun.* **2007**, 4113-4115.
77. C. G. Piscopo, A. Adorni, R. Maggi, G. Sartori, *Chimica Oggi / Chemistry Today* **2011**, 29 (supplement: Milestones in Chemistry), 6-8.
78. J. A. Melero, R. van Grieken, G. Morales, M. Paniagua, *Energy & Fuels* **2007**, 21, 1782-1791.
79. I. K. Mbaraka, B. H. Shanks, *J. Catal.* **2006**, 244, 78-85.

80. (a) C. G. Piscopo, S. Loebbecke, R. Maggi, G. Sartori, *Adv. Synth. Catal.* **2010**, 352, 1625-1629; (b) R. Maggi, S. Chitsaz, S. Loebbecke, C. G. Piscopo, G. Sartori, M. Schwarzer, *Green Chem.* **2011**, 13, 1121-1123; (c) C. G. Piscopo, S. Bühler, G. Sartori, R. Maggi, *Catal. Sci. Technol.* **2012**, 2, 2449-2452.
81. R. D. Badley, W. T. Ford, *J. Org. Chem.* **1989**, 54, 5437-5443.
82. S. Leveneur, D. Y. Murzin, T. Salmi, *J. Mol. Catal. A: Chem.* **2009**, 303, 148-155.
83. (a) T. Lu, Z. Lu, Z.-X. Ma, Y. Zhang, R. P. Hsung, *Chem. Rev.* **2013**, 113, 4862-4904; (b) K. E. O. Ylijoki, J. M. Stryker, *Chem. Rev.* **2013**, 113, 2244-2266. (c) A. G. Lohse, R. P. Hsung, *Chem.-Eur. J.* **2011**, 17, 3812-3822. (d) T. V. Nguyen, J. M. Hartmann, D. Enders, *Synthesis* **2013**, 45(7), 845-873. (e) H. Pellissier, *Adv. Synth. Catal.* **2011**, 353, 189-218. (f) B. M. Trost, M. U. Frederiksen, M. T. Rudd, *Angew. Chem., Int. Ed.* **2005**, 44, 6630-6666; (g) P. A. Wender, N. M. Deschamps, R. Sun, *Angew. Chem., Int. Ed.* **2006**, 45, 3954-3957.
84. (a) J.-J. Feng, J. Zhang, *J. Am. Chem. Soc.* **2011**, 133, 7304-7307; (b) M.-B. Zhou, R.-J. Song, C.-Y. Wang, J.-H. Li, *Angew. Chem., Int. Ed.* **2013**, 52, 10805-10808; (c) P. A. Wender, T. M. Pedersen, M. J. C. Scanio, *J. Am. Chem. Soc.* **2002**, 124, 15154-15155.
85. (a) A. Ueda, A. Yamamoto, D. Kato, Y. Kishi, *J. Am. Chem. Soc.* **2014**, 136, 5171-5176; (b) A. B. Smith, S. Dong, J. B. Brennehan, R. J. Fox, *J. Am. Chem. Soc.* **2009**, 131, 12109-12111; (c) M. J. Campbell, J. S. Johnson, *J. Am. Chem. Soc.* **2009**, 131, 10370-10371; (d) H. Kim, H. Lee, D. Lee, S. Kim, D. Kim, *J. Am. Chem. Soc.* **2007**, 129, 2269-2274.
86. (a) H.-Q. Zhang, C.-B. Zhang, *J. Heterocycl. Chem.* **2012**, 49, 1-8; (b) D. M. Podgorski, S. W. Krabbe, L. N. Le, P. R. Sierszulski, R. S. Mohan, *Synthesis* **2010**, 16, 2771-2775; (c) I. Nakamura, Y. Kudo, M. Terada, *Angew. Chem., Int. Ed.* **2013**, 52, 7536-7539; (d) R. Guo, K.-N. Li, L.-Z. Gong, *Org. Biomol. Chem.* **2013**, 11, 6707-6712; (e) X. Guo, W. Liu, W. Hu, *Chem.-Asian J.* **2014**, 9, 117-120.
87. Y.-Q. Zhou, N.-X. Wang, S.-B. Zhou, Z. Huang, L. Cao, *J. Org. Chem.* **2011**, 76, 669-672.

88. (a) C. Perego, R. Millini, *Chem. Soc. Rev.* **2013**, 42, 3956-3976; (b) R. Gounder, E. Iglesia, *Acc. Chem. Res.* **2012**, 45, 229-238; (c) C. Martínez, A. Corma, *Coord. Chem. Rev.* **2011**, 255, 1558-1580; (d) R. Maggi, G. Bosica, S. Gherardi, C. Oro, G. Sartori, *Green Chem.* **2005**, 7, 182-184; (e) R. Ballini, F. Bigi, E. Gogni, R. Maggi, G. Sartori, *J. Catal.* **2000**, 191 (2), 348-353; (f) F. Bigi, B. Frullanti, R. Maggi, G. Sartori, E. Zambonin, *J. Org. Chem.* **1999**, 64, 1004-1006.
89. For a recent example of DFT as a tool to rationalize diastereoselectivity: V. Narbonne, P. Retailleau, G. Maestri, M. Malacria, *Org. Lett.* **2014**, 16, 628-631.
90. (a) B. T. Whiting, G. W. Coates, *J. Am. Chem. Soc.* **2013**, 135, 10974-10977; (b) A. Ahmed, S. D. R. Christie, M. R. J. Elsegood, G. Pritchard, *J. Chem. Commun.* **2013**, 49, 7489-7491; (c) G. D. Yadav, P. S. Surve, *Ind. Eng. Chem. Res.* **2013**, 52, 6129-6137.
91. (a) A. de Roy, C. Forano, K. El Mliki, J.P. Besse, in “*Expanded Clays and Other Microporous Solids*”, eds. M.L. Occelli, H.E. Robson, Rynholdn N.Y., **1992**, vol. 2, 108-169; (b) J. I. Di Cosimo, V. K. Díez, M. Xu, E. Iglesia, C. R. Apesteguía, *Journal of Catalysis*, **1998**, 178, 499-510.
92. F. Cavani, F. Trifirò, A. Vaccari, *Catal. Today*, **1991**, 11, 173-302.
93. B.F. Sels, D.E. De Vos, P.A. Jacobs, *Catal. Rev.* **2001**, 43, 433-488.
94. A. Corma, V. Fornes, R. M. Martín Aranda, F. Rey, *J. Catal.*, **1992**, 134, 58-65.
95. W.T. Reichle, *J. Catal.*, **1985**, 94, 547-557.
96. D. P. Debecker, E. M. Gaigneaux, G. Busca, *Chem. Eur. J.* **2009**, 15, 3920-3935.
97. (a) F. R. Hartly, in *The Chemistry of Organo Phosphorous Compounds*, John Wiley and Sons, New York, USA, **1990**; (b) O. I. Kolodiazhnyi, *Tetrahedron Asymmetry* **2005**, 16, 3295-3450.
98. (a) D. V. Patel, K. Rielly-Gauvin, D. E. Ryono, C. A. Free, W. L. Rogers, S. A. Smith, J. M. DeForrest, R. S. Oehl and E. W. Petrillo, Jr., *J. Med. Chem.* **1995**, 38, 4557-4569; (b) M. Tao, R. Bihovsky, G. J. Wells and J. P. Mallamo, *J. Med. Chem.* **1998**, 41, 3912-3916; (c) A. J. Ganzhorn, J. Hoflack, P. D. Pelton, F. Strasser, M.-C. Chanal and S. R. Piettrek, *Bioorgan. Med. Chem.* **1998**, 6, 1865-1874.

99. Ó. Lopez, J. G. Fernandez-Bolaños, M. V. Gil, *Green Chem.* **2005**, 7, 431-442.
100. D. Q. Shi, Z. L. Sheng, X. P. Liu, H. Wu, *Heteroatom Chem.* **2003**, 14, 266-268.
101. S. J. Hecker, M. D. Erion, *J. Med. Chem.* **2008**, 51, 2328-2345.
102. R. U. Pokalwar, R. V. Hangarge, P. V. Maske, M. S. Shingare, *Arkivoc* **2006**, 11, 196-204.
103. A. Szymanska, M. Szymczak, J. Boryski, J. Stawinski, A. Kraszewski, G. Collu, G. Sanna, G. Giliberti, R. Loddo, P. La Colla, *Bioorgan. Med. Chem.* **2006**, 14, 1924-1934.
104. (a) D. Leca, L. Fensterbank, E. Lacôte, M. Malacria, *Chem Soc Rev.* **2005**, 10, 858-865; (b) H. Yorimitsu, *J. Org. Chem.* **2013**, 9, 1269-1277.
105. G. O. Doak, L. D. Freedman, *Chem. Rev.* **1961**, 61, 31-44.
106. (a) K. S. Kumar, C. B. Reddy, M. V. Narayana Reddy, C. R. Rani, C. S. Reddy, *Org. Commun.* **2012**, 5, 50-57; (b) R. G. de Noronha, P. J. Costa, C. C. Romao, M. J. Calhorda, A. C. Fernandes, *Organometallics* **2009**, 28, 6206-6212; (c) F. Wang, X. Liu, X. Cui, Y. Xiong, X. Zhou, X. Feng, *Chem. Eur. J.* **2009**, 15, 589-592; (d) X. Zhou, X. Liu, X. Yang, D. Shang, J. Xin, X. Feng, *Angew. Chem. Int. Ed.* **2008**, 47, 392-394; (e) B. Saito, H. Egami, T. Katsuki, *J. Am. Chem. Soc.* **2007**, 129, 1978-1986; (f) J. P. Abell, H. Yamamoto, *J. Am. Chem. Soc.* **2008**, 130, 10521-10523.
107. (a) M. Pandi, P. K. Chanani, S. Govindasamy, *Appl. Catal. A: Gen.* **2012**, (441-442), 119-124; (b) B. Kaboudin, M. Karimi, *Arkivoc* **2007**, 13, 124-132; (c) B. Kaboudin, M. Karimi, *Bioorgan. Med. Chem. Lett.* **2006**, 16, 5324-5327; (d) E. Martinez-Castro, O. Lopez, I. Maya, J. G. Fernandez-Bolaños, M. Petrini, *Green Chem.* **2010**, 12, 1171-1174; (f) G. Keglevich, V. R. Toth, L. Drahos, *Heteroatom Chem.* **2011**, 22, 15-17; (g) P. G. Mandhane, R. S. Joshi, D. R. Nagargoje, C. H. Gill, *Tetrahedron Lett.* **2010**, 51, 1490-1492; (h) L. Zhao, H. Ding, B. Zhao, C. Lu, Y. Yao, *Polyhedron* **2014**, 83, 50-59.
108. (a) D. Simoni, R. Rondanin, M. Morini, R. Baruchello, F. P. Invidiata, *Tetrahedron Lett.* **2000**, 41, 1607-1610; (b) T. Angelini, S. Bonollo, D. Lanari, F. Pizzo, L. Vaccaro, *Org. Biomol. Chem.* **2013**, 11, 5042-5046; (c) S. S. Weng,

- G. Y. Lin, H. C. Li, K. C. Yang, T. M. Yang, H. C. Liu, S. H. Sie, *Appl. Organometal. Chem.* **2012**, 26, 455-460.
109. For a microwave-promoted synthesis, limited to aromatic aldehydes see: S. Kumari, A. Shekhar, D. D. Pathak, *Chem. Sci. Trans.* **2014**, 3, 45-54.
110. D. P. Debecker, E. M. Gaigneaux, G. Busca, *Chem. Eur. J.* **2009**, 15, 3920-3935.
111. D. Uraguchi, T. Ito, T. Ooi, *J. Am. Chem. Soc.* **2009**, 131, 3836-3837.
112. J. C. A. A. Roelofs, D. J. Lensveld, A. J. van Dillen, K. P. de Jong, *J. Catal.* **2001**, 203, 184-191.
113. F. Bigi, L. Chesini, R. Maggi, G. Sartori, *J. Org. Chem.* **1999**, 64, 1033-1035.
114. J. Otera, *Modern Carbonyl Chemistry*; Wiley-VCH: New York, NY, USA, **2000**.
115. B. M. Trost, D. L. Van Vranken, *Chem. Rev.*, **1996**, 96, 395-422.
116. (a) M. Noji, Y. Konno, K. Ishii, *J. Org. Chem.* **2007**, 72, 5161-5167; (b) H.-J. Zhang, B. Demerseman, Z. Xi, C. Bruneau, *Adv. Synth. Catal.* **2009**, 351, 2724-2728.
117. H. Noda, K. Motokura, A. Miyaji, T. Baba, *Adv. Synth. Catal.* **2013**, 355, 973-980.
118. A. Cauvel, G. Renard, D. Brunel, *J. Org. Chem.*, **1997**, 62, 749-751.
119. Montgomery, *Introduction to factorial designs; The advantages of factorials*, Section 5-2, **2001**.